Design, Fabrication and Assembly of a Flapping-Wing with Integrated Compliant Hinge

Application in a Bio-Inspired, Resonant Micro Air Vehicle

Meindert Ras

Master of Science Thesis

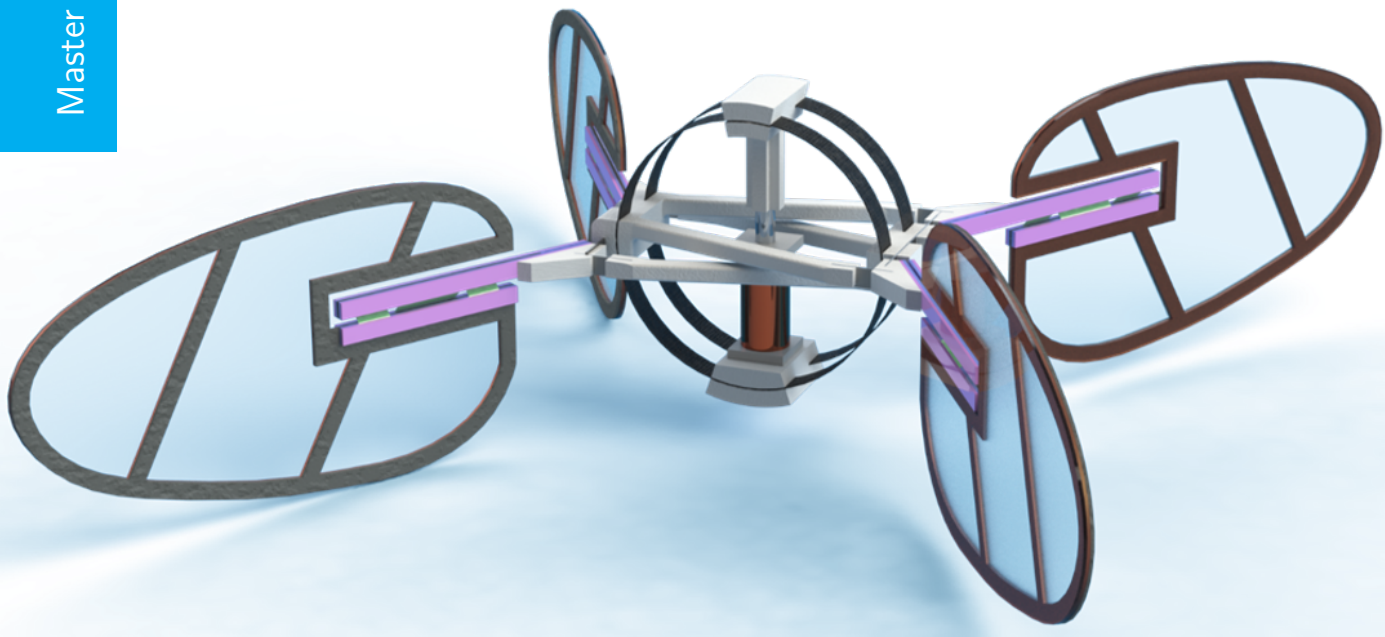

TU Delft Delft University of Technology

Department of Precision and Microsystems Engineering

Design, Fabrication and Assembly of a Flapping-Wing with Integrated Compliant Hinge

Application in a Bio-Inspired, Resonant Micro Air Vehicle

Master of Science Thesis

For the degree of Master of Science in Mechanical Engineering at Delft University of Technology

Meindert Ras

June 29, 2020

Faculty of Mechanical, Maritime and Materials Engineering (3mE) · Delft University of Technology

Delft University of Technology
Department of
Precision and Microsystems Engineering (pme)

The undersigned hereby certify that they have read and recommend to the Faculty of Mechanical, Maritime and Materials Engineering (3mE) for acceptance a thesis entitled

Design, Fabrication and Assembly of a Flapping-Wing with Integrated Compliant Hinge

by

Meindert Ras

in partial fulfillment of the requirements for the degree of

Master of Science Mechanical Engineering

Dated: June 29, 2020

Supervisor(s):

Dr.ir. J.F.L. Goosen

Reader(s):

Dr.ir. J.F.L. Goosen

Dr.ir.N.Tolou

ir.L.Zhang

Abstract

The Atalanta is a palm-sized, resonant, compliant mechanism developed by the University of Technology Delft. It is an insect-inspired, flapping-wing micro air vehicle with better hovering capabilities compared to rotary or fixed wing aircraft. In its current form, the Atalanta has a lift-to-mass ratio of 0.12 which inhibits it from taking off. Getting the Atalanta to fly would greatly benefit the research into areas such as aerodynamic modelling, on-board electronics, chemical actuators and more.

Designing and realizing a new, energy-efficient wing-system capable of producing 1.5 g lift is found to be the most effective solution to increasing the lift-to-mass ratio. Developing this new wing-system requires the design, manufacturing and integration of two parts: a wing and a compliant hinge. The wing is the wing-shaped, rigid plate that pushes air around to generate lift. The hinge is the interface between the Atalanta body and the wing, and allows the wing to passively rotate, i.e.: pitch, around its spanwise axis.

The design of the wing has two important features: the wing shape and the pitching axis. These two features have been optimized and presented in earlier research and are used as the basis for the new wing. Different fabrication methods are researched with the conclusion being that the Smart Composite Microstructure method is the one best suited. Here a hybrid structure is created by stacking sheets of different materials on top of each other, each with its own purpose. The sheets are laser cut before assembly to distributed material only where needed. The result is a wing consisting of a carbon frame for stiffness, a Mylar sheet for enclosing the wing surface area and a double-sided adhesive layer to bond the two together.

For the compliant pitching hinge, little to no experience was available within the Atalanta project. Because of this, multiple concepts are researched and their performance graded. The result is a cross axis, compliant pivot hinge consisting of three leaf-flexures arranged into an X-shape. The combined pure bending motion of all three flexures allows the wing to rotate around its pitching axis. The flexures are fabricated and subsequently integrated into the wing structure, forming the new wing-system.

Several tests are conducted to quantify the performance of the wing, the hinge and the wing-system. The first test analysis the shape and dimensions of the wing. When the laser cuts lines into a sheet of material, it automatically cuts a predefined amount of extra lines parallel to that initial line; it basically widens the cut. This way the laser light can still penetrate into the material at deeper levels. This effect causes the wingspan to be 2.78 % smaller which can reduce the lift generation by 6.2 %. Another test shows that the angular bending

stiffness between two hinges can vary up to 16.4 %. This again can influence the generated lift by approximately 2 %. The variation among hinges is most likely to be caused by an imprecise way of cutting the hinge flexures to the right size. The third test is concerned with measuring the absolute stiffness of four hinges. The average overall stiffness is a factor 27.8 higher than what was expected. Measurement errors, incorrect input parameters, hinge flexure misalignment and corrugation at the edges of the flexures all can reduce the factor to 13.9, but the dominant reason is estimated to be curving of the flexures along their width. The last test determines the right flapping frequency of the new wing-system and states it to be 8.5 Hz. This is lower than the desired 27.5 Hz but can be accounted for by the factor 5.9 increase in moment of inertia around the pitching axis. The higher moment of inertia slows down the pitching of the wing, which in turn requires the sweeping motion to slow down as well for the wing-system to maintain its optimal kinematic profile. Because the kinematic profile is close to optimal, the energy efficiency of the system is estimated to be an improvement over that of the current wing-system. The 8.5 Hz flapping frequency does hurt the lift production meaning that the Atlanta would not fly with these new wing-systems. However, reducing the mass of the wing and optimizing its topology should lower the moment of inertia significantly which directly increases the flapping frequency, and with it the lift production. This last test also measured the durability of two wing-systems to be 18 min and 54 min respectively.

The weakest link of this wing-system is the fabrication of the hinge; ample improvements can be made in this area. Nevertheless, this project presents an Atalanta wing-system that certainly is a step forward. With some weight saving improvements, the wing-system should be more energy efficient while producing more lift compared to the current wing-system. The design and manufacturing processes are more flexible and consistent which makes experimental optimization of the mechanical properties of the wing-system easier. The novel cross axis hinge concept proves to be a valuable addition to the wing. Slow motion footage shows the hinge functioning as a 1-DOF system which reduces unwanted motion of the wing-system.

Table of Contents

List of Figures

List of Tables

Acknowledgements

It is strange to realize that this thesis is the end of seven years at the University of Technology Delft. Somehow I never really thought it possible to get to this point. It requires a lot of hard work, and I'm proud to say that I gave it my very best. Studying for me wasn't something I had to go through; it felt like an exciting and organized way of learning the things I wanted to learn anyway. I have truly enjoyed these seven years and I am extremely grateful for the opportunities I have been given. But this achievement is far from my own.

First and foremost I want to thank my parents, my sister and my brothers. My parents taught me to never loose track of what is really important and believed in me and supported me no matter what. My sister and brothers have inspired me in so many ways; I am the person I am today by simply following their lead. You guys are the best!

I want to thank my room mates who have always been there for me. We have had some great times and I can guarantee we'll have them for many years to come. During these seven years I met a lot of new people who have become great friends. Without them, studying would be just that, so thank you all.

Lastly I want to thank Hans and the technical support staff. In the six years leading up to my thesis I learned a lot about mechanical systems etc., but during my thesis I learned how to be an engineer, and that is all thanks to Hans. He could have told me on day one what I should do and how I should do it; it would probably have saved both of us a lot of time. But he merely suggested some things and let me figure it out on my own. That's where I learned how to ask the right questions, learned how to answer and verify them. Working on this thesis with Hans opened up a new level of thinking about mechanical systems, that in a way, is more valuable than knowing all the equations. Hans, I wish you all the best. The members of the technical support team should be thanked as well. If there is a limit to how many times you can ask for their help, I have probably exceeded it twice over. Thank all of you for your time and valuable insights, you certainly made this thesis possible.

For the reader: I hope you enjoy this thesis!

University of Technology Delft — Meindert Ras
June 29, 2020

Chapter 1

Introduction

1-1 Background

1-1-1 Flapping-wing micro air vehicle

A flapping-wing micro air vehicle - or FWMAV - is in its simplest form a small drone that uses flapping wings for attitude control and lift generation. Its size and method of propulsion are two prominent features since they give this class of drones capabilities that are not often seen in other classes.
Regarding its size, a FWMAV has generally a wingspan of up to 15 cm [13]. An important reason for these smaller drones to exist, is that they provide increased manoeuvrability compared to their larger counterparts since moment of inertia scales favourably with the characteristic dimension of a drone [14]. Other reasons can include: low power consumption due to low drone mass [2], flying in confined spaces [15], ease of transportation and difficulty to detect [13].
Secondly: flapping wings. There are three categories when it comes to lift generation in drones: flapping wing, fixed wing and rotary wings. Fixed wing MAVs - similarly to an air-plane - create lift by generating an airflow over fixed wings with an airfoil cross-section. Rotary wing MAVs - similarly to a helicopter - have one or more spinning blades that push the air down creating lift. These two categories have some critical disadvantages that give rise to the flapping wing MAVs, namely: fixed wing MAVs have to be in forward motion to generate the required airflow and thus typically cannot hover, and rotary wing MAVs are difficult to scale down since they need sufficient blade surface area to create lift [13, 16].
A great example illustrating the benefits of flapping wing MAVs over fixed wing or rotary wing MAVs are search and rescue missions after an earthquake. Small, energy efficient, highly manoeuvrable flapping wing drones capable of hovering could be used to get into the unsafe, collapsed buildings to search for survivors and communicate their location to rescue teams.

1-1-2 The TU Delft Atalanta

A review article published in 2019 [15] lists 51 FWMAV projects around the world. Across the board these drones display incredible research into propulsion, control, compliant mechanisms, energy storage, aerodynamics and much more. One of the drones on the list is the Atalanta from the department of Precision and Microsystems Engineering at the University of Technology Delft (see fig. 1-1 C, fig. A-2 for additional images). The project started in 2006 and since then at least 3 PhD candidates, 16 master students and 10 bachelor groups have contributed to its research covering a wide range of topics. The drone itself has a mass of 7.82 g and a wingspan of about 13 cm. Its most recent complete prototype produced 0.9 g lift [1] which amounts to a lift-to-mass ratio of 0.12.

The Atalanta - similar to many FMWAVs - is heavily inspired by nature. Its wing design, kinematics, drive mechanism and body are directly linked to that of a flying insect of the order *Diptera* [1]; and for good reasons. Insects can perform precise hovering flight [15], are capable of sophisticated and agile manoeuvring [16], can change the size and shape of their wings [17] and show remarkable flight endurance and energy efficiency compared to man-made drones [1, 15]. One key feature of insects that yields this impressive energy efficiency, is the use of resonance. The thorax (body of the insect containing the muscles and the wing-driving mechanism, see fig. 1-1 A,B) and wings of an insect form a tuned mass-spring-damper system that, when excited at the right frequency, drives the wings while requiring a minimum amount of energy [1, 18]. Amongst the 51 projects, the Atalanta is - to the authors knowledge - the only FWMAV that mimics this insect behaviour so closely.

For the Atalanta to mimic this behaviour, it basically utilizes four components: an actuator, wings, a compliant amplification mechanism and a ring-shaped frame (fig. 1-1 C). The actuator is placed inside the ring and deforms it (fig. 1-1 D) at the lowest eigenfrequency of the system. A compliant four-bar mechanism is attached to the ring and translates and amplifies the deformation of the ring into a sweeping motion of the four wings.

As mentioned, exploiting resonance increases the energy efficiency of the system which means that less power is required to operate the drone. Normally the power consumption of a FWMAV has three components: 1) aerodynamic power to overcome the aerodynamic drag on the wings, 2) inertial power needed to accelerate the wings and the fluid surrounding them, 3) elastic power to compensate for the elastic deformation of the wings, frame etc [2]. But since resonance is applied, the cycle-averaged elastic and inertia power will be zero since this energy is continuously stored in the ring-shaped thorax. The actuator therefore only has to provide enough energy to overcome the aerodynamic drag on the wings which is dissipative [1] and acts as a damper within the mass-spring-damper system. Reducing the power consumption within the system is highly important since this allows the use of a smaller, less powerful actuator keeping the mass of the system low. Additionally, using resonance - and with it compliant mechanisms - lowers the complexity of the system due to integration of parts, reduces frictional losses and allows for a lightweight, scalable design.

1-2 Problem definition

The latest Atalanta prototype (manufactured by Bolsman in 2010 [1]), as mentioned above, has a lift-to-mass ratio of 0.12. This means that the drone is currently not able to take off; let

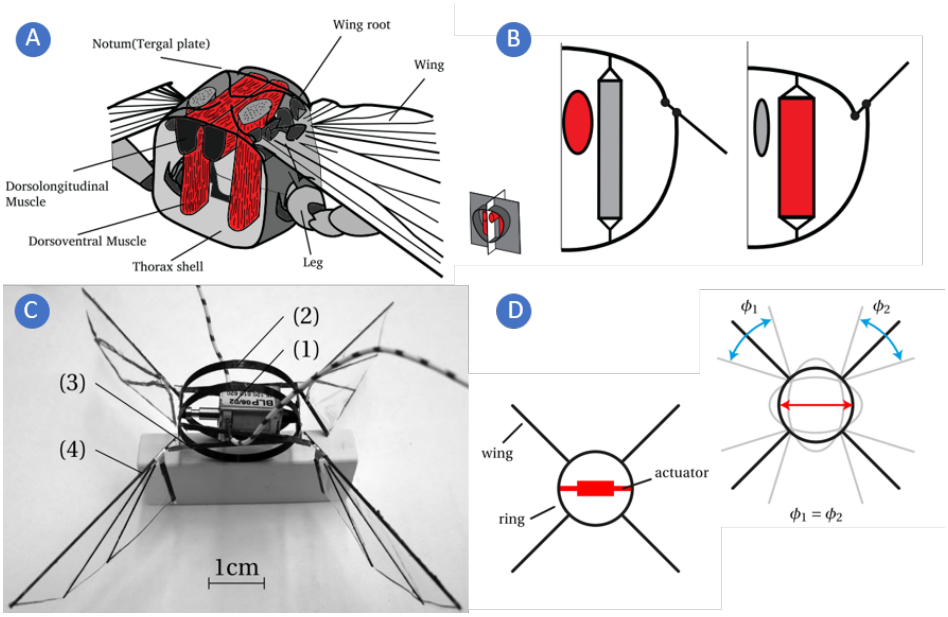

Figure 1-1: **A:** Cross-section of the thorax (body) of an insect from the order of the *Diptera*. Several parts are labeled but the important parts are coloured red; these are the two muscle groups that deform the thorax shell which in turn drives the wings via the wing root. **B:** Schematic representation of the thorax shell, muscles and wings of an insect. The muscles deform the shell pushing the wing up and down. **C:** The Atalanta FWMAV: (1) linear actuator, (2) deformable ring (similar to thorax shell), (3) amplification mechanism/wing driving mechanism, (4) wings. **D:** Simplified representation of how the Atalanta wings are actuated due to resonance of the system. Images **A** and **B** courtesy from Bolsman [1], **C** from Wang [2] and **D** from Peters [3].

alone hover, fly or perform aerial manoeuvres. These capabilities are important since research into topics such as aerodynamic modeling, attitude control, obstacle avoidance, antonymous flight etc. would be greatly aided if a fully functioning Atalanta drone was available.

Therefore the problem as intended to be solved within the bound of this thesis project is defined as follows:

The Atalanta FWMAV, as developed by the department of Precision and Microsystems Engineering from the University of Technology Delft, is not able to produce enough lift to compensate for its own weight.

1-3 Aim

The aim of this project is to increase the lift-to-mass ratio of the Atalanta. This can be achieved several ways which will be discussed in the next chapter. In general the aim can be described in three steps:

1. Map the current state of the Atalanta to identify critical improvement areas. These are components or systems of the Atalanta that when improved sufficiently, should yield a significant increase in lift performance.

2. Research possible improvements for these areas and single out the ones that are in line with the predetermined requirements.

3. Lastly implement the selected improvements and subsequently determine their success. This will also give an indication to what degree the initial problem of not being able to take off, was resolved.

1-4 Thesis structure and overview

Chapter 1 provides the backdrop to this report where the Atalanta is introduced and its problem is identified. The goal here is to define a starting point and an end point together with the stating the importance of making this journey.

Chapter 2 gives an overview of the current state of the Atalanta. This helps in narrowing the focus of this project. Four critical areas are presented and rated to indicate the one most suited in providing a solution to the problem. The conclusion of this chapter is that designing, fabricating and testing a theoretically optimal wing-system is the solution path with the highest potential.

Chapter 3 then shows the process and final solution of designing and fabricating the wing. To avoid confusion: the wing-system consists of a wing and a hinge that together form the wing-system. The wing is the flat, wing-shaped rigid plate that generates lift. The hinge is a compliant, 1 degree of freedom pivot hinge that allows for the pitching of the wing. Some wing-tests are performed to see if the final prototype meets the predefined requirements.

Chapter 4 is similar to chapter 3 in structure, but now the subject is the passive pitching hinge. Requirements for the design, fabrication and performance are defined and a final prototype is developed and tested.

Chapter 5 takes the results of the previous two chapters and combines them into a functioning wing-system. The entire manufacturing process is presented, together with the final prototype. Three tests are conducted for a qualitative assessment of the performance of the wing-system. Results of the tests conducted in chapters 3 to 5 are placed within their respective chapters.

Chapter 6 discusses the results of all tests. The goal here is to see whether the results are sensible, and if not, what the reason might be for the result not to be as expected.

Chapter 7 reflects on the entire project from the authors personal point of view. Results are judged in their entirety, not just their scientific outcome.

Chapter 8 concludes the report with some possible improvements that can be implemented in future work.

Chapter 2

Literature research

As of yet, the Atlanta doesn't produce enough lift to compensate for its own weight. In order to solve this problem - or at least get a step closer - there are four general paths: 1) reduce the mass of the drone, 2) increase the lift produced by the drone, 3) increase the efficiency of the system, and 4) a combination of all of the above. To determine what path(s) to take, this chapter provides a summarized state of the art of the Atalanta project which functions as a springboard into the actual project and narrows down its focus. For a more extended literature review, please read the authors dedicated literature survey [19].

2-1 Atalanta state of the art

The state of the art in this chapter dates to the time of Q4 2019. In order to get a birds-eye view of the Atalanta project, it is divided into multiple 'areas', shown in Figure 2-1. These areas can be components, sub-systems or even research activities. The figure gives a short summary of the current state of the area, a list of references to the bachelor/master/PhD projects that delve deeper into the area and a three-colour rating. (The three PhD reports are listed under references [1–3]; all BEP and master projects are listed under references [20–38]. Note that the BEP and master reports are not publicly available; for access contact Dr.ir. J.F.L. Goosen.) These ratings are important because they indicate whether an area is critical in achieving lift-off, how much work already has been done and how much there is left to do. All of this combined shows the best way forward.

The figure implies that a 🟢🟡🔴 rating points at the area with the highest potential within the bounds of this thesis project. 🟢🟡🔴 means that the area is a bit of a road-block in achieving lift-off, that there has been some successful work in the past but that it is not enough and that more knowledge is needed. Looking at the figure there are four areas that could be considered frontrunners: wings, actuator, fabrication and assembly, testing/experimental optimization. Each of these four area's will be looked at in more detail in the next section.

Area	Reference	A	B	C
Gearbox	[28]			
Bachelor project successfully produces a large-scale linear and rotational frequency divider				
Future work includes scaling down and testing on full FWMAV prototype				
Control	[3] [24] [25] [27] [32] [34] [38]			
Research done into a.o. control through variable structure stiffness, control using optic flow sensors and wing kinematic control through active hinges using electrostatics				
Scaling down components and reducing weight has to be done before integration into Atlanta drone				
Wings	[2] [26] [30]			
Extensive research has been done; optimal dimensions, mass distribution, operating frequency etc. are known				
Gathering relevant information for the realization of this optimal wing is not been done				
Thorax	[1] [33] [36] [37]			
Resonating rings coupled with an amplification mechanism proven to work				
Some research done on triangular velocity-position function for the wing using a torsional thorax structure				
Actuator	[22] [29] [31] [35]			
Linear electromagnetic actuator proven to work; mass, efficiency, energy density a.o. not optimized				
Significant progress made on the development of a chemical actuator; no prototype ready for implementation				
Fabrication and assembly	[23]			
Very limited information available on dimensions and fabrication method of body and wing-system				
Fabrication and assembly processes barely researched; optimization of both not done				
Simulation and modelling	[21]			
Extensive models available on almost all topics; simulator built to test viability of optic flow based control				
No model exists that outputs optimized design parameters for a full Atalanta				
Testing/experimental optimization	[20]			
Tests performed on first full Atalanta prototype; further tests done on (active) wings, chemical actuators, ...				

Figure 2-1: This table shows the different areas of the Atalanta project together with a short summary of their current status. References to the projects related to each area are listed in the column under **Reference**. Columns **A**-**C** are defined as follows. **A** shows the importance to achieving take-off, i.e. how critical this area is (■ = most critical). **B** shows the extent of successful implementation into the drone, i.e. how much work already has been done (■ = no successful implementation). **C** shows the amount of knowledge available indicating how much work there is left to do (■ = significant amount of work to do).

2-2 In-depths research into four focus areas

In this section each of the four areas is looked at in more detail. Each area contains an explanation of why the color rating as seen in fig. 2-1 is the way it is. The letters **A**, **B** and **C** refer to the columns containing the rating in fig. 2-1.

2-2-1 Wings

This area is concerned with everything wing-related before it is fabricated and assembled. In short it is set to determine what the optimal properties are of a wing custom made for the Atalanta drone. Think of shape, mass, mass distribution, operating frequency, hinge stiffness, generated lift, energy efficiency etc.

Rating

A ■ Wings are critical in achieving lift-off. Wings are the actual parts that generate the lift and if they are not operated the right way, their efficiency drops and with it the generated lift [2, 39]. Furthermore, if the energy efficiency is high, a less powerful actuator is required which reduces the mass of the drone. Since the mass of the actuator accounts for approximately 95% in the Bolsman prototype [1], reducing it would be a significant step forward.

B ■ The optimal properties for a rigid wing with a 1 DOF pitching hinge are known [2](see fig. 3-2). The reason why this rating is not green, is because the optimized wing does not include a design for the hinge and the mass distribution is not optimized.

C ■ As already implied, there is extensive information available on this topic. Further research is still needed on wings where the dedicated pitching hinge is replaced with a compliant wing structure, but this shouldn't be necessary in achieving lift-off.

2-2-2 Actuator

This area is concerned with the power source of the Atalanta. Originally a linear electromagnetic actuator (see fig. 1-1 C) was used, but research in this area is heavily geared towards chemical actuators for their superior power density [29].

Rating

A ■ The actuator is critical as well. As mentioned before, the total mass of the Atalanta is dominated by the actuator. Reducing its mass or increasing its power density would be significant steps towards achieving lift-off.

B ■ The successful implementation so far consists of a linear electromagnetic actuator that was able to drive the original prototype (see fig. 1-1 C) well enough to produce lift. Future work within the domain of this type of actuator, is to find or develop one that is lighter and/or has a higher power density. One day of research resulted in finding an actuator that could be an improvement over the old one (see fig. 2-2). No fully working, stand-alone, Atalanta-sized chemical actuator has been manufactured yet although it shouldn't take long as of now.

C ■ The reason for this yellow rating is that there is little information about the current linear electromagnetic actuator. Some basic properties were determined and an actuator was selected but no extensive optimization has been done. More research has been done on a chemical actuator but still not enough to produce a stand-alone prototype.

	A: Bolsman [1]	**B**: New [31]
Mass [g]	8.25	5.5
Power [W]	1.5	0.8
Power density [W/kg]	182	145
Input voltage [V]	12	3
Stroke [mm]	6	1-4
Dimensions [mm]	10x12.5x21.5	10x8x20

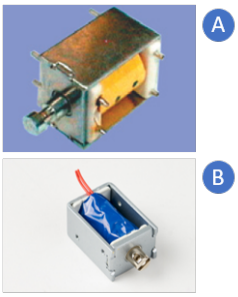

Figure 2-2: Comparison of the linear electromagnetic actuator used by Bolsman (**A**) in his original Atalanta prototype [1] and a new model (**B**,[4]) that could be an improvement if it meets the power requirements. An important feature is the mass reduction by 2.75 g.

2-2-3 Fabrication and assembly

This area is pretty self-explanatory: it is concerned with the fabrication of all Atalanta parts and their subsequent assembly. Bolsman predominantly fabricated and assembled his Atalanta prototype by hand, cutting parts with scissors and gluing them together. The only parts not fabricated using a cut-and-glue method were the 3D-printed body parts as shown in fig. 1-1 C.

Rating

A ■ This area is critical since the Atalanta's size fits right in-between two categories of fabrication methods [40]. Smaller drones are generally fabricated and assembled using methods such as Smart Composite Microstructures [7, 41–43] and MEMS [6, 44–47] because they require high precision. Larger drones [48, 49] are often fabricated using a method closer to cut-and-glue with tools like scissors, mills and laser cutters. Since the Atalanta is a compliant resonator, the mechanical properties of its parts like mass, size and stiffness are important; a fabrication or assembly error could influence its performance significantly.

B ■ This rating is yellow since a successful Atalanta was built but there is ample room for improvement. Due to fabrication and/or assembly errors, the wings on the original prototype did not show the same dynamic behaviour with respect to each other [1]. This influences their respective performance which can hurt the stable hovering capabilities of the drone.

C ■ This rating refers to the fact that there is almost no information or research on fabrication or assembly methods within the Atalanta project or even within similar projects in the rest of the world. There is a lot of work to do within this area.

2-2-4 Experimental optimization

This area is included since - although very useful - a significant amount of Atalanta projects have had a purely theoretical approach. The knowledge gained from these projects is necessary in moving forward, but without any experimental projects it is difficult to determine whether the knowledge would actually result in the intended real-life achievements. This area is included in order to get an overview of which theories are confirmed, and which still need some work.
Certain Atalanta projects had their own test setups and performed some form of experimental optimization, but since the original prototype in 2010 [1] there has been no project - to the authors knowledge - with the sole purpose of developing a new and improved, functioning Atalanta using experimental optimization. This seems necessary in achieving lift-off since the Atalanta is a complex system where multiple parameters have to be perfectly tuned.

Rating

A ■ As already indicated, this area is critical as well since the whole goal of the entire Atalanta project is to develop a FWMAV that is, first and foremost, able to hover and fly slowly and autonomously [1]. Without any actual testing of components, systems, theories etc. this does not seem possible.

B ■ There has been a lot of testing on a multitude of parts/systems/theories etc. The reason why this rating is yellow however, is because not all tests contribute to making the Atalanta fly as well as others. Experimental results on, for example, the subject of on-board navigation electronics are not going to get us closer to achieving lift-off at this point in time. There is still a need for experimental optimization on an updated version of a complete Atalanta drone.

C ■ This rating is green because throughout the years multiple test setups have been developed (see fig. 2-3 for some examples) that are able to measure the lift force of a wing, the total lift force produced by the Atalanta, the motion of a wing etc. [1, 2, 5, 20]. All of this combined should be sufficient in assessing the actual performance of an updated Atalanta drone.

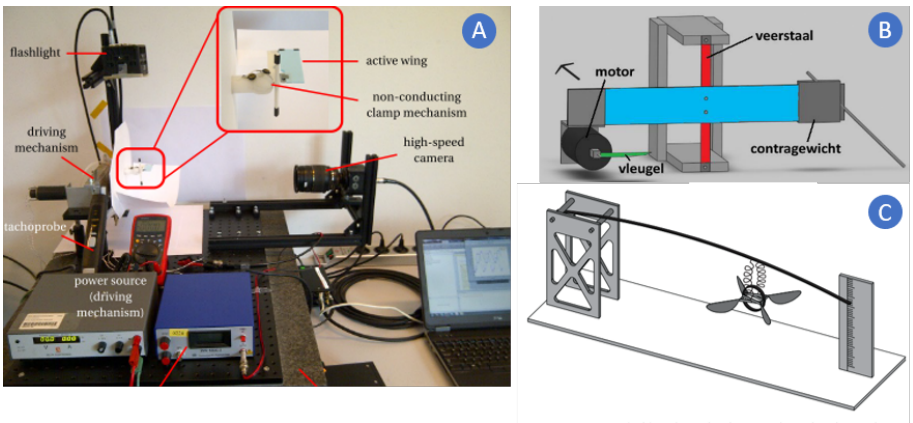

Figure 2-3: **A:** setup for flapping a wing-system and recording its movement [2]. **B:** setup for measuring the generated lift force per wing [5]. **C:** setup for measuring the total generated lift [1].

2-3 Thesis outset

With research in place on the Atalanta project in its entirety and the four focus areas in particular, a solution path for the remainder of this project has to be selected. This section aims to do that by combining all of the information in the previous two sections into a project with the purpose of making significant progress in achieving lift-off most effectively.

2-3-1 Solution paths and selection criteria

The paths as mentioned at the beginning of this chapter are: 1) reduce the mass of the drone, 2) increase the lift produced by the drone, 3) increase the efficiency of the system, and 4) a combination of all of the above. The selection criteria are: A) contribution to achieving lift-off, B) extent of successful implementation, and C) amount of work left to do.

2-3-2 Recap and solution path selection

The previous section can be summarized as follows:

Wings The properties of a theoretically optimal wing are known [2]. The only thing left to do is transform these properties into an actual design including a pitching hinge. This would increase the lift produced per wing compared the current wings [1].

Actuator Linear electromagnetic actuators are proven to work [1]. Finding or developing a new linear electromagnetic actuator with a lower mass but high enough power density would mean a significant step forward because the total mass of the drone would decrease.

Fabrication and assembly This is a critical step in achieving lift-off because to do so you need an actual drone. There is an abundance of work left to do in this area and it could lead to an increased efficiency of the system due to fewer fabrication and assembly errors.

Experimental optimization A lot of good setups for quantifying the performance of the drone and its sub-systems are available. What is left to do is supply these setups with improved components.

There is a way to combine all of these four areas into a project that reaps the benefits of all four. The idea is to design an actual wing conform the optimal properties, develop a new fabrication and assembly method for this wing, manufacture the new wing and subsequently test its performance using the already available setups. If successful this would result in a wing able to produce approximately 6.5 times more lift compared to the current wing [1, 2]. Because this - now real - optimal wing is only able to produce its lift if the system driving it is tuned perfectly, this would mean that the efficiency of the drone would increase. In turn, this would mean that a less powerful and less heavy actuator would be required when compared to the less efficient system developed by Bolsman [1].

The following chapters will work out this idea and evaluate it with respect to the overall goal of getting closer to achieving lift-off of the Atalanta FWMAV from the University of Technology Delft.

Chapter 3

Wing

The previous chapter provided a path forward for the remaining chapters. This would be the design, manufacturing and testing of a new and improved wing-system. To, once more, clarify the terminology: a wing-system is the combination of a wing (the rigid plate that generates lift) and the hinge (the part that allows passive pitching). These two parts are worked out individually in chapter 3 and chapter 4 before being combined in chapter 5.

3-1 Research

This section provides some background information on the Atalanta wing-system in its current form. This will function as a baseline to which the new wing-system will be compared. Some research into wings of similar projects is also presented from which inspiration is drawn.

3-1-1 Current Atalanta wing; the baseline

Casper Bolsman during his PhD designed, manufactured and tested the wing as shown in fig. 3-1. He was the first to do so and his work included some mechanical and aerodynamic modelling and optimization of the chord length at different positions along the length of the wing [1]. He manufactured the wing using a cut-and-glue method.

Each wing could produce about 0.225 g of lift with a total of 0.9 g for four wings. Because the total mass of the Atalanta was approximately 8 g, the wings did not succeed in making the Atalanta take off. Bolsman lists some improvements with respect to the wings at the end of his thesis:

- A more complex wing design has to be developed, optimizing all wing parameters
- There is need for a more accurate aerodynamic model combined with a tunable mechanical model

- Reducing the number of components by better integration of various individual parts is recommended

- Exploration of different manufacturing techniques such as rapid prototyping is required to simplify the design and realization cycle

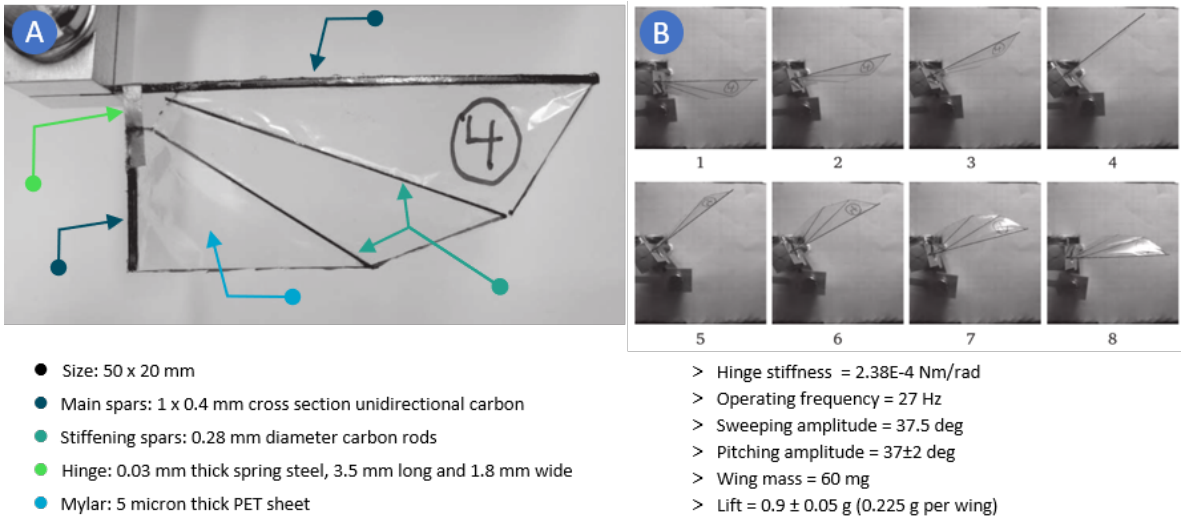

Figure 3-1: A: single wing developed by Bolsman [1] with all parts highlighted by coloured arrows. **B:** first eight frames of a full sweep, captured with a high-speed camera. All main performance parameters are listed as well.

3-1-2 The theoretically optimal Atalanta wing

After Bolsman, another PhD candidate joined the project: Qi Wang. His contribution, among others, was to optimize the shape and the pitching axis of the wing (both shown in fig. 3-2) which can save up to 33 % of power during hovering flight compared to traditional wings used in most FWMAVs [2]. This improvement should result in a higher lift force and energy efficiency compared to Bolsman's wing.

Wang did this by developing a quasi-steady aerodynamic model including four aerodynamic loading terms. This model is proven to accurately predict the aerodynamic force and torque acting on a wing during its flapping cycle. Compared to quasi-steady models, this model does not rely on empirical parameters which improves its predictive capability allowing for a comprehensive optimization of the shape and kinematics of flapping wings [2].

In short: the developed optimization algorithm provides the optimal shape, pitching axis, required power, pitching angle, flapping frequency and wing motion (sweeping and pitching angles) for a range of required lift and for two cross sections. The constraints are the mass and maximum dimensions.

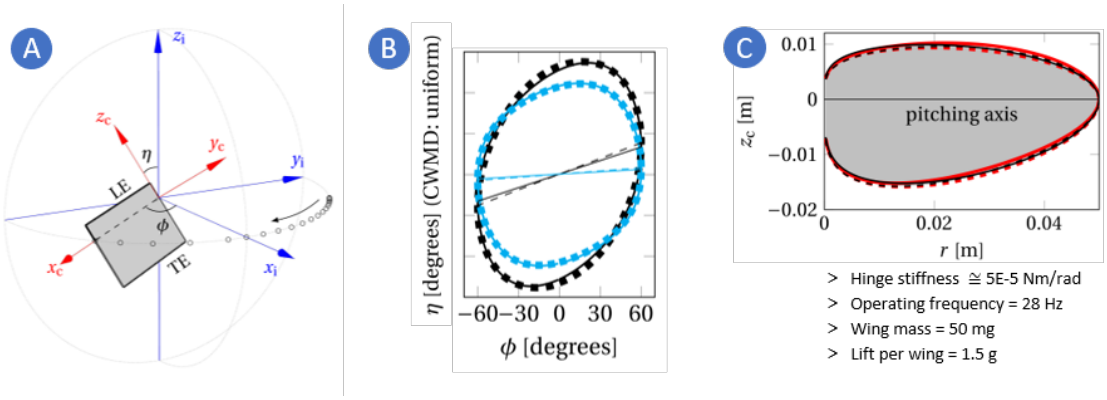

Figure 3-2: Overview of optimized Atalanta wing as developed by Wang [2]. **A:** wing before optimization with its sweeping and pitching angle indicated by ϕ and η respectively. 'LE' stands for leading edge, 'TE' for trailing edge. The wing pitches around the x axis of the co-rotating frame c. The pitching hinge is imaginary and located in the origin of the fixed frame i. **B:** Graph of the optimal kinematics of the optimized wing, expressed in the sweeping and pitching angles. **C:** optimized wing shape and pitching axis. Some important parameters are also listed. Note that the hinge stiffness, operating frequency, generated lift etc. are all linked. If one changes, all other parameters change. The listed values are "average" or typical values so to say.

3-1-3 Wing fabrication and assembly methods

Within the Atalanta project there is extensive knowledge on the optimal wing shape, kinematics etc.; but there is little knowledge on wing fabrication. In this section, four commonly used wing fabrication methods as seen in other FWMAV projects are presented. The goal is to assess their usefulness for the Atalanta within the bounds of this thesis project.

- **Cut-and-glue** This method is generally used for FWMAVs with wings larger than 9 cm [40]. At this scale the influence of fabrication and assembly errors resulting from the usage of simple tools and jigs is less significant. An advantage of using this method is its low cost. The Microbat form Caltech University [50] is a project where the wings consisted of carbon rods and Mylar film glued together by hand (similar to Bolsman [1]). Their assessment of this process is that the glue makes it difficult to produce identical wings, making the study of design variables and their affect on the performance ineffective and inefficient [51].
- **Micro-electromechanical Systems** This method is used in the past to produce wings with a length of 3 cm [6] and 15 cm [52] making it quite versatile. This process generally includes the deposition of thin film of material followed by a curing step. Next a pattern is created in the material, for example, by etching. After this the whole process can be repeated creating a 3D-structure consisting of multiple layers of different materials, each with a specific 2D shape. MEMS allows for the fabrication of precise and consistent wings with complex geometries. Disadvantages can be having to perform multiple, complex steps and the relatively low turn-around time. A project that used this method is the OVMI from the University of Valenciennes [6].
- **Smart Composite Microstructures** This technique is a novel and innovative one. First proposed by Wood et al. [42], this method addresses the void when it comes to

mesoscale manufacturing [8]. Here material layers are bulk laser-micromachined and laminated together by using adhesives in a monolithic, planar fashion. From a planer configuration, the structures can acquire their 3D shape by folding [41] in different directions similarly to a pop-up book. This process yields small-scale structures of high precision where multiple parts can be integrated and made at once. The RoboBee from Harvard university [8] and the piezo MAV from Carnegie Mellon university [53] were created using this method. This technique is mainly beneficial at the scale of about 5 cm.

- **Additive manufacturing** 3D-printing is often used to describe the process of material extrusion where material is dispensed through a nozzle in layers; but this is just one example of an additive manufacturing technique. Jaffar-Bandjee et al. [54] list seven additive manufacturing techniques, their resolutions, advantages/disadvantages and their ability of printing multiple materials. Goh et al. [55] similarly discuss additive manufacturing but on a somewhat broader scope, namely with respect to unmanned aerial vehicles. They praise additive manufacturing for its agile nature enabling rapid production without the need for major changes in the manufacturing setup. A project that uses this method is the mechanical insect (see fig. 3-3) from Cornell university [9]. They mention the benefit of being able to produce a prototype in a matter of minutes. Some disadvantages of additive manufacturing [55] are: limited choice of high performance materials, anisotropic material properties, manufacturing-induced porosity, ill defined mechanical properties of AM parts, small build volume and high cost per unit for large amounts of products.

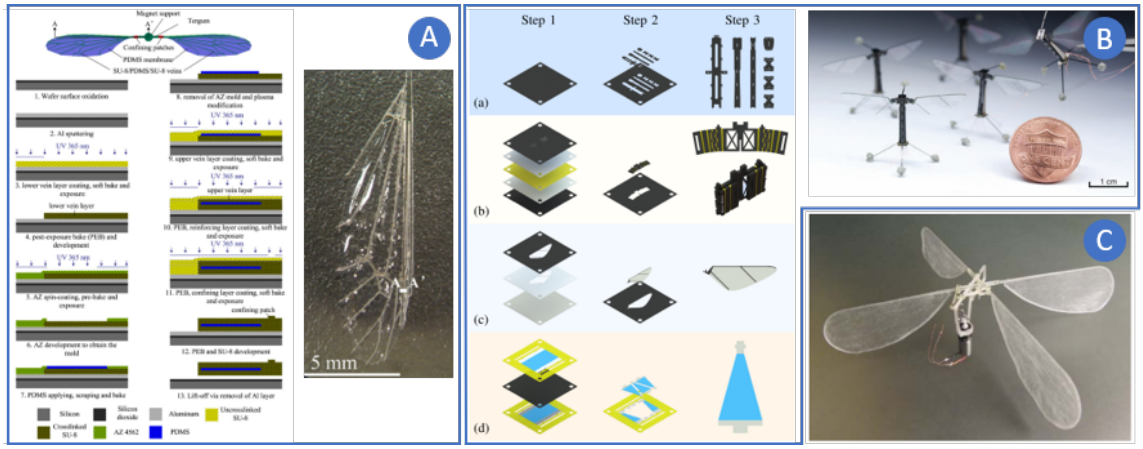

Figure 3-3: **A:** illustration of a MEMS fabrication method used to fabricate wings [6]. **B:** illustration of the SCM fabrication method [7] as used for the Harvard RoboBee [8]. **C:** 3D-printed FWMAV [9].

3-2 Requirements

Before designing and manufacturing the wing, some requirements should be defined that guide the engineering choices made during this process. These requirements are split up into three categories and are based on the information provided in the previous two sections.

3-2-1 Design

- The shape of the wing has to be equal to optimized shape [2], see fig. 3-2 B. This shape will increase the lift generated by each wing and will require less power to operate.
- The mass of the wing has to be as low as possible because this lowers the total mass of the Atalanta, which in turn will require less lift to be generated.
- The materials used to fabricate the wing should be relatively easy to come by. This will allow a shorter turn-around time which leaves more time for design iterations.
- Since Wang's optimized wing did not account for a passive pitching hinge, the new wing should accommodate such a hinge. This integration should be as elegant as possible, minimizing its effect on the shape and dimensions of the wing.

3-2-2 Fabrication and assembly

- Consistency between multiple wings has to be maximized. This means that random fabrication and assembly errors should be minimized. The result will be that different wings will have close to identical performances which will benefit uncontrolled, stable hovering of the Atalanta.
- The fabrication and assembly process should be flexible. This means that the process can accommodate design changes relatively easily without needing to overhaul the manufacturing process. Experimental optimization and testing will be more effective this way since implementing new ideas into the design will be quicker.
- The tools required for the fabrication and assembly process should be readily available. Preferably the tools are owned by the PME department since this means easy access and full control.
- The tools used during the fabrication and assembly process should be able to produce fine features and produce them consistently; meaning: the resolution and precision of the tools should be high enough.

3-2-3 Performance

- The wing has to have mechanical properties as close to a rigid plate as possible. This is the assumption made by Wang [2] and will deliver the best performance. Any unwanted deformation of the wing may lead to parasitic motion which influences the wing's performance negatively.

3-3 The actual wing

3-3-1 Fabrication and assembly

The requirements for the fabrication and assembly process are more constricting compared to the design or performance requirements. Hence the choice for a certain fabrication and assembly method is made first.

Of the four options as described in section 3-1-3, MEMS is the only one not implemented during this project. The Atalanta wings are 5 cm long and don't have very intricate features so the fine precision and small scale benefits of a MEMS approach are not needed. Additionally, the process consists of more complex and time-consuming steps compared to the other three fabrication options.

3D-printing, cut-and-glue and SCM are implemented; also in that chronological order. An overview of this "evolutionary" process can be seen in fig. 3-4 where the time axis is horizontal and is pointed to the right. Below, these three fabrication methods are worked out in more detail.

3D-printing (see fig. 3-4 B)

Since additive manufacturing is a potential fabrication method for the Atalanta wings, the first 3D-printed wing (fig. 3-4 A, top wing) was made mimicking the shape and structure of the baseline wing (fig. 3-4 A). No hinge was included in this design because the main objective was to determine if 3D-printing was a viable option.

The printer used for this experiment is the Prusa i3 MK3S with PLA material. The process was relatively simple and consisted of two steps. First a Mylar sheet would be taped to the printing bed and then the structure would be printed on top of it. Due to the heat in the extruded PLA, the material would stick to the Mylar. After completion, the wing would be cut out from the surrounding Mylar. This simple, initial test was successful so two more wings were printed having a more complex shape and vein structure (fig. 3-4 B, bottom two wings).

Although 3D-printing is a very easy and flexible method, it doesn't fulfil all the requirements listed in section 3-2. The smaller features of the wing are too fine for the printer and the consistency between wings is not good enough. Additionally, the adhesion of the Mylar to the PLA is not durable enough; the Mylar would come loose if the wing was not picked up carefully enough. 3D-printing should still be possible but it would require optimization of the printer settings and materials for a start.

Cut-and-glue (see fig. 3-4 C)

This method was researched for two reasons: 1) to get a better feeling of the optimal wing shape in combination with the passive pitching hinge, and 2) to get an indication of whether or not the cut-and-glue method would be a viable fabrication and assembly method of the wing.

The wings were made by tracing the optimal wing shape onto a styrofoam sheet and cutting it out with scissors. The pitching axis is indicated by the blue line running across the length of the wing. The hinges were made by cutting strips of carbon steel and glueing them to multiple pieces of carbon strips. The first two wings have a hinge with just a single piece of steel; the third wing uses two strips in order to reduce the torsional deflection of the wing at the ends of its sweeping motion. The fourth wing uses four steel strips in order to get a symmetrical distribution of carbon around the pitching axis.

As can be expected, using scissors and glue to manually manufacture wings doesn't result in consistent wings. The process is very tedious and is prone to a lot of small errors. Bolsman [1] mentions these flaws when discussing why his wings did not all perform identically. Although this method does not satisfy all the requirements, it did provide a lot of knowledge on the passive pitching hinge. When analysing the motion of these cut-and-glue wings, it was apparent that the hinges functioned as if they had two or even three degrees of freedom. The angular bending stiffness needed for the passive pitching motion is very low (on the order of $10^{-5}\,\mathrm{N\,m\,rad^{-1}}$). To obtain this stiffness using carbon steel, the dimensions had to be very small; this resulted in a low torsional stiffness which is not preferred. The hinge would torsion at the end of the sweeping stroke and thus have a larger sweeping angle than intended. As a result of the bending and torsion, a slight heaving motion was also observed. All of this makes the motion of the wing unpredictable and chaotic. This in turn results in additional forces acting on the hinge structure which can cause it to fail.

Smart Composite Mircrostructures (SCM, see fig. 3-4 D)

This method, in its simplest form, has the following steps: 1) cut custom 2D shapes into multiple sheets of different materials including two-sided adhesive layers, and 2) stack them using certain alignment features. Figure 3-4 D shows two columns. The first represents figuring out the right feature sizes, hinge placement and design, laser cutter settings, adhesive selection, testing the assembly method and more. The second column shows four fully assembled wing-systems after the fabrication and assembly processes were optimized.

Considering all the research and results of different fabrication methods, SCM was ultimately selected for this project. The fabrication and assembly processes satisfy the requirements mentioned in the previous section. The designs cut into every sheet can be changed easily using any 3D-CAD software. This makes the process flexible, allowing design changes without overhauling the fabrication and assembly process. All sheets are cut using the same high resolution laser cutter meaning that random fabrication errors are less likely to occur. Systematic errors can still occur but if the laser cutter is calibrated and its precision is high enough the number of systematic errors can be reduced.

3-3-2 Design

This subsection is concerned with the actual design of the wing which consists of four parts: 1) the overall shape, 2) the stiffening spars, 3) the hinge support structure, and 4) the width of the carbon parts.

Overall shape

The selection of the shape is fairly straightforward. The shape is taken from the results presented in the PhD report of Qi Wang [2]. This shape will give the wing its optimal performance within the context of the Atalanta project which is exactly what is required for this thesis project. The shape is traced and implemented into a Solidworks file.

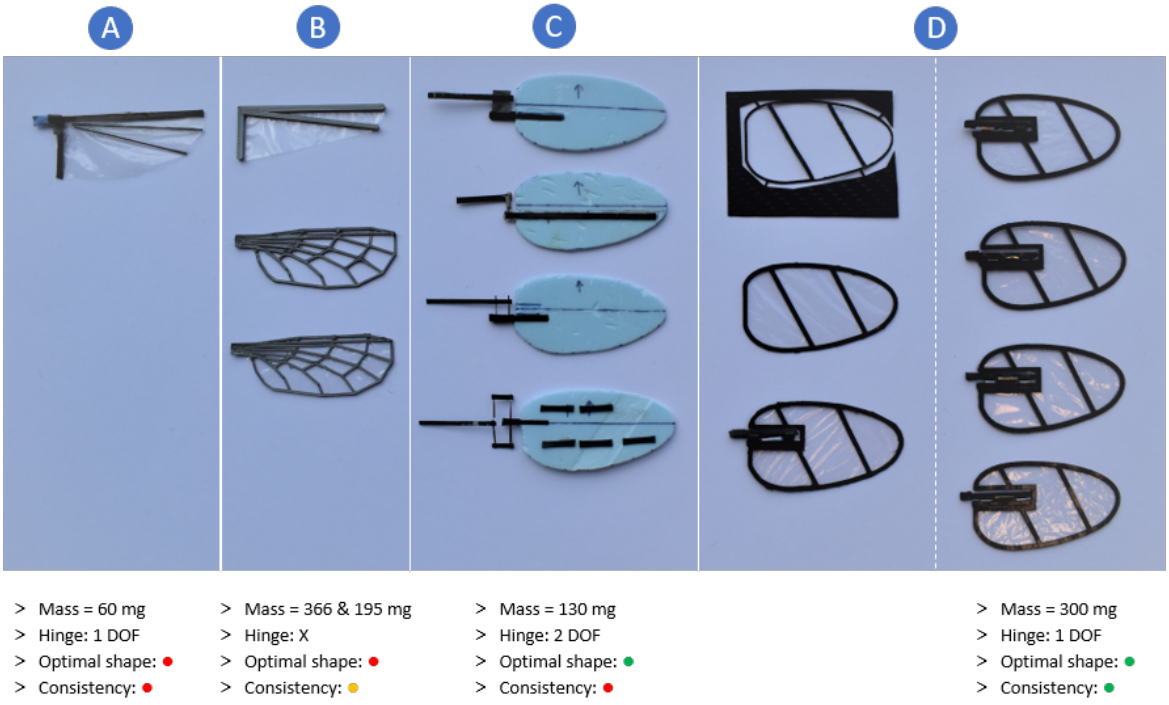

Figure 3-4: "Evolution" of the wing-system from left to right. The mass and hinge functionality of each wing is provided. The hinge functionality is defined as the degrees of freedom (DOF) it has. The 'Optimal shape' refers to whether or not the wing is shaped according to the optimized shape [2]. 'Consistency' indicates how consistent the dimensions and functionality are of multiple wing-systems fabricated using the same method. **A:** cut-and-glue wing-system developed by Bolsman [1]. This wing is regarded as the baseline for this project. **B:** 3D-printed wings. These wings don't have a pitching hinge. **C:** cut-and-glue wings with different external pitching hinge configurations. The hinges are considered as two DOF systems since their torsional stiffness is too low compared to the bending stiffness. This means the wings extend beyond their maximum sweeping amplitude, which is undesirable. **D:** wing-systems fabricated using the SCM method.

Stiffening spars

The stiffening spars (blue boxes in fig. 3-5) are the two diagonal bars that run form the top of the wing to the bottom. In theory, the wing has to be a rigid plate. These spars don't accomplish that but get close enough. Adding more material can increase the stiffness but also increases the mass of the wing which is not preferred so there is a balance to be struck. For this project the required wing stiffness is not calculated; the maximum allowable mass of the wing is unknown as well. Future work would have to include these criteria and a topology optimization should be performed to optimize the material placement. For the wings fabricated during this project the spars are placed somewhat randomly.

Hinge support structure

As will be explained in more detail in chapter 4, the hinge is placed within the wing. This means that the hinge support structure (red box in fig. 3-5) has to be incorporated into the structure of the wing. The placement of the hinge support structure is determined by the

length of the hinge and the location of the pitching axis. The shape of the structure allows the hinge to be attached to the wing and allows the adhesive to still stick to the wing without overlapping the hinge.

Width of carbon parts

The width of all the carbon parts is 1.7 mm except for the bottom part of the hinge support structure; the width there is two times 1.7 mm (i.e. 3.4 mm) to make sure the hinge and adhesive layer do not overlap. These values are not optimized analytically. Smaller widths have been tested (see fig. 3-4 D, rectangular sheet) but if the width became too small, the structure would become very fragile and the structure would warp due to the heat of the laser. At 1.7 mm the structure seemed stiff and strong enough and no warping occurred.

3-3-3 Final result

The result of the work described above can be seen in fig. 3-5. The image shows a wing still connected with small tabs to its support material. The sheet is a 0.3 mm thick piece of cured 0°/90° carbon, acquired at Conrad [56]. The different features are highlighted in red, blue and green. More information on the adhesive layer, the Mylar and the assembly in chapter 5.

The Photonics Industries DCH-355-3 diode-pumped solid-state laser from the department of Precision and Microsystems Engineering was used for cutting this and all other parts. The diode current was set to 5.0 A and the cutting speed to 120 $\mathrm{m\,s^{-1}}$. 5 drills were used, spaced 0.02 mm apart (drilling step). 4 levels were used with a Z-step of −0.1 mm. All cuts were repeated 3 times. Cutting this carbon sheet with these settings takes 12:53 minutes.

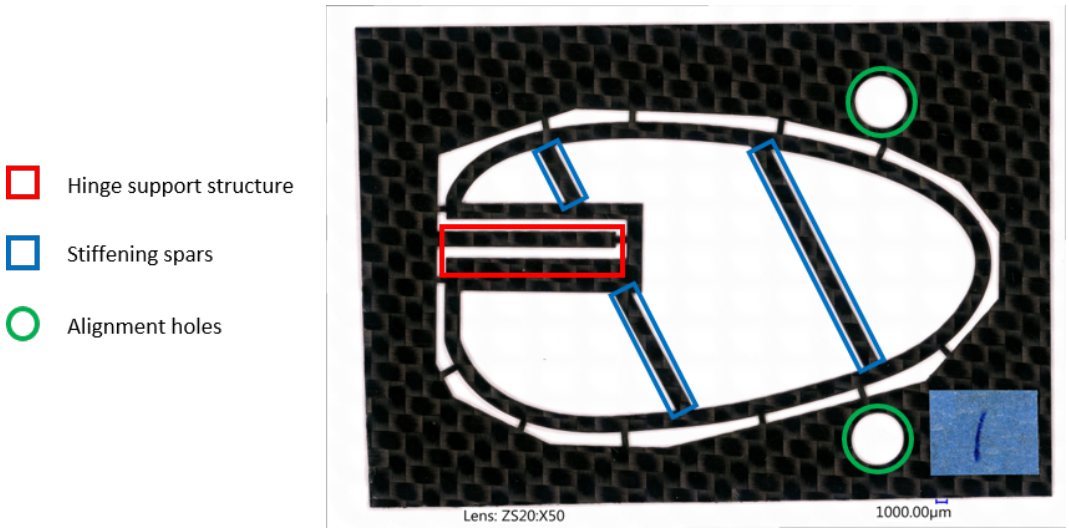

Figure 3-5: Carbon wing sheet with the hinge support structure, stiffening spars and alignment holes indicated in red, blue and green respectively. Note that this wing sheet is not the final wing design. For the actual final design, the hinge was moved a bit further into the wing (see fig. 5-2).

3-4 Testing

Of all the requirements mentioned in section 3-2 that are applicable to the fabrication and assembly of the wing-section of the wing-system, two could be tested. These two requirements are that the wing should mimic a rigid plate, and that dimensions and shape of multiple wings should be consistent. No values are attached to these requirements since this project is more qualitative in nature than quantitative. The results in this project are meant to indicate whether or not the ideas and designs put forward have potential; a proof-of-concept so to speak.

The rigid-plate requirement is not tested in this project because there was no time to do so. However, visual inspection of the slow motion footage of a wing during its sweeping motion doesn't show any significant wing structure deformation due to bending or torsion. This indicates that, within the bounds of this project, the wing structure can be assumed to be stiff enough. The second requirement is tested and the results are shown in the section below.

3-4-1 Shape and dimensional analysis

For this test, four wing structures were fabricated as described above; the first of these wings is shown in fig. 5-2. Next, four features were selected to be measured (indicated by numbers [1]-[4] in fig. 3-6). These four features are:

1. Width of the bottom part of the hinge support structure
2. Width of vertical straight bar at the base of the wing
3. Width of the first diagonal stiffening spar
4. Wingspan of the wing

For each wing, four photos were made using the VHX6000 digital microscope to measure the four features mentioned above. For feature [1] an image of the full carbon sheet at 50X magnification was made. Because this could not be done at once, an automatic stitching feature was performed putting multiple images together resulting in the image seen in fig. 3-6. The features [2], [3] and [4] were all photographed separately with a 200X magnification. The magnification for these images is higher because the feature size is smaller and a higher magnification allows for more precise measurements.

The features were measured using the measuring tools available within the microscope software. When drawing a line on the image, the software would know the length of this line. This measuring tool was not calibrated by the author.

Since the measurements were made by drawing a straight line between two points on a digital image using a computer mouse, the results include a measuring error, i.e. a "visual, clicking error". In an effort to improve the results, each measurement was performed ten times. To clarify: in total 160 measurements were made (4 wings with each 4 features that were each measured 10 times; $4 \cdot 4 \cdot 10 = 160$).

Figure 3-6 shows the results of this test. Wing number one is shown with the four features indicated by the red lines and the numbers [1]-[4]. The numbers on the left show the results

for each of the four features per wing. Each result shows two values: 1) the median of all ten measurements for each feature, and 2) the standard deviation between all ten measurements. The bold value next to the feature number is the distance when measured digitally in the 3D-CAD model, i.e. the distance the feature should be.

[1] Supposed to be: 3.4 mm
Wing 1: 3.1726 ± 0.0040667 mm
Wing 2: 3.1258 ± 0.092896 mm
Wing 3: 3.1465 ± 0.006971 mm
Wing 4: 3.1364 ± 0.0052842 mm

[2] Supposed to be: 1.7 mm
Wing 1: 1.4733 ± 0.004176 mm
Wing 2: 1.4726 ± 0.0023064 mm
Wing 3: 1.472 ± 0.0021176 mm
Wing 4: 1.476 ± 0.0020137 mm

[3] Supposed to be: 1.7 mm
Wing 1: 1.4598 ± 0.0061101 mm
Wing 2: 1.4698 ± 0.0038367 mm
Wing 3: 1.4655 ± 0.0020393 mm
Wing 4: 1.4678 ± 0.0036331 mm

[4] Supposed to be: 53.89
Wing 1: 51.7938 ± 0.0045078 mm
Wing 2: 52.5991 ± 0.0086402 mm
Wing 3: 52.5785 ± 0.0033561 mm
Wing 4: 52.5915 ± 0.00583 mm

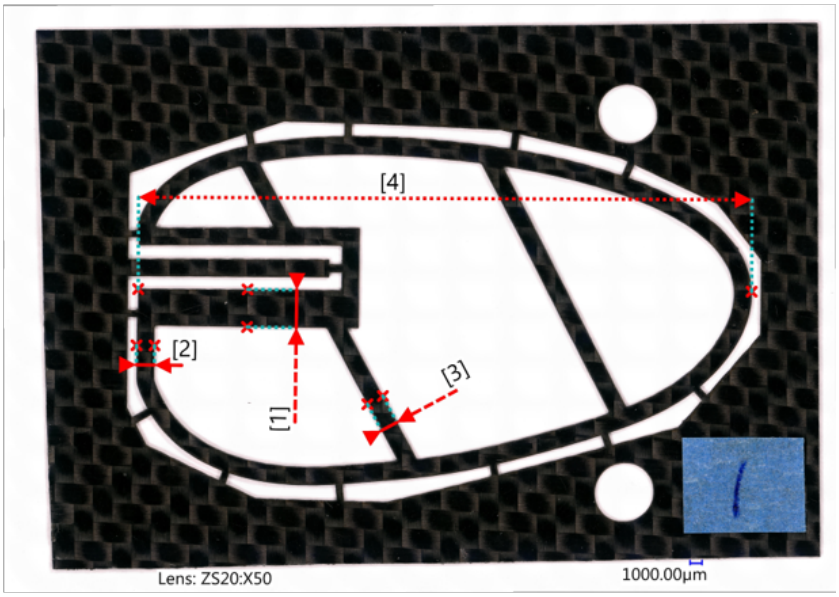

Figure 3-6: Wing number one of four that was tested. The test consisted of measuring four feature sizes and comparing them to their digital value. The four measured features are labelled [1]-[4] and shown in the image with red arrow lines. The data on the left shows the test results per feature, per wing.

Chapter 4

Hinge

This chapter works out the passive pitching hinge prior to it being integrated into the wing described in the previous chapter. The pitching motion of a wing is - in this project - defined as the rotation about the local x-axis of the wing (see fig. 3-2 A). This pitching is necessary for the wing to produce its lift and within the Atalanta project this is done passively. This means that the pitching motion is a result of the interplay between the inertia of the wing, its motion and the aerodynamic forces acting on the wing. All of this is in equilibrium with the angular stiffness of the hinge that allows for this motion. In this chapter the requirements for such a hinge are defined, some literature is presented, a hinge design is selected, manufactured and lastly tested.

4-1 Requirements

The requirements for the hinge are similar in certain ways to the requirements of the wing; but there are some differences. Note also that these requirements are not meant to be hard constraints, they are guidelines. The aim of this project is to find a design and manufacturing process for the wings that has potential. Quantifying exactly how successful the ideas presented in this thesis are with respect to a fully functioning Atalanta drone is difficult and outside the scope of this project. That is why, for example, the mass requirement states that the mass should be minimized, not below a certain value.

4-1-1 Design

- The dimensions of the hinge have to be relatively small. An original requirement for the entire drone was for the Atalanta to be small [1]; a compact hinge is in line with that requirement.
- The mass of the hinge has to be as low as possible to keep the mass of Atalanta to a minimum.

- The materials used to fabricate the hinge should be relatively easy to come by. This will allow a shorter turn-around time which leaves more time for design iterations.
- The integration of the hinge with the wing should be as elegant as possible, minimizing its effect on the shape and dimensions of the wing.

4-1-2 Fabrication and assembly

- Consistency between multiple wing-systems has to be maximized. This means that random fabrication and assembly errors should be minimized. The result will be that different wing-systems will have close to identical performances which will benefit uncontrolled, stable hovering of the Atalanta.
- The fabrication and assembly process should be flexible. This means that the process can accommodate design changes relatively easily without needing to overhaul the manufacturing process. Experimental optimization and testing will be more effective this way since implementing new ideas into the design will be quicker.
- The tools required for the fabrication and assembly process should be readily available. Preferably the tools are owned by the PME department since this means easy access and full control.
- The tools used during the fabrication and assembly process should be able to produce fine features and produce them consistently; meaning: the resolution and precision of the tools should be high enough.

4-1-3 Performance

- The angular hinge stiffness around the x-axis should be in the order of $10^{-5}\,\mathrm{N\,m\,rad^{-1}}$ [2].
- The stiffness of the hinge for the other five degrees of freedom should be at least 150 times [57] higher compared to the pitching stiffness. This makes sure that the hinge operates as a single DOF system and thus reduces the parasitic motion of the wing.

4-2 Research

4-2-1 Perfect pitching stiffness

The theoretically optimal wing as described in section 3-1-2, has an optimized angular pitching hinge stiffness. This value depends on many parameters, so to recap: for a wing with the shape as shown in fig. 3-2 C (red line), a mass of 50 mg, a kite profile for the chord-wise mass distribution [2], a required lift production of 1.5 g and using the kinetic energy recovery system (KERS, a.k.a: the thorax structure resonating at its natural frequency), the angular stiffness of the passive pitching hinge should be $4.2 \times 10^{-5}\,\mathrm{N\,m\,rad^{-1}}$.

Now, as is clear from the previous chapter, the wing designed for this project is different from the theoretically optimal wing. The wing in this project doesn't have a kite profile cross section, doesn't have a uniform mass distribution, the mass is higher and the wing shape is not fully closed (i.e. the hinge is incorporated into the wing instead of being outside the wing). All of this means that the perfect hinge stiffness for the actual wing is different from the $4.2 \times 10^{-5}\,\mathrm{N\,m\,rad^{-1}}$. Calculating what the hinge stiffness should be would require implementing the new design into the optimizer developed by Wang [2] and running it; this is outside the scope of the project. Doing this is not even necessary since the question is not *"What is the perfect hinge stiffness?"*, but *"Is it possible to design and manufacture a hinge that could have the perfect hinge stiffness if it was known?"*.

Thus, within the bounds of this project, the perfect hinge can be described as follows: the design is simple and compact, its angular pitching stiffness is in the order of $10^{-5}\,\mathrm{N\,m\,rad^{-1}}$, the other five stiffnesses are significantly higher making the hinge a 1 DOF system, the hinge is made using easily available materials and tools and the consistency between multiple hinges is maximized. It goes without saying that the hinge should be a compliant hinge since the Atalanta's kinetic energy recovery system only works if the entire Atalanta can be seen as a compliant mechanism.

4-2-2 Compliant hinges

Machekposhti et al. [10] list 26 compliant revolute joints and analyses them in a normalized manner so different hinge concepts can be compared to each other. All 26 hinges are categorized according to their flexure type but for this project the second part of the analysis is more valuable. In the second part, most of the hinges are given values for their respective range of motion, axis drift, on-axis stiffness and off-axis stiffness. This analysis is perfect since it allows for the selection of the best hinge based on its performance and whether or not it is sufficient for the Atalanta project.

Looking at the available data, a hinge concept with potential is defined as follows:

- The range of motion should be large enough. The maximum pitching angle for a wing with optimal kinematics is about 40° (40° one way so 80° in total). In this case the threshold is set at 0.5 rad which is 28.6° but note that the actual dimensions and materials of the hinge can be changed to increase the range of motion.
- The on-axis stiffness has to be as low as possible so it can reach $10^{-5}\,\mathrm{N\,m\,rad^{-1}}$ with certain dimensional and material changes. The lowest on-axis stiffness presented is $2.7 \times 10^{-3}\,\mathrm{N\,m\,rad^{-1}}$.
- The off-axis stiffness should be large compared to the on-axis stiffness (a factor of at least 150 [57]). Especially the torsional stiffness (around the local z-axis, seefig. 3-2) should be 150 times larger.

Of the 26 options, six hinge concepts pass the test (see fig. 4-1). It should be said that the data for some hinges is not present [10], so the choice is not airtight.

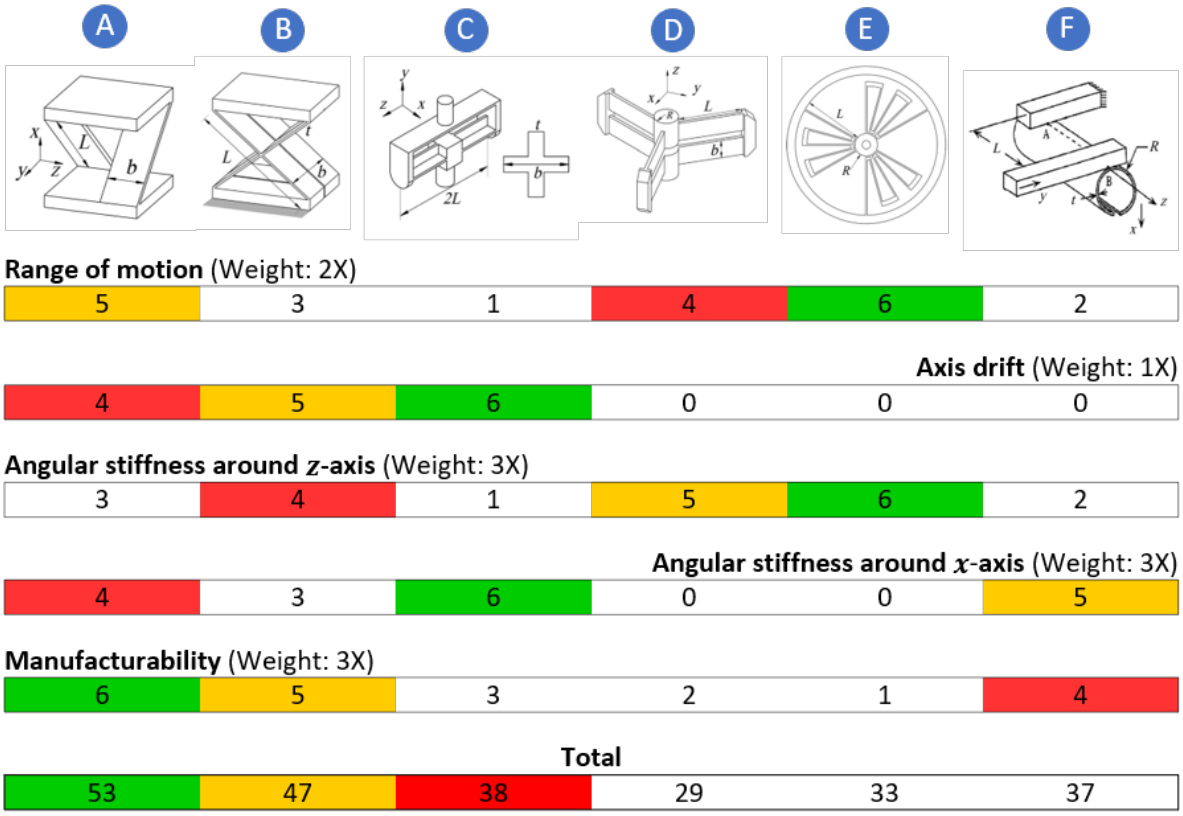

Figure 4-1: This figure shows six compliant, pivot hinges: Cross axis (**A**), X2 (**B**), CR-1 (**C**), CR-3 (**D**), Multileaf (**E**), Split-tube (**F**). Each hinge is rated for its performance on a scale of 1-6 with 6 being the best score (the colors indicate the top three hinges in each category). A 0 score means that no data was available. Every performance category has a weight factor that is multiplied with the performance score. The final ranking is shown at the bottom.

4-2-3 Hinge selection

With six frontrunners, one new selection criteria is added to better determine the best hinge concept. This criteria has to do with how easy the hinge can be fabricated and integrated into the wing design. An overview of the six hinges and their scores with respect to the five selection criteria can be seen in fig. 4-1. It is clear from the figure that the cross axis hinge is the best option for the Atalanta project. Its stiffness around x over the stiffness around z ratio is 267. This satisfies the requirement and promises a 1 DOF hinge. Note that the cross axis hinge would have the highest score even if all weight factors are set to one, and also if the rows with zeros (axis drift and stiffness around x) would not be counted.

The data for the cross axis hinge as presented in [10] is based on: $b = 4\,\text{mm}$, $L = 20\,\text{mm}$, $t = 0.15\,\text{mm}$, $\phi = 45°$, $E = 70\,\text{GPa}$, $\nu = 0.33$, $S_y = 440\,\text{MPa}$ (high strength aluminium wrought alloy EN AW 2024).

The equation used to calculate the angular stiffness around the compliant axis is the following:

$$k = \frac{E \cdot w \cdot t^3}{12 \cdot L} = \frac{E \cdot (2 \cdot b) \cdot t^3}{12 \cdot L} \quad \frac{Nm}{rad} \tag{4-1}$$

For the data mentioned above, this equation yields $k = 7.9 \times 10^{-3}\,\mathrm{N\,m\,rad^{-1}}$ which is two orders of magnitude higher than what this project aims for. But if the input parameters are changed to $b = 7\,\mathrm{mm}$, $E = 210\,\mathrm{GPa}$ (carbon spring steel), $t = 0.01\,\mathrm{mm}$ and $L = 10\,\mathrm{mm}$ the stiffness yields $k = 2.45 \times 10^{-5}\,\mathrm{N\,m\,rad^{-1}}$. This means that obtaining a stiffness of the order $10^{-5}\,\mathrm{N\,m\,rad^{-1}}$ is possible in theory.

The range of motion is also sufficient since with the original design parameters the range of motion was 1.676 rad which corresponds to 96° which is more than enough. Lastly, the cross-axis hinge also seems to be the easiest to fabricate and incorporate into the wing compared to the other five.

4-2-4 Three-piece cross axis hinge

With the cross axis hinge selected as the compliant pivot hinge to be used for this project, the details need to be worked out. One more conceptual design change is implemented based on the research conducted by Tielen et al. [58]. Instead of using two leaf flexures, three are used in a double X-shape (see fig. 4-2).

A standard cross axis hinge (fig. 4-2 A) has non-diagonal stiffness values in its stiffness matrix. Due to symmetry in the three-piece cross axis hinge (fig. 4-2 B), the non-diagonal stiffness terms for the forces in the z and y directions (see fig. 4-2 C) are eliminated. This should result in less parasitic motion when the hinge is operated. It is important to have a clean motion of the wing and adding this symmetry should help accomplish that. The three-piece hinge does increase the pitching stiffness by a factor two compared to the two-piece, but as is demonstrated earlier, the design parameters still allow the hinge to have the required pitching stiffness. Plus, the three-piece hinge also increases the stiffnesses in other directions which is beneficial.

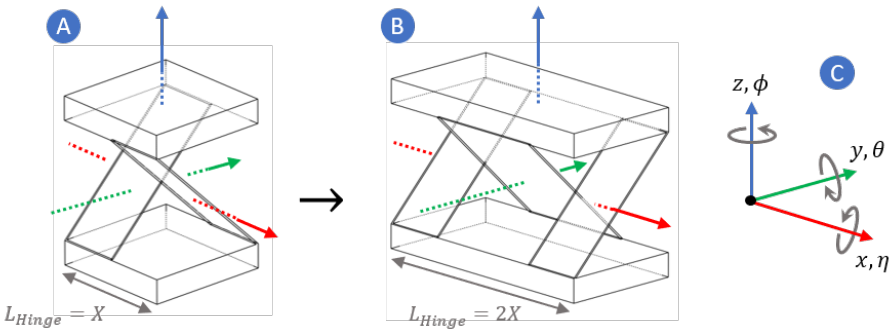

Figure 4-2: **A:** schematic representation of a two-piece, cross axis pivot hinge. The width of both leaf flexures is identical and is half the length of the base (x) if there is no gap between the leaf flexures. **B:** three-piece cross axis pivot hinge. This configuration is obtained by mirroring the two-piece hinge which is why the length of the base is twice as long (2x). The width of the middle leaf flexure is twice the width of the outer leaf flexures. **C:** coordinate system that is used by Wang [2] (see fig. 3-2) and is adopted in this thesis project. Pitching of the wing (η) happens around the red/x axis, sweeping (ϕ) of the wing happens around the blue/z axis. Note that this coordinate system is different from the one used by Machekposhti et al. [10] (see fig. 4-1 A).

4-3 Design

With the three-piece, cross axis, compliant pivot hinge selected as the concept of choice, this section provides the detailed design. The two most important characteristics of the hinge are its angular bending stiffness and its dimensions. The stiffness is linked to the performance of the wing-system, and the dimensions determine how neatly the hinge integrates into the wing.

4-3-1 Design parameters

For the stiffness, eq. (4-2) and eq. (4-3) are used [58]. Equation (4-2) shows the applied load, which is equal to a certain stiffness multiplied by a certain deflection of the hinge; eq. (4-3) shows the actual stiffness equations. Note that Tielen et al. [58] use a different coordinate system so the force and moment loads below don't follow a standard x, y, z pattern. The equations below are applicable to the coordinate system as presented in fig. 4-2 C. Also note that w in all equations is the length of the entire hinge, or in other words, the width of all leaf flexures added up. L and t are the length and thickness of a single leaf flexure.

$$\begin{bmatrix} F_z \\ F_y \\ F_x \\ M_\phi \\ M_\theta \\ M_\eta \end{bmatrix} = \begin{bmatrix} k_{F_z,z} & 0 & 0 & 0 & 0 & 0 \\ 0 & k_{F_y,y} & 0 & 0 & 0 & 0 \\ 0 & 0 & k_{F_x,x} & 0 & 0 & 0 \\ 0 & 0 & 0 & k_{M_\phi,\phi} & k_{M_\phi,\theta} & 0 \\ 0 & 0 & 0 & k_{M_\theta,\phi} & k_{M_\theta,\theta} & 0 \\ 0 & 0 & 0 & 0 & 0 & k_{M_\eta,\eta} \end{bmatrix} \cdot \begin{bmatrix} \Delta_z \\ \Delta_y \\ \Delta_x \\ \Delta_\phi \\ \Delta_\theta \\ \Delta_\eta \end{bmatrix} \tag{4-2}$$

$$\begin{aligned} k_{F_z,z} &= \frac{Ewt}{2L} + \frac{Ewt^3}{2L^3} & k_{M_\phi,\phi} &= \frac{5Ew^3t}{768L} + \frac{9Ew^3t^3}{128L^3} + \frac{Ewt^3}{12L(\nu+1)} \\ k_{F_y,y} &= \frac{Ewt}{2L} + \frac{Ewt^3}{2L^3} & k_{M_\theta,\theta} &= \frac{59Ew^3t}{768L} + \frac{Ewt^3}{12L(\nu+1)} \\ k_{F_x,x} &= \frac{5Ew^3t}{32L^3} & k_{M_\eta,\eta} &= \frac{Ewt^3}{12L} \\ k_{M_\theta,\phi} &= \frac{Ew^3t}{256L} & k_{M_\phi,\theta} &= \frac{Ew^3t}{256L} \end{aligned} \tag{4-3}$$

The requirements state that the materials and tools to fabricate the hinge should be easily available. The material available is carbon steel with a thickness of 0.01 mm. This material has a Young's modulus of 210 GPa and paissons ratio of 0.33. This means that the width (w) and the length (L) are the two variables left.

4-3-2 Final design

The final design and dimensions can be seen in fig. 4-3. There are multiple options for w and L that all result in the right functionality of the hinge. But since L is a function

of the width of the hinge (w_{Hinge} in fig. 4-3 C), and the width of the hinge equals three carbon layers (each with a thickness of 0.3 mm), the length of the leaf flexures equals 1.27 mm ($L = \sqrt{{w_{Hinge}}^2 + {h_{Hinge}}^2} = \sqrt{2 \cdot (0.9 \times 10^{-3})^2} = 1.27 \times 10^{-3}$ m). With this, w is selected to be 14 mm which is the addition of w_1, w_2 and w_3 (see fig. 4-3 B). This combination of L and w should give the hinge an angular pitching stiffness of:

$$k_{M_\eta,\eta} = \frac{Ewt^3}{12L} = \frac{210 \times 10^9 \cdot 14 \times 10^{-3} \cdot (0.01 \times 10^{-3})^3}{12 \cdot 1.27 \times 10^{-3}} = 1.9249 \times 10^{-4} \quad \frac{Nm}{rad} \tag{4-4}$$

Note that the stiffness is not in the order of 10^{-5} N m rad^{-1} which is one of the requirements. When designing the hinge, the width of the hinge (w in eq. (4-4)) was thought to be the width of the middle leaf flexure (7 mm). This factor two increases the hinge stiffness to a value of the order 10^{-5} N m rad^{-1}. This error can, for example, be corrected for by halving the width of each leaf flexure.

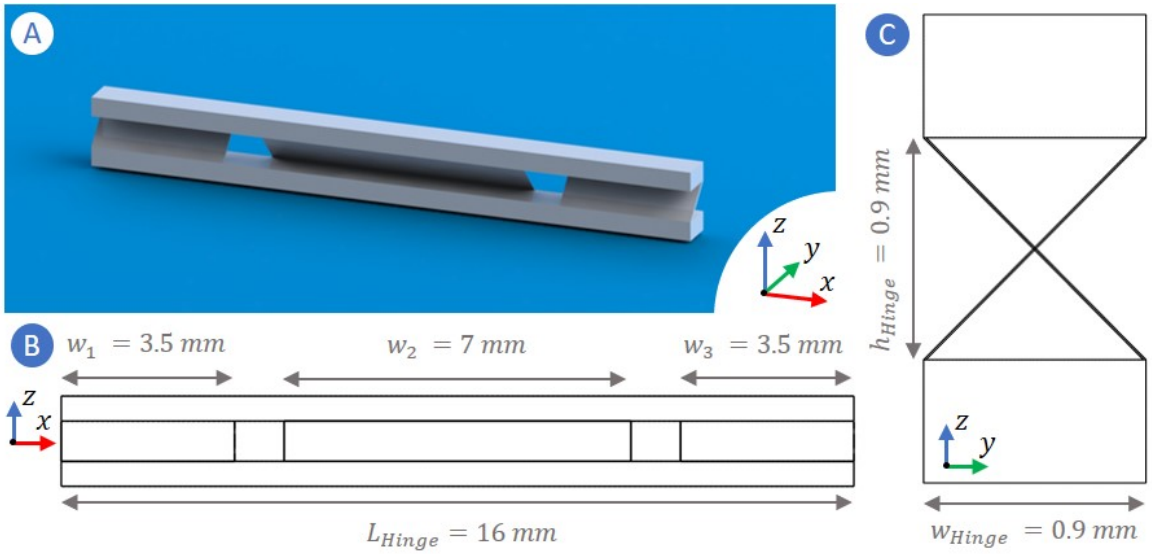

Figure 4-3: Overview of the final design of the three-piece, cross axis pivot hinge. **A:** rendering of the hinge with its coordinate system in the bottom right. **B:** side view of the hinge with the dimensions of the flexures and the length of the hinge. The spacing between the flexures is 1 mm. **C:** front view of the hinge. The X-shape is square which gives each flexure a length of 1.27 mm. The thickness of all flexures is 0.01 mm.

4-4 Realisation

The hinge basically consists of three individual leaf flexures with parallel edges, cut to the right width. The flexures are made from a rolled-up, 12.7 mm wide and 5 m long piece of carbon steel. Since the width of all three flexures added up is at least 14 mm, the three hinges cannot be made from a single strip of steel.

To fabricate these three flexures, initially the same laser cutter was used that cut all the wing parts. The flexures are very thin and warp easily when heat is applied which is what

happened when the laser cutter was used. A number of tests (see fig. 4-4) were performed to find the optimal laser cutter settings but none was found. The laser either didn't cut through the material (fig. 4-4 A) or it cut through the material while warping and burning it (fig. 4-4 B, C). The best result (fig. 4-4 D) had no smooth edges, was slightly warped and took 32 minutes to cut.

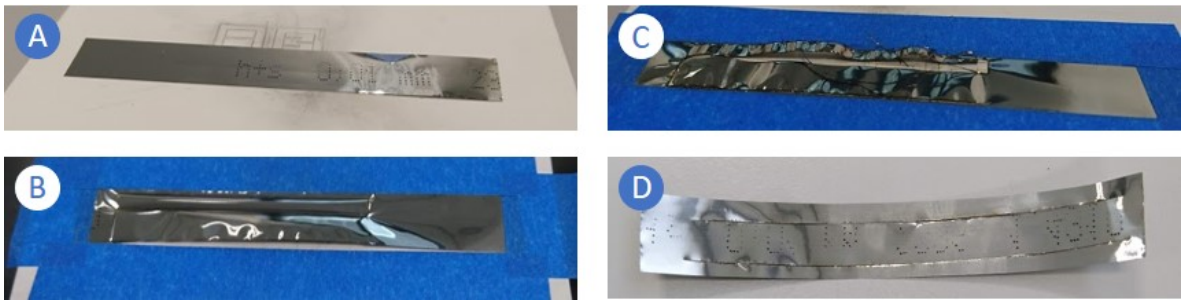

Figure 4-4: Some results from experimenting with the laser as a tool for fabricating the leaf flexures. The cutting times are as follows: 00:03 min (**A**), 00:57 min (**B**), 03:15 min (**C**), 32:15 min (**D**).

Cutting the steel with either scissors or a scalpel is relatively easy so the second approach in fabricating the leaf flexures was a more 'cut-and-glue' method. A metal jig was laser cut with gaps equal to the width of the flexures. This jig was then clamped to a hard surface with a piece of steel in between. Using a scalpel, the flexures were then cut out.

This method isn't perfect as well. Some known problems are:

- The cutting is less consistent because the angle of the scalpel with respect to the material can vary significantly.
- The width of the flexure depends on the width of the gap in the metal jig. If this jig is improperly made, this directly translates to a poor fabrication of the flexure.
- Cutting the steel using a scalpel results in 'waves' forming along the cut edges; more on this in chapter 6.
- Cutting the steel with a scalpel results in the steel curling slightly. The axis around which the steel curls is orthogonal to the cutting direction and parallel to the cutting surface.

The fabrication of the leaf flexures is certainly not optimized and can be improved significantly. Some suggestions are made in chapter 8.

4-5 Testing

4-5-1 Hinge angular stiffness test

The idea

Since the angular stiffness of the hinge is closely related to the performance of the wing, its value should ideally match the intended value. The theoretical value, as calculated using

eq. (4-4), is $1.9249 \times 10^{-4}\,\mathrm{N\,m\,rad^{-1}}$. This 'Stiffness test' should determine how close the actual stiffness is to the theoretical stiffness.

The simplest way to measure the actual stiffness of a hinge is to apply a known load and measure the angular deflection. The applied moment can be a known mass at a known distance from the axis of rotation:

$$k_{M_\eta,\eta} = \frac{M_\eta}{\Delta_\eta} = \frac{F \cdot R}{\Delta_\eta} = \frac{m \cdot g \cdot R}{\Delta_\eta} \quad \frac{Nm}{rad} \tag{4-5}$$

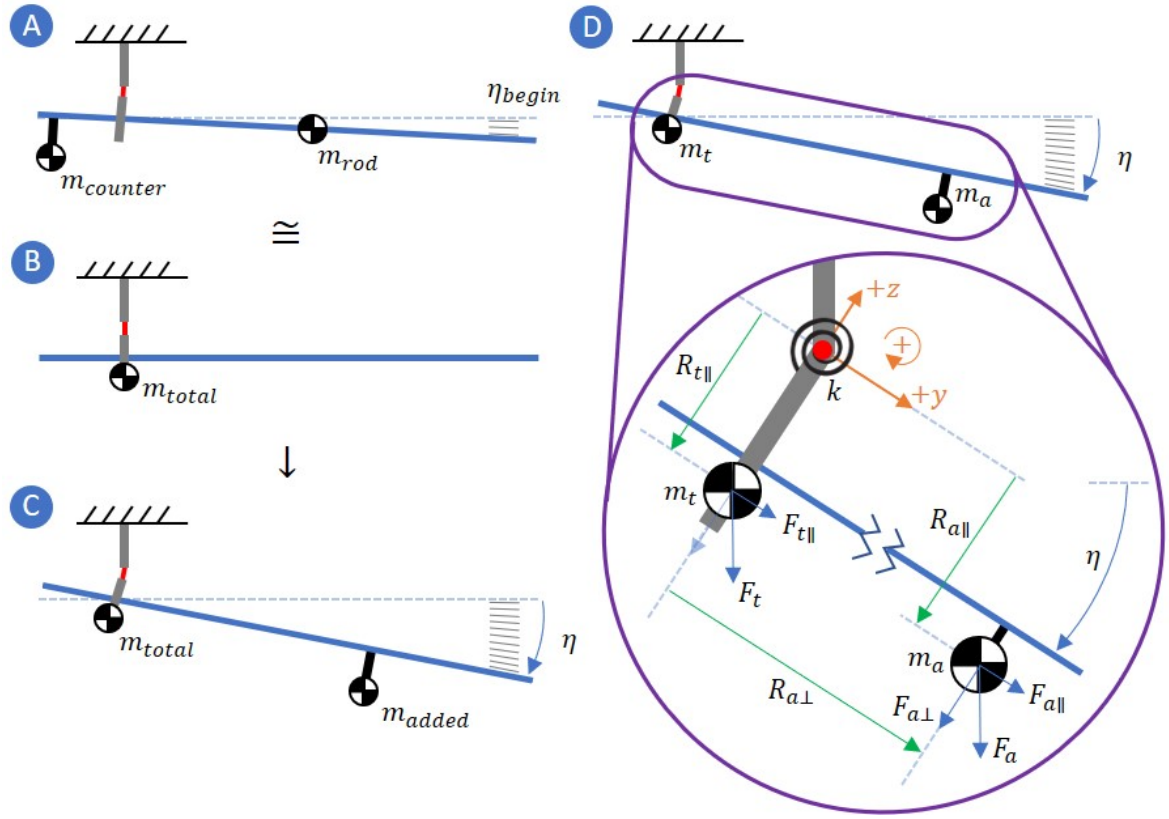

Figure 4-5: Schematic representation of the stiffness test. **A:** start of the experiment where M_η is not applied yet. The two masses in the system are the counter mass ($m_{counter}$) and the mass of the rod (m_{rod}). η_{begin} is the pitching angle before applying the load and is meant to be as close to $0°$ as possible. The counter mass can be moved along the rod to accomplish this. **B:** resulting model with a single mass (m_{total}). **C:** deflection angle η as a result of applying the mass (m_{added}). **D:** mechanical model of the hinge with all forces and distances added in. The hinge is assumed to function as a torsional spring; this assumption is discussed in chapter 6.

Figure 4-5 shows the general idea of the test. The hinge is fabricated and clamped in to the "ceiling". A rod (blue line in fig. 4-5) goes through the bottom part of the hinge and has a center of mass m_{rod} located to the right of the hinge. A counter mass $m_{counter}$ is located to the left of the hinge. The counter mass can be moved along the rod; this is done to make sure that η_{begin} is close to $0°$ as possible. Now the model can be changed to virtually having a single mass located under the hinge. This means the center of mass of the rod doesn't need to be determined. Now a third mass is added: m_{added}. This mass is known and its distance

to the hinge is known. This gives us the moment it induces on the hinge. As a result, the rod rotates clockwise and is displaced by a certain angle η.

Two corrections have to be included in the equations:

1. When the rod rotates (fig. 4-5 D), force F_a doesn't rotate with it since it is a gravitational force. F_a can be decomposed into two forces which each contribute to the moment applied to the hinge.
2. Since m_t is located a distance $R_{t\|}$ under the effective axis of rotation of the hinge, when the rod rotates, m_t drifts a bit to the left of the hinge creating a counter moment. This moment should be subtracted from the moment applied by m_a in order to calculate M_h which is the moment acting on the hinge.

Based on fig. 4-5 D, the actual pitching stiffness of the hinge can be calculated as follows:

$$\begin{aligned} k_{M_\eta,\eta} &= \frac{M_\eta}{\Delta_\eta} \cong \frac{-(M_a + M_t)}{\eta} \\ &= \frac{-(F_{t\|} \cdot -R_{t\|}) - \Big[(-F_{a\perp} \cdot R_{a\perp}) + (F_{a\|} \cdot R_{a\|})\Big]}{\eta} \quad \frac{Nm}{rad} \\ &with \\ F_{t\|} &= F_t \cdot sin(\eta) = [(m_{rod} + m_{counter}) \cdot g] \cdot sin(\eta) \quad N \\ F_{a\perp} &= F_a \cdot cos(\eta) = (m_{added} \cdot g) \cdot cos(\eta) \quad N \\ F_{a\|} &= F_a \cdot sin(\eta) = (m_{added} \cdot g) \cdot sin(\eta) \quad N \end{aligned} \tag{4-6}$$

The parameters that need to be measured are: added mass (m_a), mass of the rod (m_r), counter mass (m_c), distances ($R_{t\|}$), ($R_{a\perp}$), ($R_{a\|}$) and of course the angle of deflection (η).

The hinge holder assembly can be seen in fig. 4-6. The hinge holder consists of five carbon plates each with a thickness of 0.3 mm. Three plates are glued together using super glue; the two holes at the top function as alignment features. When the three plates are joined, the three flexures are installed using the 'hinge-holder alignment sheet' (see fig. 5-1). Now the two remaining carbon plates are glued to the main body in order to hold the flexures in place. When this is all done, the small tab just below the two alignment holes is cut through. This is to separate the top and bottom parts of the hinge holder; the two parts are now solely held together by the three flexures. The single hole at the bottom is used to hold the rod.

The setup used for this test can be seen in fig. 4-7. In Solidworks, a schematic was drawn up with all the angular deflection marks; this schematic was printed onto an A3-sized paper and taped to a carbon plate. The marks go from 0° to 30° with increments of 0.1°. The rod consists of two parts: a long piece of M2 threaded aluminium, and a strip of 2 by 4 mm carbon. At the tip of the rod, a small piece of carbon strip is glued orthogonal to the rod to make measuring the deflection easier. The counter weight is a block of aluminium that holds its orientation with respect to the rod when the rod rotates. The added mass on the right of the hinge is a resistor clamped in between two bolts. This item was used because it was small enough and could be hanged on to the rod. The resistor also retains its orientation with respect to the rod when the rod rotates.

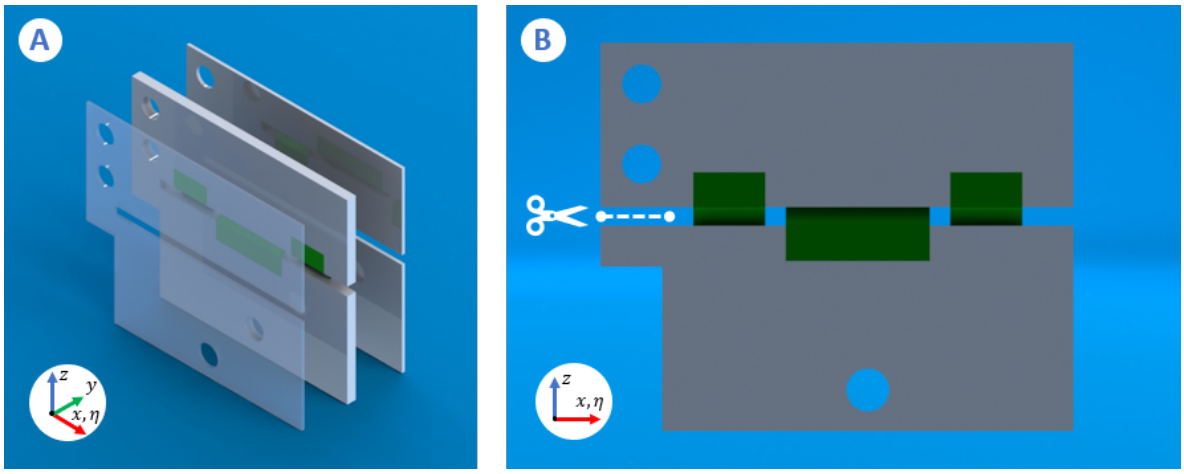

Figure 4-6: Hinge holder assembly used for measuring the angular pitching stiffness of the hinge. **A:** exploded view of the assembly with the first carbon plate made transparent. The leaf flexures are coloured green for better visibility. The assembly consists of five carbon plates glued together: the middle three give the flexures the right configuration, the outside two keep the flexures in place. **B:** side view of the assembly. The tab connecting the top and bottom parts together, is cut away (white, dashed line). The top two holes are used to align the plates; the bottom hole holds the rod (see fig. 4-5 and fig. 4-7).

The test

The stiffness test actually consists of two smaller tests, each performed three different ways, and all of that done for four separate hinges. This makes a total of 24 measurements ($2\ tests \cdot 3\ variations \cdot 4\ hinges = 24$). All six tests performed on each hinge are illustrated in fig. 4-8.

The two types of tests are:

1. **T1:** measuring the angular deflection for three different positions R_{1-3} of the same added mass (m_a). For an increasing R, the deflection is expected to increase as well.

2. **T2:** measuring the angular deflection for three different masses m_{a1-3}. Again, for a larger mass the deflection should be larger as well.

One general thing to be observed in the results is that the stiffness should be higher for larger deflections because the hinge stiffness is non-linear. In the equations in this chapter the hinge is assumed to be linear but this is merely an assumption to simplify the equations. In other words: the measured stiffness should be higher for larger rotations with respect to a hinge in its rest position, i.e. no rotation at all. The results of all the tests are shown in fig. 4-9.

One thing that becomes immediately clear from the results is that the overall average stiffnesses of the four hinges is $5.3540 \times 10^{-3}\,\mathrm{N\,m\,rad^{-1}}$. The designed theoretical stiffness is $1.9249 \times 10^{-4}\,\mathrm{N\,m\,rad^{-1}}$ which means that there is a difference in stiffness of a factor 27.8; let's say 28. The possible reasons for this mismatch are discussed in chapter 6.

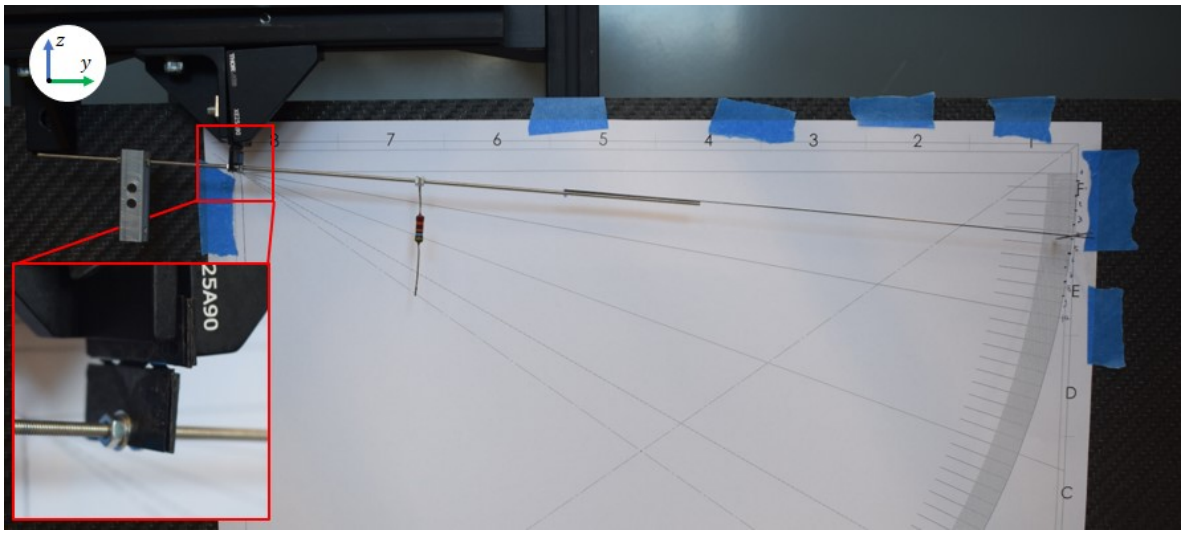

Figure 4-7: Test setup for measuring the angular pitching stiffness of the hinge. The aluminium block on the left is the counter mass (m_c); the resistor on the right is the added mass (m_a).

4-5-2 Hinge configuration test

This test aims to check whether the alignment of the flexures within their carbon hinge assembly is correct. If a flexure is not aligned properly, it can increase the effective length and/or width of the hinge, which in turn can change its effective stiffness.

Each of the four hinges was photographed using a Keyence VHX-6000 digital microscope [59] using a 30X magnification. Subsequently, two parameters were measured for each hinge: 1) the angle between a flexure and the carbon plate (this should be 90°), and 2) the distance between the top and bottom parts of the hinge assembly (this should be 0.9 mm, see fig. 4-3). These measurements were taken using the measurement software that comes with the VHX-6000 microscope. Using that software, it is possible to select multiple points on the image and determine the angle/distance/etc. between them. Because this is a visual measurement prone to human error, and the carbon/flexure edges are not perfectly straight/parallel, the results may not be exactly true. The results are purely meant to indicate to what order of magnitude the parameters differ from their theoretical value. The results for all four hinges are: the angle ranges from 90.5 to 92.5°; the gap ranges from 0.77 to 1.05 mm. The results are discussed in chapter 6.

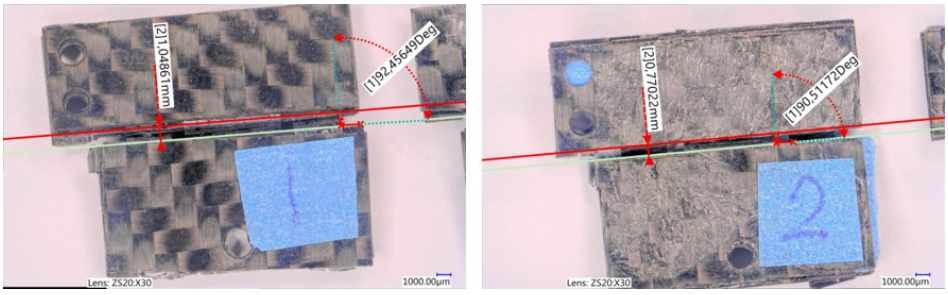

Figure 4-10: Images of two of the four hinge assemblies. The gap between the top and bottom part is measured, as well as the angle between a flexure and the carbon.

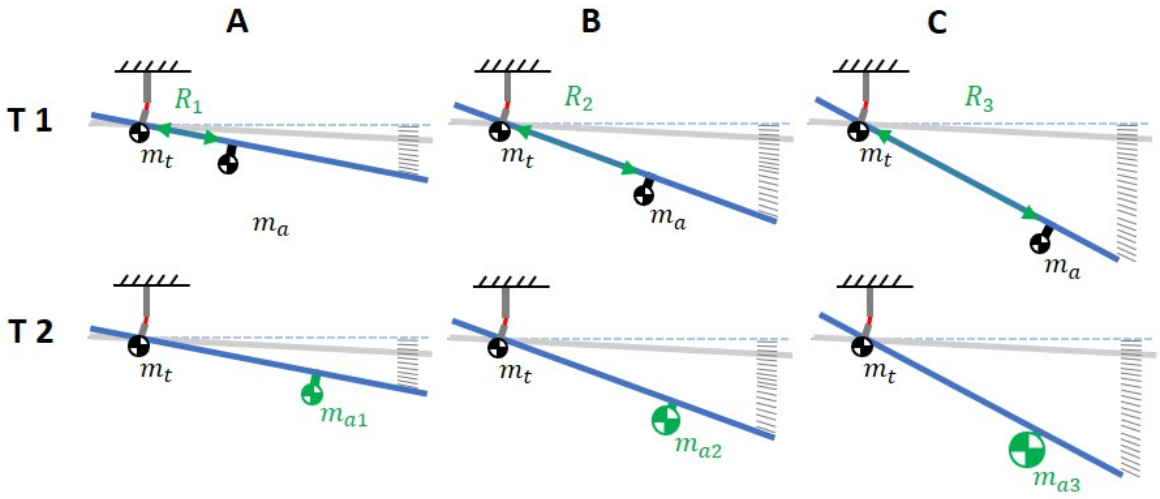

Figure 4-8: Schematic representation of all six tests performed for each of four hinges. **T1** and **T2** represent tests 1 and 2. Categories **A** through **C** represent the three variations on each test with the moment load increasing from **A** to **C**.

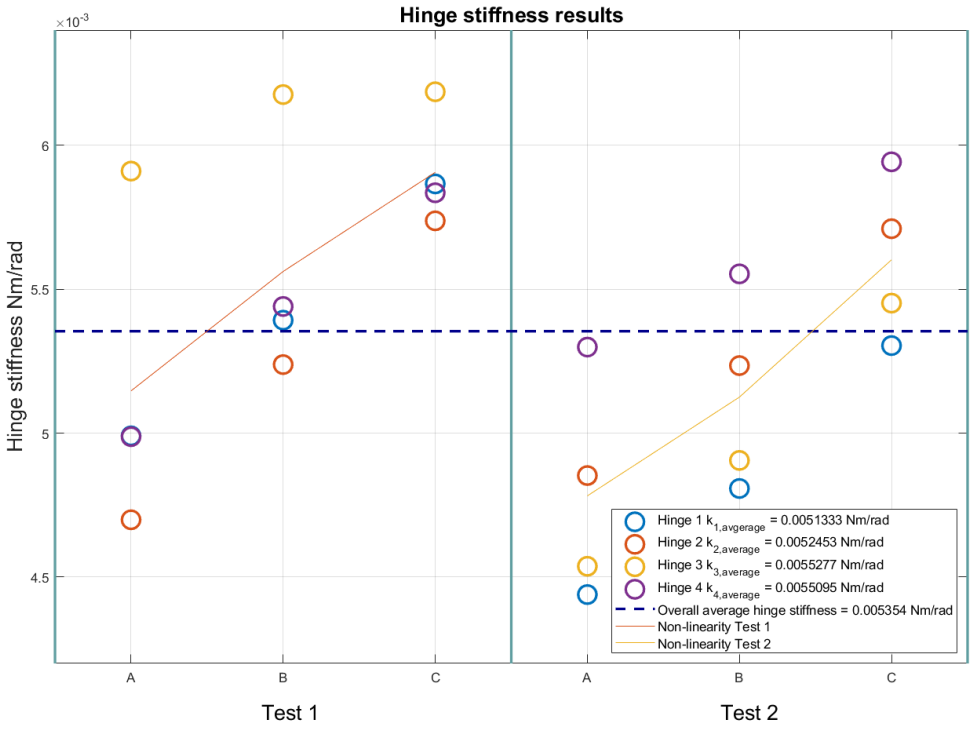

Figure 4-9: Results from the stiffness test. The horizontal axis shows tests **A** through **C** for both test **1** and **2**. The vertical axis shows the calculated hinge stiffness. Each hinge has its own coloured, circle marker. The blue, dashed line indicates the average stiffness for all 24 results. The solid red and yellow lines show the non-linear tendency for tests **1** and **2**. See the legend for the average stiffness of each individual hinge.

Chapter 5

Integration

This chapter is concerned with the integration of the previous two chapters. The wing and the hinge are designed and fabricated separately, and now this chapter brings them together. The entire fabrication and assembly process is shown and explained step by step. The final, completed wing-system is presented and tested.

5-1 Requirements

The requirements for the integration process come down to consistency and flexibility. 'Consistency' means that when two or more wing-systems are assembled, their respective performance is consistent. The goal is to have four wing-systems that produce the same lift, have the same flapping frequency, the same kinematics etc. When designed poorly, the integration of the hinge into the wing can lead to, for example, misalignment and misplacement which leads to inconsistencies. Making the integration process 'flexible' means that the process accommodates design changes to the wing and/or hinge relatively easily. If, for example, the length of a hinge needs to be reduced to reduce its pitching stiffness, a flexible integration process facilitates this without requiring new tools, additional materials or components etc.

5-2 The concept

At this point, the wing is a sandwich of three material sheets with an integrated rectangular structure for the hinge to attach to. The hinge itself consists of three separate steel flexures that need to be integrated into the wing to form the wing-system. Important here is the right alignment of the three flexures with the wing, and the alignment between the three flexures.

To do all this, a 'hinge-integration-jig' is developed; this is the orange sheet shown in fig. 5-1. Essentially this is 0.3 mm thick carbon plate (same material as the wing frame) with two features: 1) it has the same alignment holes as are present in the wing sheet, and 2) it has three slots for the hinge flexures to fit in. These two features combined allow for the hinge

flexures to be integrated into the wing in the right place and with the right orientation; the process can be seen in fig. 5-1 B-G.

This concept satisfies the requirements to a certain extent for two reasons. Firstly, the jig is cut with the same laser cutter as the other parts and made from the same material as the wing frame. This means that, if the hinge dimensions need to change, a new jig can be made fairly easily, i.e. flexibility. Secondly, using the same tool and material means that any fabrication errors are present in both parts. This benefits the consistency between multiple wing-systems.

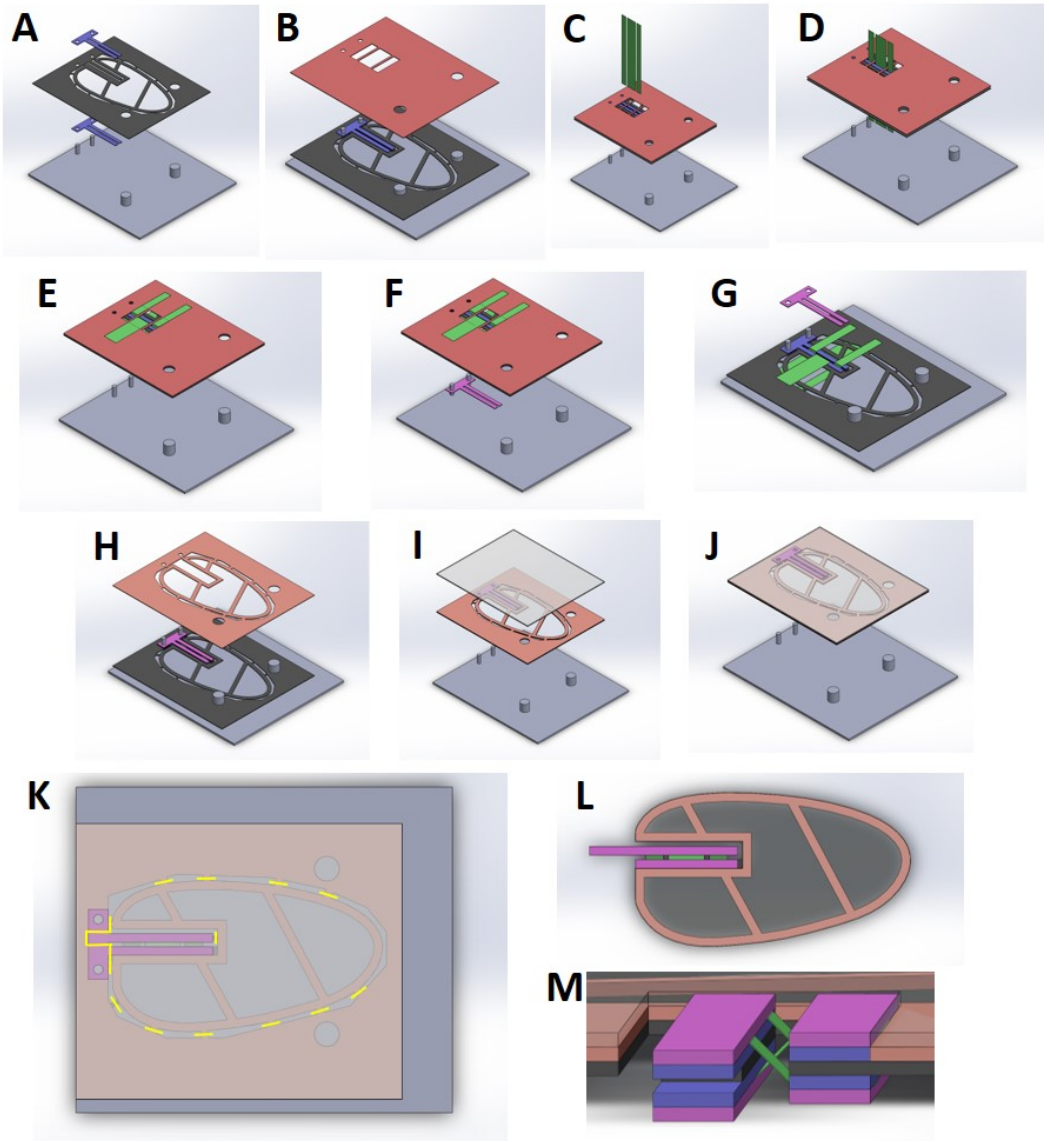

Figure 5-1: The process of manufacturing a fully functioning wing-system is described here. Steps **A**-**B** and **H**-**K** show the wing fabrication. Steps **C**-**G** show the integration of the hinge flexures into the wing. **L** and **M** show the final product. For an exploded view of the wing-system see fig. A-1.

5-3 The process

The process of manufacturing a fully functioning wing-system is described here. Some information may overlap with previous chapters; it is included here to present an overview of the process from start to finish. The bold letters below refer to a certain step in the process as shown in fig. 5-1.

A Laser cut the carbon wing sheet (black part) and the carbon spacers (blue parts). Place the wing sheet on the alignment tool (grey part), apply glue to the hinge support structure and place a spacer on the wing sheet; repeat this for the second spacer which should be glued to the other side of the wing sheet.

B Laser cut the hinge alignment sheet (orange part) and place it over the wing sheet. The wing sheet and hinge alignment sheet can be temporarily held together using small pieces of tape.

C Cut the three hinge flexures (green parts) using a scalpel and a cutting jig.

D Weave the hinge flexures through the hinge support structure using the hinge alignment sheet to get the placement right.

E Form an X-shape by folding the three hinge flexures over the hinge alignment sheet. Align the hinge flexures using the slots in the hinge alignment sheet and hold them in place by taping them to the wing sheet (bottom) and hinge alignment sheet (top).

F Place a hinge fastener (pink part; same shape as carbon spacer) on the alignment tool. Apply glue to the hinge support structure on the bottom side of the wing assembly (not shown in the image). Place the wing assembly on the alignment tool; the hinge fastener will be attached to the assembly. This clamps the three hinge flexures in between two pieces of carbon ensuring a rigid connection.

G Get rid of the hinge alignment sheet. The hinge flexures will stay in place because they are now glued to the wing sheet on the bottom side. Tape the hinge flexures to the wing sheet making sure that they are, again, fastened at both ends. Apply glue to the hinge support structure and place the last hinge fastener onto it. The hinge is now integrated into the wing and excess material can be cut away.

H Laser cut the double-sided adhesive sheet (light orange part). Remove the protective layer on the bottom and glue the sheet to the wing sheet using the alignment tool as a guide.

I Remove the second protective layer and lay a piece of Mylar film (see through part) over the wing assembly.

J Gently press the Mylar to the wing sheet to ensure a good connection.

K Using a scalpel, cut away the Mylar covering the hinge support structure. With the same scalpel, cut through all the tabs indicated by the yellow lines. The wing-system can now be released from its support material and is ready to be used.

L This image shows the final wing-system. The colors are added to all images to clearly indicate which part is which; they do not represent their actual color.

M This is a close-up of the hinge. The 'hinge support structure' is the combination of all the carbon parts (pink, blue, black) that hold the hinge flexures (green parts) in place.

5-4 The completed wing-system

The product that is the result of this project is a functioning wing-system with the optimal shape and pitching axis, and an improved off-axis hinge stiffness. This product is shown in fig. 5-2 and fig. A-1. Within the Atalanta project, the novelty of this thesis is the fabrication and assembly of the wing-system using the Smart Composite Microstructures method. It is also the first time that the theoretically optimal shape and pitching axis are implemented into an actual wing-system. The creative part of this thesis is mostly concentrated in the hinge; namely, using a three-piece, cross axis configuration and integrating it into the wing area.

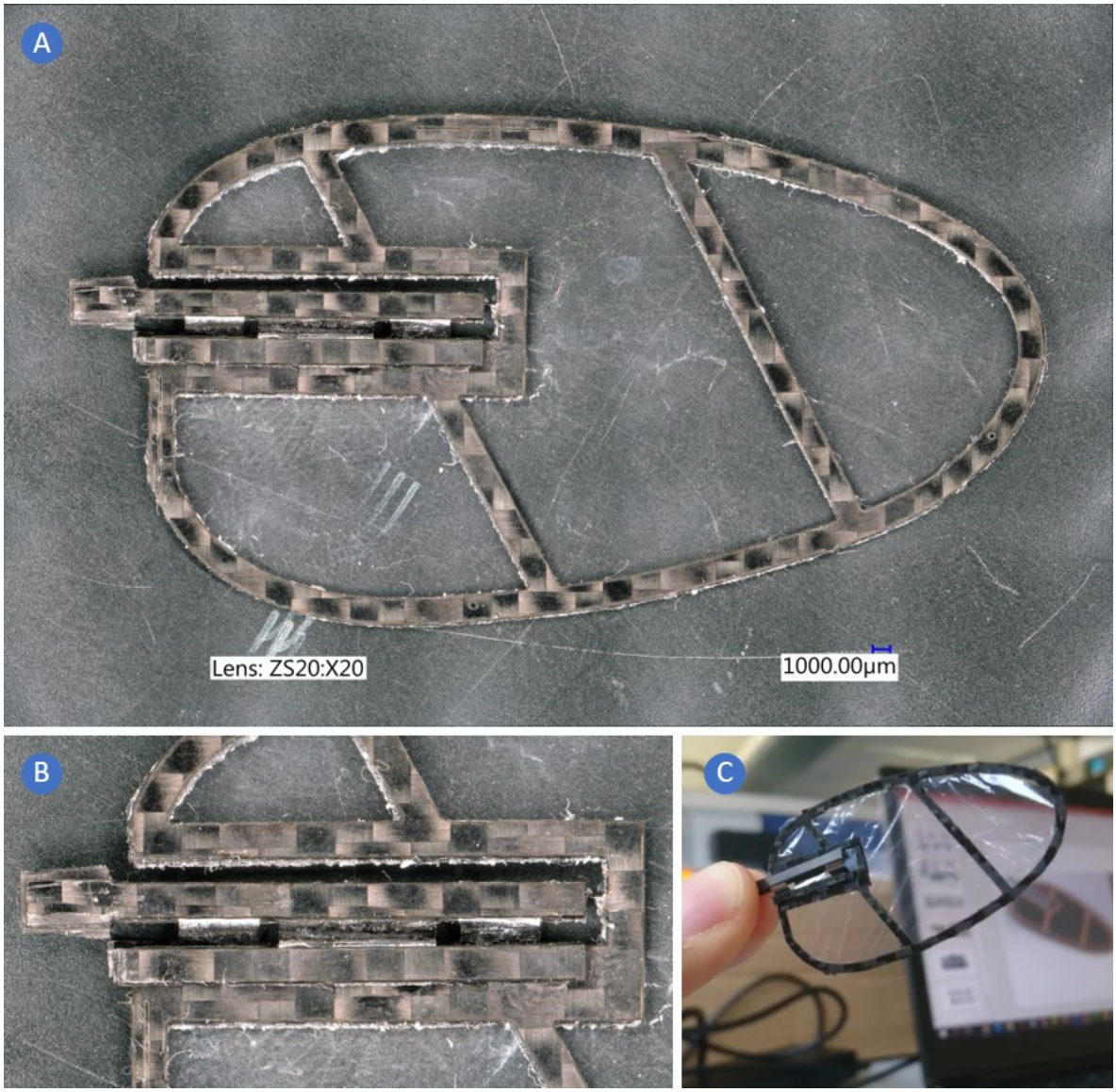

Figure 5-2: A: image of the completed wing-system, taken with the Keyence VHX-6000 microscope. The Mylar film and double-sided adhesive sheet are difficult to see because they are both transparent. **B:** hinge support structure with the leaf flexures installed. **C:** photo taken to show the Mylar film.

5-5 Testing

This section, similar to previous chapters, describes some some experiments performed to quantify the result achieved up till now. With the wing and hinge designed, fabricated, assembled and now integrated, the performance of the entire wing-system will be validated.

To do this three tests are performed. These tests are small and simple and are not sufficient to exactly determine how well this wing-system would perform when used to actually fly the Atalanta. The tests aim to provide some support to the question whether the results of this project are potentially an improvement over the existing wing-system.

5-5-1 Wing-system mass evaluation

The mass of the wing-system does not influence the energy efficiency of the wing, but it does influence the wing kinematics and lift requirement of the Atalanta. The kinematics will be discussed later, but heavier wings mean a heavier Atlanta drone which should all be compensated by the cumulative lift generated by the four wings.

If the wing-system is seen as a mass-spring-damper system, the total mass of the system would be the dedicated mass plus the mass of the spring. In this case that means weighing the entire wing-system minus the top of the hinge support structure, i.e., the structural part connecting the Atalanta to the hinge. The wing-system you are left with can be seen in fig. 5-3.

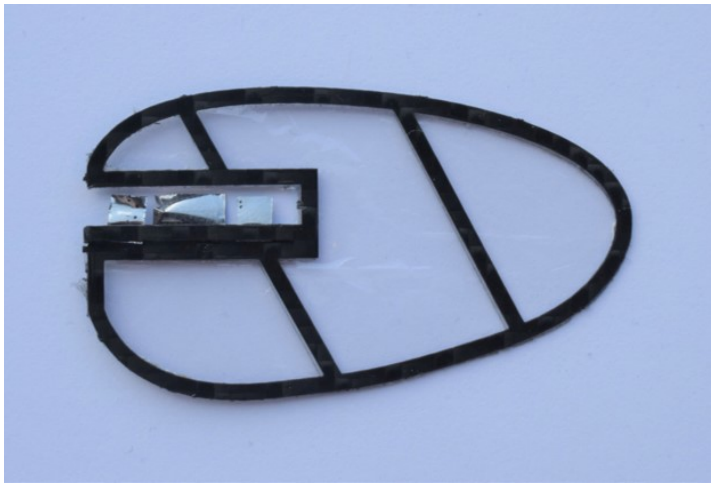

Figure 5-3: Wing system without the top of the hinge support structure, a.k.a. the carbon bar that connects the hinge to the Atalanta. This part is the mass of the wing-system.

Eight wing-system were fabricated and weighed for this test; the results can be seen in table 5-1. The table shows two types of wings: *Standard* and *Engraved*. This is because four of the eight wings were engraved with the laser cutter in order to put some marks on the wings for a test that was ultimately cancelled. This is all to say that the *Engraved* wings should weigh less because material was taken out compared to the *Standard* wings. These marks were very small so the mass difference due to the engraving is far less dominant than due to, for example, fabrication errors; this is clear from the results.

Wing	Standard	Engraved
1	283.15 mg	304.53 mg
2	290.02 mg	281.97 mg
3	294.52 mg	316.37 mg
4	296.54 mg	314.88 mg

Table 5-1: Results of weighing eight wing-systems without the top part of the hinge support structure. The scale used for the measurements was a Mettler Toledo AX 105 with an accuracy of 0.01 mg.

Clearly the design of this wing-system with these materials results in a wing-system that is approximately five times heavier compared to the wing-system designed by Bolsman [1]. But these wings should also produce more lift and do that more efficiently. To get an indication of how close a new Atalanta drone with the new wing-system would be to achieving lift-off compared to the drone manufactured by Bolsman, an overview is made in table 5-2.

Table 5-2 shows the masses of the sub-systems of the Atlanta drone for the Bolsman prototype in the first column. Bolsman got rid of the metal frame for the actuator which reduced its mass. With everything added up, his prototype had a lift-to-mass ratio of 0.12. If for a new prototype the actuator (fig. 2-2 B) is used as described in section 2-2, together with the new wing-system, the total mass would be slightly less (assuming the mass of the body parts would remain the same). But a wing with an improved shape and pitching axis would be far more efficient and could produce up to 1.5 g of lift per wing [2]. This would add up to 6 g lift in total. Since the wings in this report have a cut-out for the hinge, and the fabrication is not perfect, the lift would probably be less than what is theoretically possible. Assuming 5.5 g in total is possible, the lift-to-mass ratio of the new drone would be 0.78. For the new drone to have a 0.12 lift-to-mass ratio with the new wing-system, the lift per wing would only have to be 0.21 g and 0.85 g in total. (Note that this table doesn't account for the fact that the sweeping frequency of the new wing-system is three times lower compared to what it should be; more on this in chapter 6. A lower sweeping frequency results in less lift generated per wing.)

Current Atalanta drone		**Improved Atalanta drone**	
4 wings	0.24 g	4 wings	1.2 g
Rings and body parts	0.36 g	Rings and body parts	0.36 g
Actuator	8.25 g	Actuator	5.5 g
Actuator frame	-1.03 g		
Atalanta mass	7.82 g	Atalanta mass	7.06 g
Total lift	0.9 g	Total lift (estimated)	5.5 g
Lift/mass	**0.12**	**Lift/mass**	**0.78**

Table 5-2: Overview of what the lift-to-mass ratio of an improved Atalanta could be. For this a new actuator and the wing-system concept developed during this project will be used. Assumptions are that the new actuator is powerful enough, that the wing-systems can operate at approximately 30 Hz, that the hinge cut-out doesn't influence the lift production significantly and that the mass of the Atalanta body parts remain constant.

5-5-2 Wing-system durability test

For the Atalanta to lift-off, its construction has to hold up and not give in to the loads applied to the system. The pitching hinge may be one of the most fragile parts since the dynamic loads induced by the wing motion are directly applied to it. Another weak link may be the connection between the Mylar and the carbon wing sheet. If the Mylar gets loose or ruptures, the lift produced by the wing will immediately decrease. To check the durability of the wing-system, a test is performed where the wing is operated at its natural frequency and a timer is set to see - if the wing breaks at all - how long this would take. The test with the timer is actually part B of the entire durability test. Part A consists of finding the right operating frequency of each wing-system. The frequency described by Wang [2] of approximately 27.5 Hz belongs to a wing-system with a certain mass, mass distribution and hinge stiffness. The wing-system developed in this project has different values for those parameters which means that the optimal operating frequency will be different. This frequency was not calculated or simulated but determined experimentally in part A.

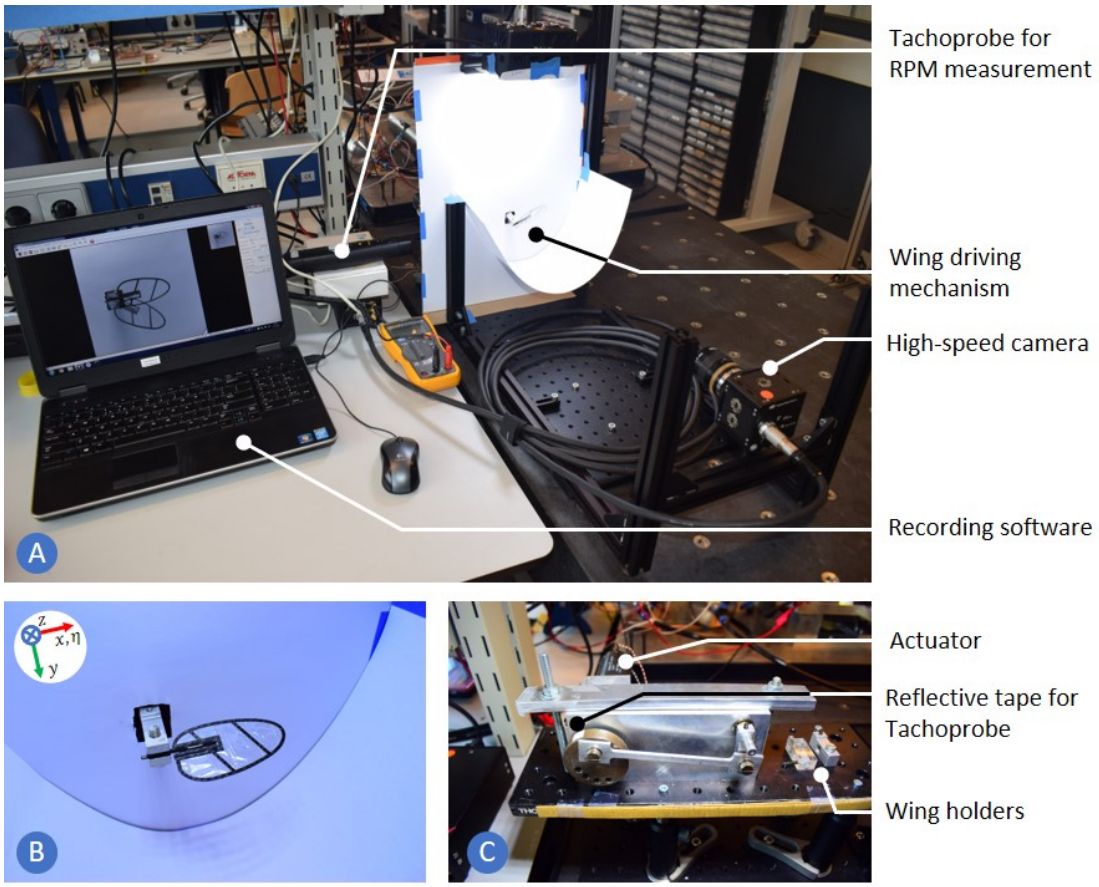

Figure 5-4: A: test setup used to record the motion of the wing-system and time its endurance; tools listed on the right. **B:** close-up of the wing holder which is connected to the driving mechanism as seen in **A**. The coordinate system is a body-fixed one. The wing-system sweeps around the z-axis which points into the background. The wing pitches around its local x-axis. **C:** wing driving mechanism that translates a rotational motion of the actuator into a oscillating motion of the wing-system.

The setup used to operate the wing-system and analyse its motion can be seen in fig. 5-4. The wing-system is driven by the mechanism seen in fig. 5-4 C and filmed by a high-speed camera. The sweeping frequency of the wing-system can be changed by changing the voltage that runs through the actuator. A Tachoprobe measures the actual RPM with the use of a reflective piece of tape attached to the outer rim of the brown disk seen in fig. 5-4 C.

The wing-system has a number of dynamic modes. For a low operating frequency the wing-system will behave according to its rigid-body mode. When the frequency is steadily increased, the wing-system goes through multiple modes, each displaying its own kinematic profile. The desired kinematic behaviour [2] is visualized in fig. 5-6. Of course this behaviour is for a 50 mg wing with a different mass distribution, hinge stiffness and no hinge cut-out. But the energy efficiency of the wing-system is only dependant on its kinematic profile [2]. So if the wing-system behaves according to this optimal motion - whatever its mechanical properties - this means the wing generates lift most efficiently.

Wing	Actuator voltage V Sweeping frequency (approximate) Hz Observations											
Engraved 1	2.6 8.4	3.1 10.5		3.6 12.5			4.2 15.0			7.0 26.6		
	Tried 7.0 V because that is close to the 27 Hz predicted by Wang [2]. Hinge broke at 7.0 V											
Engraved 2	0 0	< Continuous sweep >					4.0 14.2					
	Tried a continuous sweep without stopping in between to observe the mode changes; these can be clearly seen with the naked eye. Hinge was already damaged before this test											
Engraved 3	2.9 9.6	3.4 11.7	3.5 12.1	3.6 12.5	3.7 12.9	3.8 13.4	3.9 13.8	4.1 14.6	5.5 20.4	6.3 23.7	7.7 29.3	8.2 31.2
	Did narrower search around 3.6 V since this seems to be close to optimal frequency. Above 4 V the wing only sweeps without pitching. Hinge was partially torn sometime during this test; when this happened is not known											
Engraved 4	2.7 8.8	2.9 9.6	3.0 10.0	3.2 10.9	3.3 11.3	3.4 11.7	3.5 12.1	3.6 12.5	3.7 12.9	4.0 14.2	5.0 18.3	
	In-between two eigenmodes, the wing-system is unstable and ultimately falls back into one of the two modes. For this wing-system the hinge broke at 5.0 V. Optimal frequency seems to be lower than wing-systems 'Engraved 1' and 'Engraved 3'											
Standard 1	2.7 8.8	2.8 9.2	2.9 9.6	3.0 10.0	3.1 10.5							
	The Tachoprobe indicated a frequency of 9.6 Hz at a motor voltage of 3.0 V. At 3.1 V the wing-system only showed a sweeping motion. At 2.7 V the wing has an incorrect phase difference with respect to the sweeping motion. The glued connection of one of the hinge strips with its carbon support material came loose; no parts broke											
Stan. 2, 3, 4	2.5 8.0	2.6 8.4	2.7 8.8	2.8 9.2	2.9 9.6	3.0 10.0	3.1 10.5					
	All three remaining non-engraved wing-systems have a optimal frequency between 2.6 V and 2.8 V. Only wing-systems 3 and 4 are still fully intact											

Figure 5-5: Overview of part A of the test: finding the right operating frequencies for the wing-systems. Each wing-system was tested for multiple actuator voltages with their corresponding wing-system sweeping frequencies; these are the values listed. Some observations of the tests are also included for every wing-system. A green box shows the the frequency at which the wing-system seemed to have the right kinematic profile. An orange box shows the frequency at which the wing-system broke. Note: all these tests were conducted at a total sweeping amplitude of $60°$. The test to determine the actual kinematic profile of a wing-system was conducted at $127°$ (see section 5-5-3 and fig. 5-6).

Part A All eight wing-systems were tested with the operating frequency range narrowing for the last four wing-systems (*Standard 1-4*). The results can be seen in fig. 5-5.

Part B In this part the actual durability of two wing-systems is tested by timing their endurance before failure when operated at their optimal frequency. Since most wing-systems did not (fully) survive their initial test due to inappropriate operating frequencies, only two wing-systems were tested here. The results are shown below.

- Wing *Standard 4*: Tachoprobe readout determined the frequency to be 8.5 Hz (2.7 V motor voltage). After 18.12 minutes at this frequency the hinge strip closest to the tip of the wing snapped.
- Wing *Standard 3*: Again the Tachoprobe readout determined the frequency to be 8.5 Hz (2.7 V motor voltage). After 54:22 minutes of operation the test had to be stopped. No visual damage could be observed.

5-5-3 Analysing the kinematic profile of a wing-system

Every test described in the previous section was recorded with a high-speed camera setup. With a tracking software the optimal motion of this new wing-system can be visualized and compared to the theoretical optimal motion [2] (see fig. 5-6).

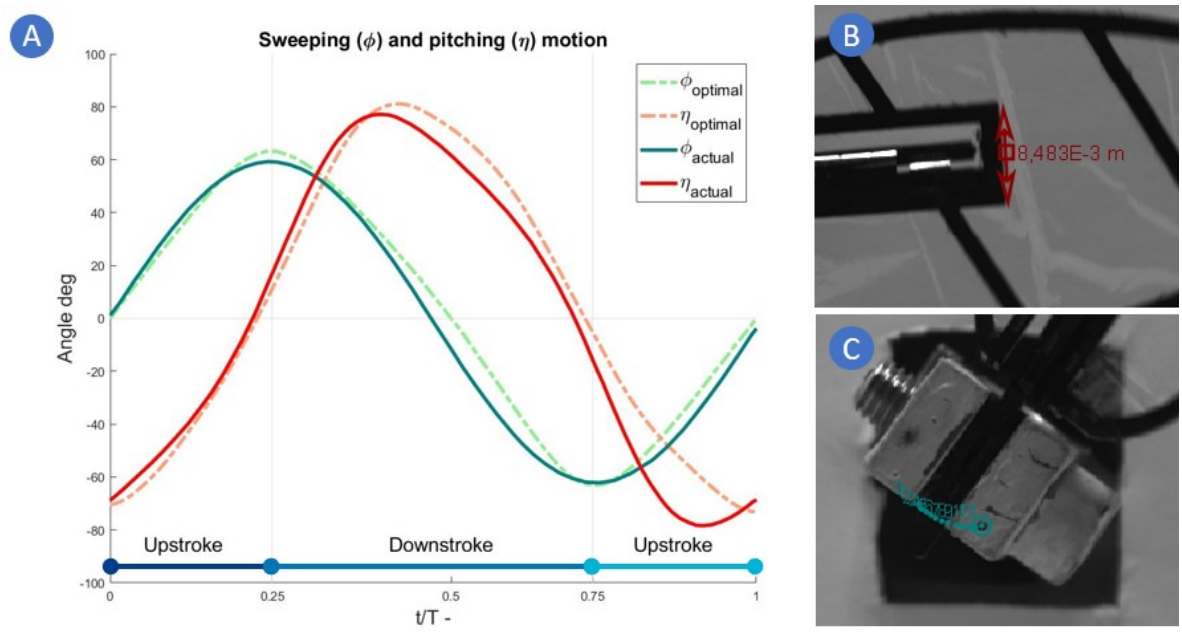

Figure 5-6: A: sweeping and pitching angles of a single stroke for the actual wing-system as well as for an optimal wing-system. **B:** tracking the length of a carbon edge to determine the pitching angles. **C:** tracking a dot on the wing-holder to determine the sweeping angles.

For this test, the *Standard 4*-wing was used. Note that the total sweeping angle is set to 127° to mimic the desired range of motion presented by Bolsman [1]. Because this range of motion

is twice the angle used for the durability test, the optimal frequency is lower for the same actuator voltage. For this test, the frequency is 8.0 Hz with a actuator voltage of 2.7 V. The video was analysed using the Tracker software [60] pre-installed on the high-speed camera laptop. The sweeping motion (ϕ) was determined by automatically tracking a black dot on the wing-holder (see fig. 5-6 C). The pitching motion (η) was determined by measuring the length of a carbon edge (see fig. 5-6 B) in every frame and translating that to a pitching angle. If you know the actual length of the carbon edge and you calibrate the image (by measuring the width of the wing-holder for example), you can calculate the pitching angle using some trigonometry. The results are not corrected for any image scaling due to the carbon edge moving up/down and away/towards the camera.

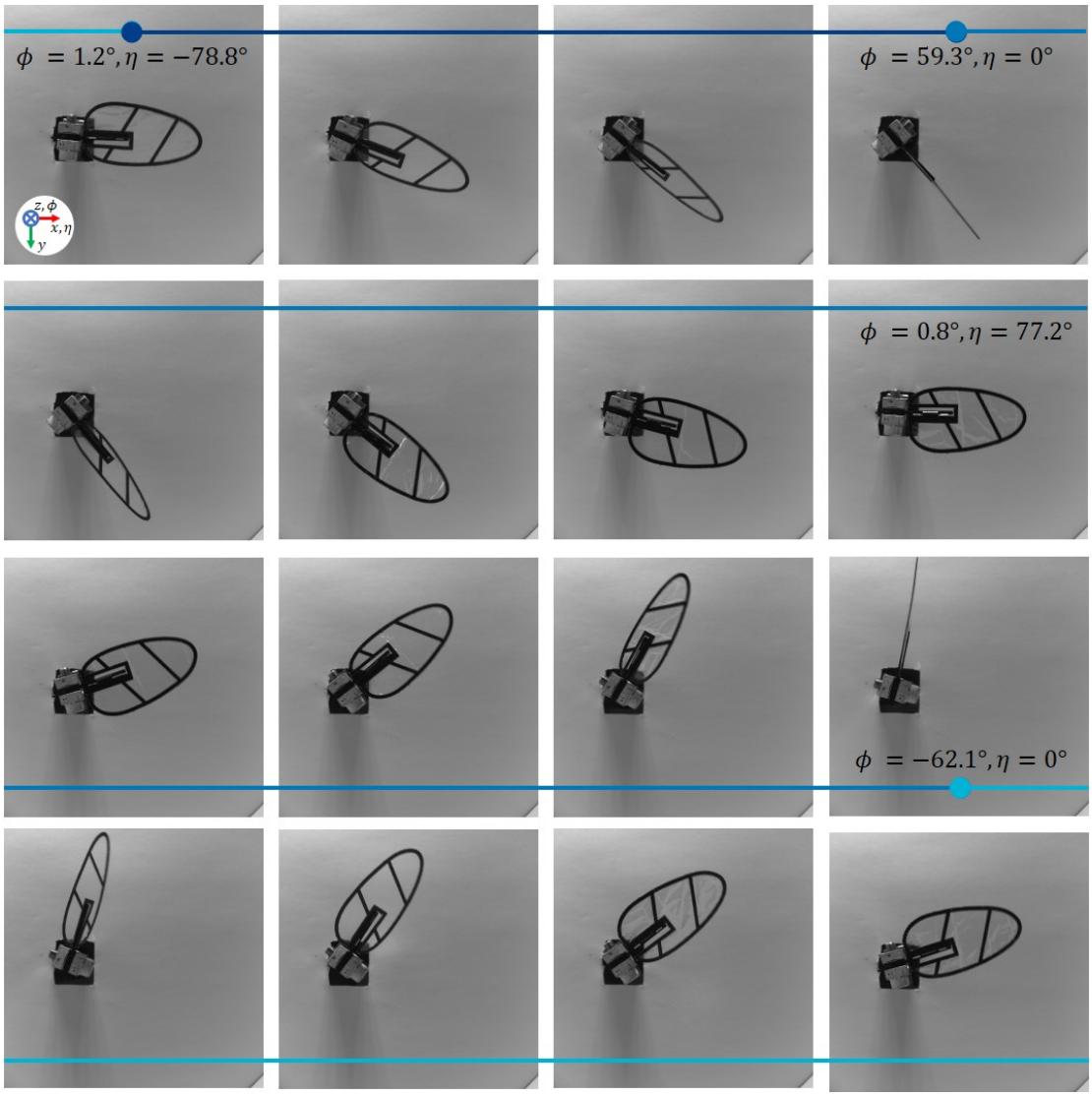

Figure 5-7: One full stroke of the newly developed Atalanta wing-system. The coordinate system seen in the first frame is a body-fixed one and is used consistently in this report (originally from [2], see fig. 3-2 A). The blue coloured bars refer to the up-/downstroke as shown in fig. 5-6. Some sweeping (ϕ) and pitching (η) values are shown at key frames; these values don't correspond exactly to fig. 5-6, more on this in chapter 6.

Chapter 6

Discussion

In this chapter, all results from previous chapters will be discussed. In general the goal is to asses the results with respect to the overall objective of getting closer to a flying Atalanta. The chapter has three parts: wing, hinge and integration. All tests discussed in previous chapters will appear in their appropriate parts. Most conclusions in this chapter are more qualitative than quantitative.

6-1 Wing

6-1-1 Shape and dimensional analysis

The results in fig. 3-6 show that, for all four measuring points, the measured distance was less than the distance it should be. If the average measured distance for each point is subtracted from its theoretical value, these are the results per point: [**1**] 0.255 mm, [**2**] 0.227 mm, [**3**] 0.234 mm and [**4**] 1.499 mm.

Clear is that for points [**1**]-[**3**] the deviation from the theoretical value is about a quarter of a millimetre, but that the deviation for point [**4**] is about 1.5 mm.

For points [**1**]-[**3**] the deviation probably originates from the fact that the laser cutter was set up in such a way that it cut five parallel lines for every line it was ordered to cut. The reason was to widen the cut so that the material wouldn't block the laser when the laser would move to the next level (i.e. further into the material). An example of this can be seen in fig. 6-1. Each cut is actually five cuts next to each other. The laser cutter software places these extra lines automatically and for this it has two options: place the extra lines on the inside of the material or on the outside. The blue and yellow arrows in fig. 6-1 indicate these two options. For points [**1**]-[**3**] the laser cutter placed the extra lines on the inside of the material. The lines are separated by 0.02 mm which adds up to a total of 0.08 mm for each side. The diameter of the laser beam adds another 0.01 mm in total. This adds up to a deviation of: $(2 \cdot 0.08) + 0.01 = 0.17\ mm$. This is still less than the 0.25 mm deviation measured, but that could be due to the imprecisions of the laser.

The reason why for point [**4**] the deviation is six times higher is unknown. The laser and the carbon sheet don't translate during cutting. The laser sits in the middle and its beam is redirected to different parts of the cutting area by bending the light using a lens-mechanism. Points [**1**]-[**3**] are all located in the bottom-left quadrant of the carbon sheet; point [**4**] is measured from the bottom-left quadrant to the bottom right. It could be that a certain laser error is cancelled out when the laser cuts in a single quadrant, whereas the error adds up when cutting in two opposite quadrants.

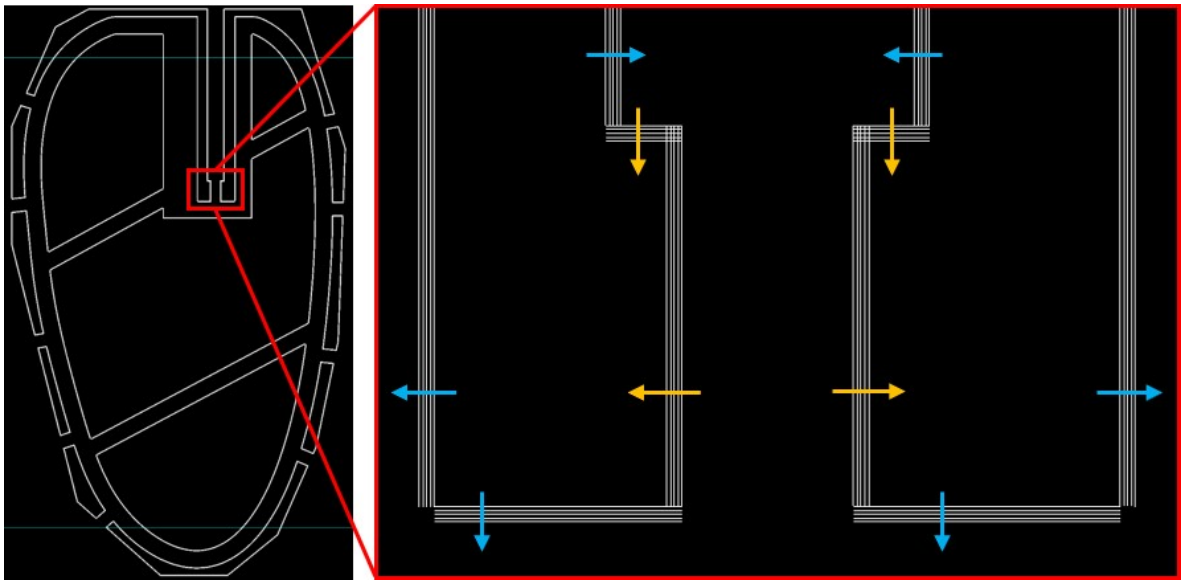

Figure 6-1: Laser cutter file for fabricating the wing. The laser cuts five parallel lines on the cutting surface to let the laser light penetrate the material more easily when cutting deeper into the material. It places these lines sometimes on the outside (blue arrows) of the material and sometimes on the inside (yellow arrows). This causes some features to have different dimensions compared to what they are supposed to have.

Deviations in dimensions due to the extra cuts and/or machine errors result in a wing surface area that is different than what it is supposed to be. A Solidworks model calculated the wing surface area to be $1323.02\,\mathrm{mm}^2$, whereas the digital microscope software calculated the actual wing surface area to be approximately $1237.54\,\mathrm{mm}^2$; a 6.9 % difference. Some additional measurements indicate that the wing did not "shrink" uniformly meaning that the shape is not exactly the optimal shape [2]. It seems that the laser cutter takes more material away the farther it gets from its origin (the middle of the cutting surface). This makes sense knowing that the laser is bent away from the center by a lens-mechanism. If the machine has a cutting error, it does make sense that the error increases with the cutting radius.

Wang performed a sensitivity analysis of all design parameters versus the lift [39]. The wing span for this project turned out to be 2.78 % smaller than what it was supposed to be. According to Wang, this smaller wing span would result in a 6.18 % reduction in lift force generated if all other parameters are kept constant. This last assumption is not the case for this project since the wing "shrinks" non-uniformly, but this calculation does give a rough estimate of the affected performance of the wing.

6-2 Hinge

6-2-1 Non-linear hinge stiffness

The first observation is that the average angular pitching stiffness of the four hinges increases from A to B to C in fig. 4-9 (solid red and yellow lines). For both tests the trend line increases when the angular deflection increases. This confirms the expectation that the hinge stiffness is non-linear and thus increases for larger angular deflections.

This thesis assumes the pitching hinge to have a linear stiffness response. This assumption, at first, seems to be wrong since the pitching deflection of the hinge is significant with a maximum of about 80°. But results presented by Bolsman [1] show that a linear spring can accurately represent the intended pitching motion. Although that spring consisted of a single leaf flexure whereas the spring presented in this thesis consists of three leaf flexures arranged in an X-shape, the mechanics are similar. A linear spring stiffness model may be good enough for now, but actually realizing a hinge with the desired stiffness based on this model is difficult (as is clear from the hinge stiffness test). Non-linear effects, however prominent, together with fabrication and assembly errors influence the hinge stiffness; fine-tuning the stiffness by experimental optimization is therefore a recommendation made by the author.

6-2-2 Average stiffness deviation between multiple hinges

The second observation is that, although all four hinges show similar performances within reasonable bounds, there are still difference between them (see legend of fig. 4-9). The differences can be due to fabrication and assembly errors, or because of measurement errors. Figure 6-2 shows the sensitivity of the hinge stiffness with respect to the generated lift [39]. The figure shows that the hinge stiffness is inversely proportional to the generated lift. The average stiffness deviation for all six tests (1A-2C) between the hinge with the highest stiffness and the lowest, is 16.4 %. As the graph shows, the lift is not that sensitive to a change in the hinge stiffness; the lift increases with less than 2 % for a 15 % decrease in hinge stiffness.

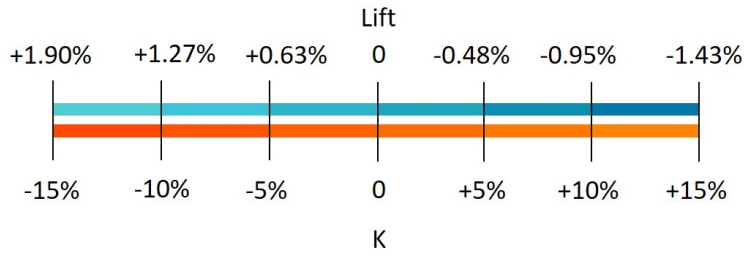

Figure 6-2: Sensitivity of the generated lift per wing with respect to a change in the hinge stiffness when all other parameters are kept constant.

6-2-3 Mismatch between theoretical and actual hinge stiffness

The third observation is the one already shortly mentioned in chapter 4. The overall average stiffness of the four hinges is $5.3540 \times 10^{-3}\,\mathrm{N\,m\,rad^{-1}}$. The designed theoretical stiffness is

$1.9249 \times 10^{-4}\,\mathrm{N\,m\,rad^{-1}}$ which means that there is a difference in stiffness of a factor 27.814; let's say 28. This is a significant difference that, as shown in chapter 5, certainly has an impact on the performance of a wing-system. The hinge stiffness partially determines the kinematics of the wing-system which in turn determines the energy efficiency of the system.

There is a list of reasons why this stiffness mismatch is observed. Some can reasonably be ruled out, others are a bit more challenging. More research is needed and the fabrication of the hinge flexures requires significant improvement; more on this in chapter 8.

The list of reasons is as follows:

1. **Measurement errors.** Tools for measuring the mass, their distance to the hinge and the deflection angle of the rod (see fig. 4-7) all have their resolutions which limit the accuracy of the readouts. Furthermore, a small gush of wind can influence the hinge stiffness setup which makes measuring the angular deflection difficult.

2. **Incorrect theoretical model.** The equation used (see eq. (4-3)) to calculate the theoretical stiffness of the hinge can be wrong.

3. **Incorrect input parameters.** The stiffness equations has the input parameters E, w, t and L. The actual values for these parameters may be different from the theoretical values (see eq. (4-4)).

4. **Hinge flexure alignment is wrong.** If one or more flexures are rotated with respect to the hinge assembly and/or each other, the effective width and length of the flexures could increase which in turn increases the stiffness of the entire hinge.

5. **Corrugation at the edges.** When cutting the flexures from the stock material using a scalpel, the edges are plastically deformed and a wave-pattern occurs along the cut edges. This effect can increase the stiffness of the flexures and thus that of the hinge.

6. **Misaligned axis of rotation.** Each hinge consists of three flexures, each with its own axis of rotation. If these axis are not aligned, the motion of the hinge can cause the flexures to pull on each other along, for example, the length of the flexures.

7. **Curved flexures.** The hinge flexures can also be bent or curved along the width of the flexures; think of a tape measure. This effect can also significantly increase the bending stiffness of the flexures.

8. **Curvature change due to tension.** The rod, counter mass and added mass (see fig. 4-7) all pull on the hinge creating tension in the flexures. This tension changes the curvature of the flexures which in turn affects the bending stiffness.

The reason for the stiffness mismatch can be either one of these reasons and it can even be a combination of multiple. In the following paragraphs each of these reasons will be discussed to determine whether or not they play a role in increasing the actual stiffness of the hinge.

1. Measurement errors Measurement errors don't seem to be able to account for the factor 28 in hinge stiffness. The three categories of parameters that are measured during the hinge stiffness test are: mass, distance and deflection angle. The tools used for these measurements have a resolution of 0.001 g, 0.005 mm and 0.1° respectively. If all parameters were to be changed in favour of decreasing the measured hinge stiffness in order to get closer to the theoretical stiffness, the factor mentioned above would decrease from 27.814 to 27.555; a 0.9 % difference. This means that potential measurement errors can not account for the significant difference between the measured stiffness and the theoretical one.

2. Incorrect theoretical model The equation used to calculate the hinge stiffness based on the design parameters is defined as follows:

$$k_{M_\eta,\eta} = \frac{EI_x}{L} = \frac{Ewt^3}{12L} \quad \frac{Nm}{rad} \tag{6-1}$$

The input parameters are the length and thickness of a single leaf flexure, the total width of all leaf flexures added up, and the Young's modulus of the material. This equation is seen to be used by Tielen et al. [58] and Machekposhti et al. [10]. The derivation is simply the multiplication of the standard, pure bending stiffness of a single beam element by the number of beams used in parallel. The equation could also be rewritten as:

$$k_{M_\eta,\eta} = \frac{E(nw_{single})t^3}{12L} \quad \frac{Nm}{rad} \tag{6-2}$$

Here n is the number of beam elements and w_{single} is the width of a single beam element. This equation implies that the X-shape does not influence the stiffness of the hinge, i.e. that all beam elements (named 'flexures' in previous parts of this thesis) are deformed by pure bending. It seems that the form of this equation is correct.

3. Incorrect input parameters The values for the four input parameters were carefully selected during the design phase. But due to, for example, fabrication and assembly errors, the actual values may differ. This in turn influences the stiffness value measured during testing. The list and table below explore the possibility of the input parameters being different, and to what extend that influences the stiffness.

- **E** The Young's modulus was selected to be 210 GPa based on the fact that the material is carbon steel. Original data sheets of this specific product can't be found so the exact value is unknown. Similar products cite a Young's modulus of 210 GPa [61]. Additionally, the material database CES Edupack [12] lists carbon steel to have a Young's modulus of 200-220 GPa.
- **w** This parameter represents the full width of all hinge flexures added up ($2 \cdot 3.5 + 7 = 14\ mm$). Using measurements from the digital microscope software, the width of the middle hinge strip varies between 6.74 and 7.02 mm and the width of the side strips vary between 3.26 and 3.69 mm. The reason for the fact that the hinge strips are not all equal, is probably because of the imprecise fabrication method (see chapter 4). The average width of the middle hinge for all four hinges is 6.94 mm.

- **L** The length of the flexure is determined by the gap in the carbon and the amount of tension applied to the hinge strips during assembly. The gap dimension between the four hinges varies from 0.77 to 1.05 mm with an average of 0.899 mm. The reason that these gaps don't match the 0.9 mm they are supposed to be, could originate from the fact that the laser cutter cuts extra lines to widen the cut. Another reason could be that during assembly, the hinge strips are not given equal tension so that when the two hinge parts are cut loose, the hinge strips 'sag', making the gap larger.
- **t** The thickness of the steel hinge flexures as mentioned on the packaging [61] is 0.01 ± 0.002 mm. For the theoretical thickness, 10 µm was selected.

The table below shows the effect on the hinge stiffness when the four input parameters are changed. For E and t the maximum values are selected too see if that bridges the gap to the actual hinge stiffness; note that the parameters could just as well be closer to their minimum values. For w and L the values are updated to more closely represent measurements done by the VHX-6000 digital microscope (see fig. 4-10).

Input parameters	Design	Change E	Change w	Change L	Change t
E [GPa]	210 *(1)*	**220** *(4)*	**220**	**220**	**220**
w [mm]	14	14	**13.88** *(5)*	**13.88**	**13.88**
L [mm]	1.273 *(2)*	1.273	1.273	**1.271** *(5)*	**1.271**
t [micron]	10 *(3)*	10	10	10	**12** *(6)*
$k_{M_\eta,\eta}$ [Nm/rad]	1.92E-4	2.02E-4	2.00E-4	2.00E-4	3.46E-4
$\frac{k_{M_\eta,\eta}}{k_{Design}}$ [-]	1	1.05	1.04	1.04	1.80

Table 6-1: *(1)*: value taken from Bolsman [1] and Wang [2]. *(2)*: $L = \sqrt{2 * 0.9^2} = 1.273\ mm$ with the hinge support structure gap being 0.9 mm tall (h_{Hinge}, see fig. 4-3). *(3)*: material thickness as mentioned on the packaging. *(4)*: upper limit of carbon steel according to material database CES Edupack [12]. *(5)*: average measured (VHX Microscope software) length of the flexures for all four hinge assemblies ($L = \sqrt{2 * 0.899^2} = 1.271\ mm$). *(6)*: upper limit of material thickness due to fabrication errors. The bottom row shows the factor with which the stiffness increases with respect to the 'Design' stiffness which is equal to the theoretical stiffness (see eq. (4-4)).

As table 6-1 shows, even when E and t are adjusted to their maximum value and w, L are adjusted to their average actual value, the stiffness still only increases by a factor 1.80 (1.7975). This means that there is some other phenomenon at play causing the significant deviation between the theoretical stiffness and the actual one.

4. Hinge flexure alignment is wrong The hinge configuration test (see section 4-5-2) set out to quantify how well the hinge flexures are aligned with respect to the hinge support structure and each other. Results from the test (see fig. 4-10) show that the angle between the hinge edge and the support material varies between 90.24° and 92.46°. This angle is ideally 90° and deviation from this ideal angle can influence the stiffness of the hinge. Figure 6-3 below shows a schematic representation of the flexure alignment with respect to the hinge support structure. The image shows that only the hinge flexure on the right is misaligned but it is possible that all three hinges are misaligned, even by different amounts and in different directions.

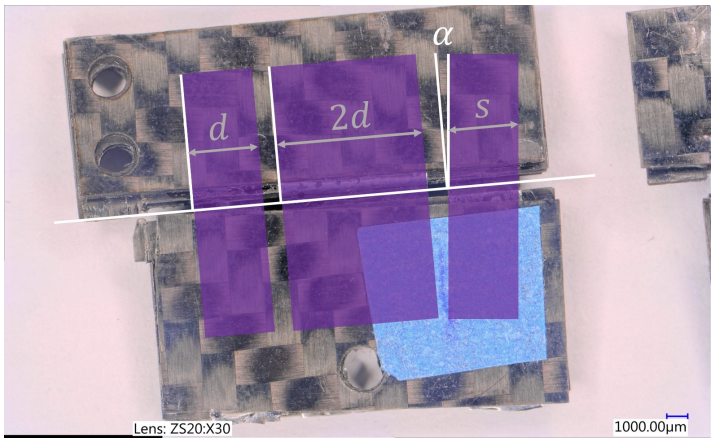

Figure 6-3: Photo of one of the hinge assemblies with a schematic representation of the hinge flexures. Normally the width of the right flexure is d, but now because it is rotated by α, the width of flexure increases and with it its bending stiffness.

Due to the misalignment the hinge flexure effectively gets wider. Since the width is an input parameter for the stiffness, this value also changes. The width of the misaligned hinge flexure is defined as follows:

$$s = \frac{d}{cos(\alpha)} \quad m \tag{6-3}$$

Here s is the width of the flexure with d being its un-rotated width. The largest measured misalignment is 2.46°. For the worst case scenario the assumption is made that all three hinge strips are misaligned by 2.46°. The stiffness of the hinge now becomes:

$$\begin{aligned} k_{M_\eta,\eta} &= \frac{Ew_{rotated}t^3}{12L} = \frac{Ewt^3}{12L \cdot cos(\alpha)} = \frac{E4dt^3}{12L \cdot cos(\alpha)} \\ &= \frac{210 \times 10^9 \cdot 14 \times 10^{-3} \cdot 0.01 \times 10^{-3^3}}{12 \cdot 1.27 \times 10^{-3} \cdot cos(2.46)} = 1.9267 \times 10^{-4} \quad \frac{Nm}{rad} \end{aligned} \tag{6-4}$$

The stiffness with perfect alignment is $1.9249 \times 10^{-4}\,\mathrm{N\,m\,rad^{-1}}$. This means that a misalignment of 2.46° on all three hinge flexures increases the stiffness of the hinge by a factor 1.0009. It can be concluded that the misalignment of the hinge flexures - although it may play a small role - is not the reason that there is such a significant difference between the theoretical and actual hinge stiffness.

5. Corrugation at the edges One of the assumptions underlying the hinge stiffness equation is that the flexures are uniform, flat plates. This doesn't seem to be the case for the flexures fabricated for this project. The hinge flexures are cut out from the stock material by laying it on a metal surface, clamping it under a metal cutting jig and then actually cutting the strips using a scalpel. This process was observed to leave a wave pattern along the cut edges (see fig. 6-4). This phenomenon occurs when a large force is applied to a single point on a thin material. The material is stretched locally which increases the length of the cut edge, and the easiest way to accommodate this lengthening is to shape it into a wave form (for more information see [62]).

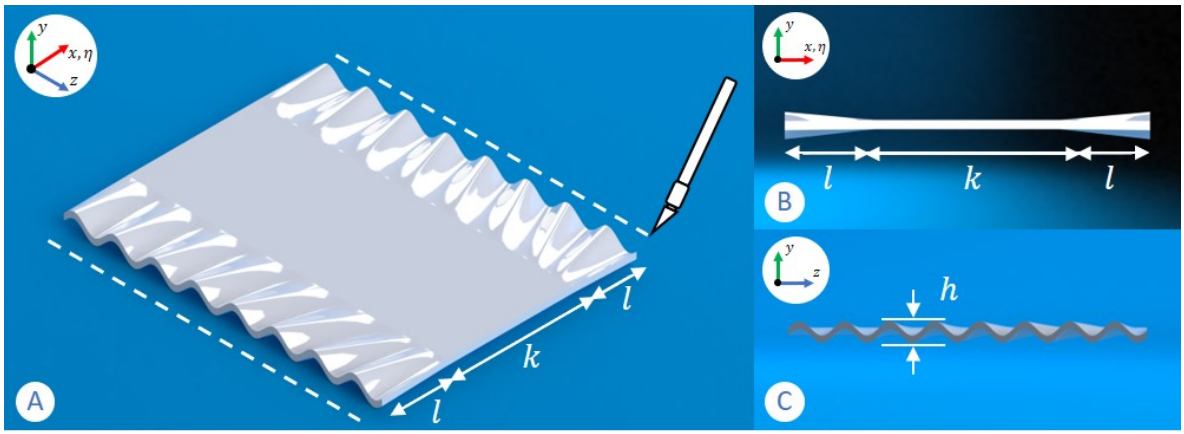

Figure 6-4: **A:** corrugation, i.e. wave pattern, along the cut edges of the hinge flexure. The corrugation has a width l into the material before it flattens out. The entire width of the flexure is $2l + k$. **B:** front view of the flexure. **C:** side view of the flexure with the height of the corrugation indicated by h. These images are not to scale, neither are the corrugation patterns.

The question is how much the corrugation influences the bending stiffness of the flexure around the x-axis. Simply modelling a plate with a constant, sinusoidal corrugation pattern throughout the entire width is already relatively complex (for more information see [63–65]); analytically defining the stiffness matrix for this part is therefore outside the scope of this project.

To get a feeling for the increased stiffness, the corrugated flexure will be modelled as an I-beam and compared to a flexure without the corrugation. The bending stiffness for a single I-beam flexure with dimensions as shown in fig. 6-4 is defined as follows:

$$k_{M_\eta,\eta} = \frac{EI_x}{L} = \frac{E(kt^3 + 2lh^3)}{12L} \quad \frac{Nm}{rad} \tag{6-5}$$

Images from the digital microscope show that the corrugation is definitely not a perfect sinusoid; in reality the amplitude and frequency of the wave are inconsistent at best. Nevertheless, the input parameters for the equation above are selected to be: $l = 0.1\,\text{mm}$, $k = (3.5\,\text{mm} - 2l) = 3.3\,\text{mm}$, $h = 0.014\,\text{mm}$, $t = 0.01\,\text{mm}$. E and L are remain the same so they cancel out. With these parameters, the bending stiffness of the I-beam is a factor 1.0695 larger than a flat plate. Here the flange of the I-beam (height of the corrugation) is only 4 µm larger than the thickness of the plate. For comparison, an I-beam with a flange height that is 10 µm larger than the thickness of the plate has a factor 1.2308 larger bending stiffness compared to a flat plate. This is because the flange height scales to the power three with the stiffness. But modelling the corrugation as the flange of an I-beam with the same dimensions seems incorrect. The corrugation is probably less stiff than the I-beam since it can fold onto itself like a harmonica when the flexure is bent; the I-beam cannot. Also, the corrugation flattens out into the material; the model for the I-beam presented here does not. Because of all this, for this thesis, the author assumes that the corrugation effect can increase the stiffness of the flexure up to a factor 1.1.

6. Misaligned axis of rotation To determine whether or not the misalignment of the axis of rotation of the three hinge flexures increases the bending stiffness of the entire hinge, the

following test was conducted.

For a single hinge assembly the bending stiffness was measured with a large and small load. Then the outer two hinge flexures were cut so the hinge assembly only consisted of the middle flexure. Then the stiffness was again measured for the same loads. These are the results:

Hinge assembly with three flexures

η_{begin}	*Mass*	η_{end}	$k_{M_\eta,\eta}$
0°	Small	2.95°	$5.9899 \times 10^{-3}\,\mathrm{N\,m\,rad^{-1}}$
0°	Large	8.4°	$6.1672 \times 10^{-3}\,\mathrm{N\,m\,rad^{-1}}$

Hinge assembly with only middle flexure

η_{begin}	*Mass*	η_{end}	$k_{M_\eta,\eta}$
0°	Small	3.05°	$5.8933 \times 10^{-3}\,\mathrm{N\,m\,rad^{-1}}$
0°	Large	8.25°	$6.2235 \times 10^{-3}\,\mathrm{N\,m\,rad^{-1}}$

Table 6-2: Results from a hinge stiffness test using the already mentioned setup (see fig. 4-7). The test indicates whether or not any possible misalignment of the axis of rotation of the flexures increases the hinge stiffness. The two tables show the results for a hinge with all three flexures and one with just the middle flexure. The tests are conducted with a small and large mass to increase the data points. The masses were all located at identical distances from the hinge.

If the axis of rotation of the three flexures were misaligned, cutting the outer two would eliminate this effect. Also, cutting the outer two flexures halves the total width of the flexures which should decrease the stiffness of the hinge. So if the misalignment of the axis of rotation did play a role, the stiffness measurements of the hinge without the outer two flexures should be far less. The results show that the stiffnesses actually hardly change. For the large mass the stiffness even increases with less flexures and a smaller angle of deflection. These results indicate that the axis of rotation for this hinge were not misaligned or at least did not increase the bending stiffness of the hinge. One could even say that the extra two flexures were beneficial to the functioning of the hinge since the stiffness for a single-flexure hinge is higher compared to having three flexures (large mass test table 6-2).

7. Curved flexures Another reason for the stiffness to be higher than expected, is a curve in the hinge along the width of the flexure (see fig. 6-5; similar to fig. 6-6). Actually measuring this curve in the hinge flexures is difficult but the reflection of the light seems to indicated that the flexure isn't flat. This phenomenon can be seen in nature where plants have evolved in such a way that their leaves can support their own weight and external dynamic forces, amongst others because of curves in their leaves [11]; this is for example true for a maize leaf [66].

There are two effects caused by this curvature that both seem to increase the bending stiffness of a flexure. One occurs before buckling (i.e. for small deflection angles) and the other after. The first effect is demonstrated in fig. 6-6. Pini et al. [11] determined the increase in bending stiffness for a piece of paper when a curvature along the clamped edge was introduced (see fig. 6-6 B). Their results show that the bending stiffness can increase up to 3.6 times just under the influence of gravity. But their model consists of a 'flexure' which is longer than it is wide; that is not the case for the flexures presented in this thesis.

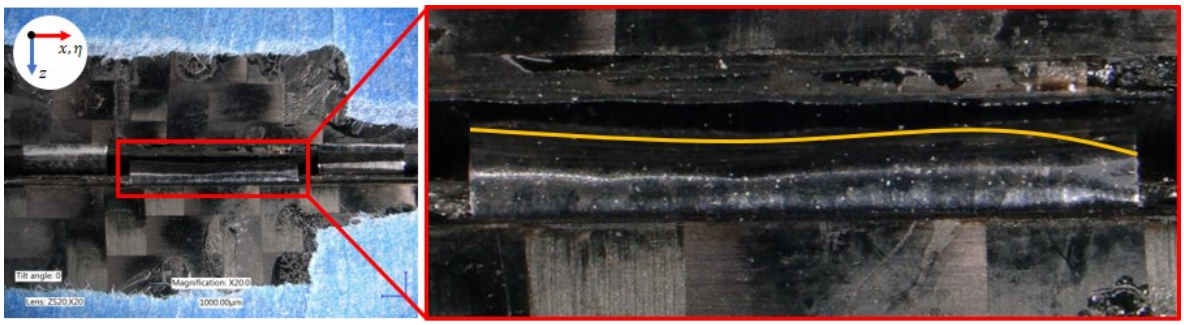

Figure 6-5: Microscope image of the three hinge flexures in their hinge assembly. The zoomed-in image on the right seems to show that the flexure is curved as indicated by the reflection of the light.

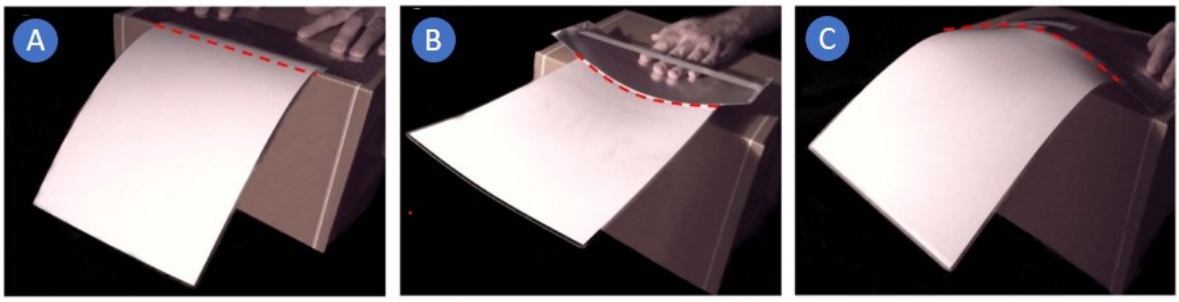

Figure 6-6: Stiffening of a piece of paper induced by transverse bending. **A:** pure bending of the paper. **B:** introducing a positive curvature along the clamped edge. **C:** introducing a negative curvature. Image courtesy of Pini et al. [11].

The second effect occurs when a curved flexure as shown in fig. 6-6 B is bent further than the linear regime. The flexure than snaps/buckles into a different position (see fig. 6-7). This effect can be felt when rotating the hinge and observed with the naked eye.

What this does, is shorten the effective length of the flexure. Before buckling the length of the flexure is equal to L (see fig. 6-7). After buckling, the length effectively shortens to S. This is because the clamped and curved part of the flexure acts as a rigid plate. This moves the axis around which the flexure rotates further into the material (red arrow). Since the bending stiffness of a flexure scales linearly with the inverse of the length of the flexure, this effect can certainly increase the stiffness of the hinge as a whole. Note that the flexures in this thesis are clamped at both ends. This means that the curve-induced-buckling effect can occur at both ends which shortens the effective length of the flexure even more. No data on the actual curvature or the effective length of the flexure are available. But since the buckling can be felt when rotating the hinge and can be seen even at this small scale, it is expected that this effect plays a dominant role in the increased hinge stiffness.

8. Curvature change due to tension The rod, counter mass and added mass (see fig. 4-7) all pull on the hinge in the negative z-direction (see fig. 6-8 B). This creates tension in the flexures, changing the curvature along the length of the flexure. A local curvature change can increase the local surface stress in the material because of material tension and/or compression. This effect is important for certain biosensors where the change in mechanical properties of a nano-

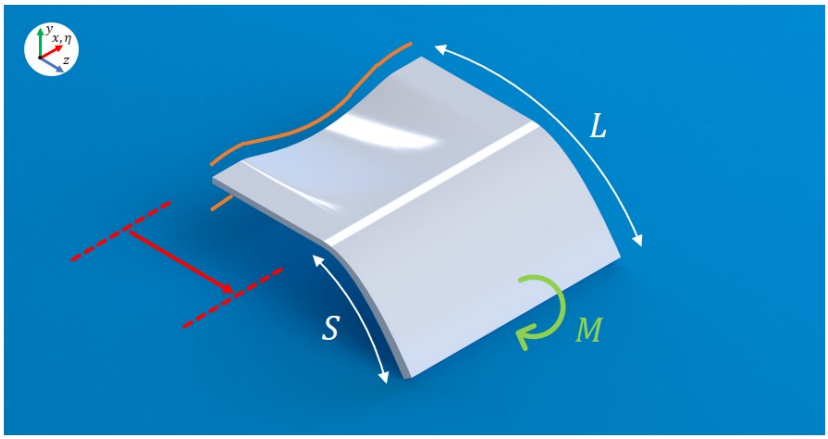

Figure 6-7: Image of a flexure that is clamped in on the left (orange lines). Due to the clamping and/or a fault in the flexure, there is a curve that runs along the width of the flexure. When a large enough moment (M) is applied, the flexure buckles. Now the flexure bends along a new axis, effectively shortening the length of the flexure and increasing the bending stiffness.

scale cantilever says something about, for example, the mass of a biological sample placed on top of it [67]. The curved flexure reacts to this surface stress by decreasing its curvature; the flexure pushes back on the applied load. An increase in curvature means an increase in surface stress, which means the flexure pushing back harder. This stiffening effect of the flexure may play a role in explaining the higher bending stiffness of the hinges as shown in chapter 4.

It is however not known to what extent this effect plays a role. The curvature at the base of the flexure (black circle in fig. 6-8) increases, but the curvature in the middle of the flexure decreases. It is possible that these two cancel each other out or at least impose opposite stiffening effects. Nevertheless, the stiffening of a thin flexure due to curvature changes along its length is still expected to be less dominant than the stiffening effect due to a curvature along the width of the hinge (see **5. Corrugation at the edges**).

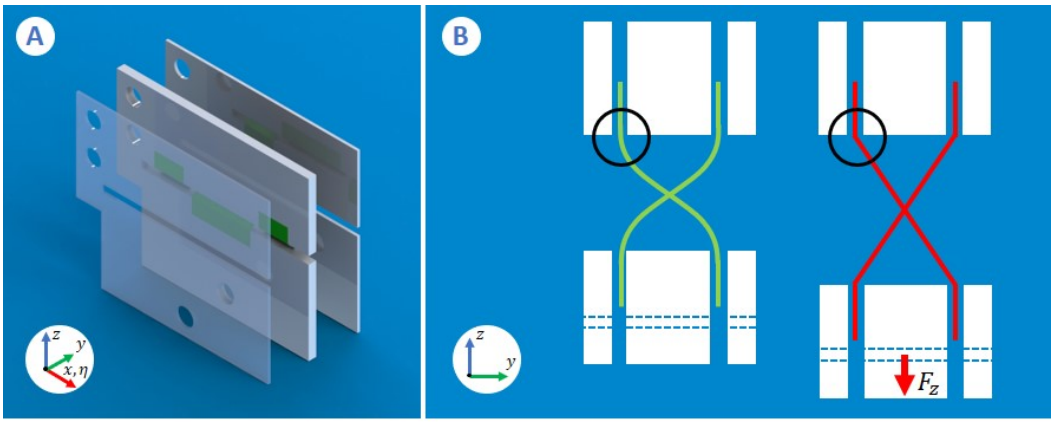

Figure 6-8: **A:** exploded view of a hinge assembly with the front plate made transparent. **B:** front view of the hinge assembly. The green flexures form an S-shape because of the way they are clamped into the hinge assembly. When a load in the negative z-direction is applied (F_z) the flexures form a Z-shape. The black circles show that the curvature for the two situations differs which may influence the bending stiffness of the hinge around the x-axis.

Summary on reasons for increased hinge stiffness Apart from reasons 2 (incorrect theoretical model) and 6 (misaligned axis of rotations), all reasons are estimated to influence the stiffness of the hinge. The difference between the theoretical and actual stiffness is a factor 27.814 and presumably a combination of reasons are the cause of this. Table 6-3 lists all reasons and their estimated role in increasing the stiffness. Note that the values are all more or less worst case scenarios. It could be the case that reasons 1-6 don't increase the stiffness at all, although this seems unlikely. For reasons 7 and 8 it is difficult to quantify their role. Nevertheless, it is estimated that reason 7, i.e. curvatures along the width of the flexure(s), is the dominant reason.

Reason	1	2	3	4	5	6	7	8
Factor [−]	1.0094	0	1.7975	1.0009	1.1	0	∗	∗

Table 6-3: Overview of all eight reasons that could influence the bending stiffness of the hinge. '**Factor**' is the scaling factor by with which a certain reason can increase the theoretical stiffness to bring it closer to the measured stiffness. '∗': no estimate available.

6-3 Integration

6-3-1 Flapping frequency and durability

Mismatch in flapping frequency

As the results show, the optimal flapping frequency of the wing-system developed during this project is approximately 8.5 Hz. This is lower than the optimal frequency of 28 Hz calculated by Wang [2]. This section will explain why the frequency is different, but first the importance of the flapping frequency is discussed.

The flapping frequency of a wing-system is more or less proportional to the lift it produces [2]. So a higher frequency means a higher lift production. But you can't simply increase the frequency because, as discussed, the entire drone is a compliant, resonating system so the flapping frequency needs to be just right. That way, the pitching frequency will be just right which results in a highly energy efficient system. The optimizer developed by Wang is capable of exactly calculating the flapping frequency, but because of time-constraints the difference in frequency will be explained in a different manner.

When comparing the wing-system developed in this project and the one used by Wang for his optimizer, there two key differences.

1. The mass of the newly developed wing-system is approximately 6 times as high.
2. The moment of inertia around the pitching axis ($I_{x_c x_c}$, see fig. 3-2) is 5.86 times higher.

Certainly there are more differences, but for now these two will be used to explain the frequency difference. Since the moment of inertia around the pitching axis is 5.86 times higher (due to a higher overall mass and a non-uniform wing), the wing will have a lower average angular pitching velocity for the same load applied to it. Now the flapping (technical term

is 'sweeping') frequency needs to be lower to give the wing enough time to rotate about its pitching axis every stroke.

Up till now only the inertial load is taken into account when discussing the net torque around the pitching axis. But the elastic load from the pitching hinge and the aerodynamic load should also be considered. For example, the hinge stiffness for the new wing-system is higher than the one used by Wang. The hinge stiffness increases with the flapping frequency so the elastic load should bring the frequencies closer together again. But it is clear that the inertial load is dominant. A higher moment of inertia means the flapping frequency has to decrease in order to still have the right kinematic profile. Improvements can certainly be made that increase the flapping frequency; more on this in chapter 8.

Wing-system durability

All four *engraved* wings broke at some point during testing. Note that all wing-systems broke at the pitching hinge; the wing itself (i.e. the carbon structure and the connection between the carbon and the Mylar) seems to be tough enough. There are three possible reasons for the failure of these wing-systems.

1. The test consisted of incrementally sweeping through different operating frequencies with a system shut down in-between each frequency. This means that the wing-system had to start from stand-still and accelerate up to the set frequency each time. This puts significant dynamic loads on the hinge each time.

2. Most frequencies were not the systems 'preferred' frequency meaning that unwanted forces would be exerted on the hinge as a result of parasitic motion of the wing.

3. Often the wing-system would be operated at up to three times the 'preferred' frequency which increases the inertial loads on the wing, which in turn are exerted on the hinge which would subsequently fail.

The two *standard* wings operated only at the right frequency lasted far longer than the *engraved* wings. It could be that the *engraved* wings are just more durable, but the hypothesis that the three above mentioned failure reasons play a significant role is more convincing in the authors opinion.

The fact that the *standard 3*-wing lasted 36:10 minutes longer than *standard 4*-wing while operated at similar frequencies shows that the fabrication and assembly errors play a role in the durability of the wing-system. What exactly causes this difference is unknown.

6-3-2 Kinematic profile of a wing-system

Figure 5-6 A shows the kinematic profile of the newly developed wing-system together with the optimal profile [2]. 'Kinematic profile' in this report means the sweeping and pitching angles of the wing-system during a single stroke. The reason why the profile is important, is because it directly influences the energy efficiency of the entire drone. The Atalanta is a compliant mechanism that operates at its natural eigenfrequency to force the entire structure

into a resonance mode. This saves a significant amount of energy. But for this to work, the mechanical properties of the Atalanta and its subsystems have to be tuned perfectly. If, for example, the wings are tuned in such a way that their preferred operating frequency differs from the eigenfrequency of the Atlanta, the dynamic behaviour of the wings will fight the desired resonant behaviour of the Atalanta. This affects the energy efficiency of the system. Note that fig. 5-6 A implies that the frequency of the new wing-system is identical to that of the optimal wing; this is not correct. As discussed earlier, these frequencies differ. Figure 5-6 A is only meant to compare the kinematic profiles, not the frequencies.

In general, the profiles seem to match, especially the sweeping motion. One observation is that the actual sweeping profile seems a bit more 'sinusoidal' compared to the optimal profile. This means that the optimal wing has a quicker turn-around time, i.e. it takes less time for the wing to reach the end of the sweeping stroke, turn around and get going back the other way. The wing-system may be more efficient this way since the angular sweeping velocities vary less.

Another observation is that the pitching profile follows the optimal profile less accurately. Especially the second upstroke is very different. The new wing-system seems to reach its maximum pitching angle before the sweeping angle is zero. This means that the pitching angle is greater just before the middle of the sweeping stroke; this seems counter-intuitive. This pitching profile also doesn't really seem to match the motion recorded by the high-speed camera (see fig. 5-7). That is why the values for the sweeping and pitching angles in that figure don't exactly match the kinematic profile. This mismatch could be an error in the tracking of the carbon edge (see chapter 5) and its subsequent translation into a pitching angle. According to Wang [2], the chordwise area distribution of the wing (orthogonal to spanwise direction) directly determines the passive pitching behaviour, including the amplitude, the phase lag from the sweeping motion and its deviation from a harmonic motion. Since the new wing has a slightly different shape and surface area compared to the optimal wing, it is not unexpected that its kinematic profile would be different.

What is undoubtedly true is the fact that the new wing-system is able to reach the desired 80° (one way) and 120° (both ways) pitching and sweeping angles respectively. A high pitching amplitude is desirable since it is inversely proportional to the aerodynamic power, which is equal to the power consumption of the drone [2].

Furthermore, since the kinematic profile and pitching axis of the new wing-system are close to optimal, it can be concluded that the new wing-system is more energy efficient than the wings developed by Bolsman [1].

Lastly, the new wing-system certainly doesn't produce enough lift to make the Atlanta take off. At 8.5 Hz flapping frequency, one wing produces approximately 0.1 g of lift. Bolsman's wing produced 0.225 g lift. But increasing the flapping frequency can be done by reducing the mass of the wing and optimizing the mass distribution. With those improvements implemented, the author estimates that the the new-wing system can produce close to 1.5 g lift per wing which should be close to sufficient for take-off.

Chapter 7

Conclusions

This thesis set out to find a solution for the fact that the Atalanta flapping-wing micro air vehicle from the University of Technology Delft is not capable of taking off. In other words, the Atalanta doesn't produce enough lift to compensate for its own weight. Fixing this problem means getting once step closer to realizing a resonant, bio-inspired and scalable FWMAV. Achieving lift-off will allow further research into areas such as attitude and position control, aerodynamic modelling, on-board electronics and more.
The plan was to 1) design a new wing with the optimal shape and pitching axis, 2) design a compliant hinge that would allow passive pitching, and 3) develop a fabrication and assembly method for both the wing and the hinge. This plan - if successful - would 1) increase the amount of lift generated per wing, and 2) decrease the power consumption due to increased energy efficiency.

The wing For the wing, 2D structures were laser cut into sheets of different materials, each with a unique purpose. These sheets were then stacked and attached to each other forming a – so to speak – 2.5D part. The wing consists of a carbon frame for stiffness, a Mylar sheet for enclosing the wing surface area and a double-sided adhesive layer to bond the two together. The assembly was done by laser cutting alignment features in all sheets and using a 3D-printed tool with alignment pins to ensure the right configuration of all sheets. The most difficult and time-consuming part here was finding the right settings for the laser cutter. The performance of the laser degraded over time which meant that the right settings changed on a weekly basis. Additionally, assembling the different sheets was not as smooth and automated as was hoped for; obtaining accurate and precise dimensions for the alignment tool using a 3D-printer is difficult. In general, however, the design-to-prototype process developed for the wing in this project proved to be relatively easy, consistent and highly flexible. Results do show that the shape and surface area of the wing are not perfect, but fixing this is simply a matter of altering the design of the wing and changing the cutting settings of the laser. Since experimental optimisation is of great importance in realizing the perfect wing-system, having this consistent and flexible design and fabrication process may be of value to future work within the Atalanta project.

The hinge The passive pitching hinge is a cross axis, compliant pivot hinge with three leaf-flexures configured into an X-shape. This design has a large range of motion, a low on-axis angular bending stiffness, a 1-DOF functionality and a compact footprint. The leaf-flexures are thin, carbon steel strips, manually cut to the right dimensions with the help of a metal cutting jig. The flexures are assembled into the wing with the help of a laser-cut alignment tool. Manually cutting these small flexures using a scalpel is far from ideal. The work is tedious, prone to errors and inconsistent. The method of integrating the flexures into the hinge support structure was good enough but can certainly be made easier. Results confirm that the fabrication process of the hinge is the weakest link. It yields hinges with inconsistent hinge stiffnesses and increases the absolute stiffness significantly. Although finetuning the mechanical properties is difficult, the general concept of the cross axis hinge has impressive potential.

The wing-system For the wing-system as a whole, the results are very positive. Certainly the flapping frequency is too low which means that the lift reduces to an estimated 0.1 g. This can be fixed by reducing the mass of the wing and optimizing its mass distribution; both of which should be relatively easy since there is abundant room for improvement in both areas. The best result is that the kinematic profile of the wing-system is close to optimal, which implies that the energy efficiency of the system is improved compared to the current wing-system. Additionally, achieving the desired sweeping and pitching amplitudes reduces the aerodynamic damping of the wing, which in turn reduces the power consumption. In terms of durability the wing-system surpasses expectations as well. When operated at the right frequency, the wing-systems can last between 18 min and an hour before the leaf-flexures give in.

Chapter 8

Recommendations

This chapter provides some possible improvements for when a 2.0 version of the wing-system would be developed. The good news is that there is enough room for improvements, all of which would someday hopefully result in the Atalanta being able to hover and fly on its own.

8-1 The wing

As mentioned earlier, the laser cutter was unreliable because its performance degraded over time. After extensive testing multiple, consistent carbon wing frames were fabricated that were certainly usable. Nevertheless, switching to a different laser cutter can greatly improve the ease with which the wings are fabricated.

The mass of the wing has to be reduced significantly. Combined with the non-uniform mass distribution, the high mass results in a moment of inertia around the pitching axis that is a factor 6 too high. The thickness of the carbon plate was 0.3 mm because no thinner option was available. The mass of the wing is proportional to the thickness of the carbon sheet so reducing the thickness to 0.1 mm drops the mass by about 65 %. Also the mass distribution can be improved. Currently the wing has material all along the trailing edge. This is unnecessary and can decrease the moment of inertia around the pitching axis significantly. The new design of the wing can than be inserted into the optimizer developed by Wang [2] to obtain the perfect and custom hinge stiffness, flapping frequency, power consumption and more.

The fabrication of the 3D-printed alignment tool can be improved as well. 3D-printing is a useful method to develop a working prototype but the standard extrusion printers available at PME are not precise enough. Dimensions often don't perfectly match their intended value and the layering process leaves a non-smooth surface texture. A better option would be to machine this part out of aluminium using a mill and lathe available in the IWS workshop. Even better would be an alignment tool with finely adjustable alignment pins. This way, any error in the laser cutting process can be corrected for with the adjustable pins. This will also allow for the pins to firmly grip the material sheets ensuring that there is no play due to oversized alignment holes.

8-2 The hinge

The fabrication of the hinge can be improved drastically. Ideally a laser cutter is used to cut all the hinge strips out of a single piece of sheet metal. This way the hinge dimensions can be perfect and it allows the hinges to be perfectly rectangular. Cutting the hinges from a single piece of metal also allows for the hinges to remain a single part until they are installed into the hinge. This reduces alignment errors and can be make the assembly process easier.
If a laser cutter is not an option, using a dedicated cutting tool is still an significant improvement. Such a tool can cut the metal and leave a smooth and straight edge, making sure that in the end the hinge stiffness better matches the designed stiffness.

Furthermore, the dimensions of the hinge are not optimized in this thesis. Ideally a new wing design will be inserted into the optimizer and the perfect hinge stiffness will drop out. Next this stiffness can be translated into dimensions of the flexures. This way the wing and hinge will be tuned perfectly with respect to each other.

The material for the hinge flexures can be optimized as well. Carbon steel was used in this thesis because it was available, but with more research and testing finding a better option should be possible.

When assembling the three individual hinge flexures into the wing, a lot of small pieces of tape are required to attach the flexures temporarily to the material sheets before they are permanently glued into place. This is not ideal since it doesn't ensure perfect alignment and makes the assembly tedious work. If the hinge flexures could be assembled into a fully functioning hinge structure before integration this would maybe make the assembly easier. Then this entire sub-assembly could be slotted into the wing at once.

All of these improvements should help in matching the theoretical bending stiffness of the hinge and the actual measured stiffness. When developing a new design and/or fabrication method for the hinge, the eight reasons mentioned in chapter 6 should be considered. These eight reasons can influence the bending stiffness of the hinge; minimizing or even eliminating their role should be a priority when developing the new design/fabrication method. Especially reason 7 is important. Reducing or eliminating any curves in the hinge flexures means getting closer to the assumption of the flexures being flat plates. This also prevents buckling effects which are estimated to have a dominant role on the bending stiffness of the hinge.

8-3 The wing-system

Getting a wing and hinge perfectly tuned with respect to each other is difficult to do without any experimental optimization. The possibility to manufacture and test multiple wing-systems a day would mean significant progress in achieving lift-off. Especially when the lift force per wing can also be measured since this is the defining performance characteristic of any wing-system. Wang [2] developed a test setup that could measure the lift force of a wing-system, as well as its motion. Additionally, from the required input power, the energy efficiency can probably also be determined. This setup can quantify the performance of a wing-system all at once, making it easier to judge whether or not that particular wing-system is good enough to be implemented into the Atalanta. Obtaining the lift force, motion and

energy efficiency of the the new wing-systems using the setup built by Wang could prove to be very insightful.

A new fabrication and assembly method for parts of the Atalanta is currently being researched in with the help of research printers. These printers can print different materials and have a wide array of settings that can be tuned to perfection. This method would allow the integral manufacturing of, for example, the wing-system all in one go without any human interaction. This would require extensive research, not only into the workings of the printer, but also into a new wing-system design since the printed materials would determine the shape and dimensions of the wing-system, as well as its functional properties. If successful, this would mean that no assembly by hand would be required, probably resulting in improved product quality and performance.

Appendix A

The Atalanta and the new wing-system

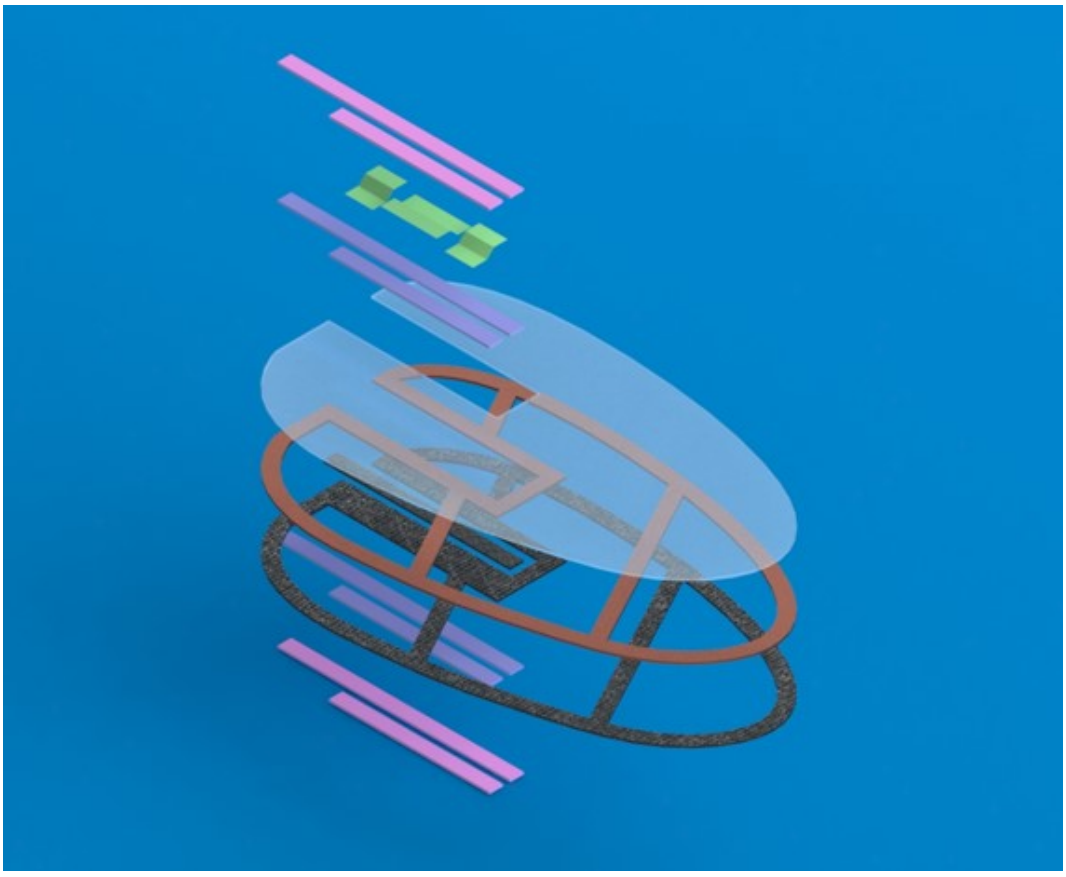

Figure A-1: Rendered image and exploded view of the new wing-system.

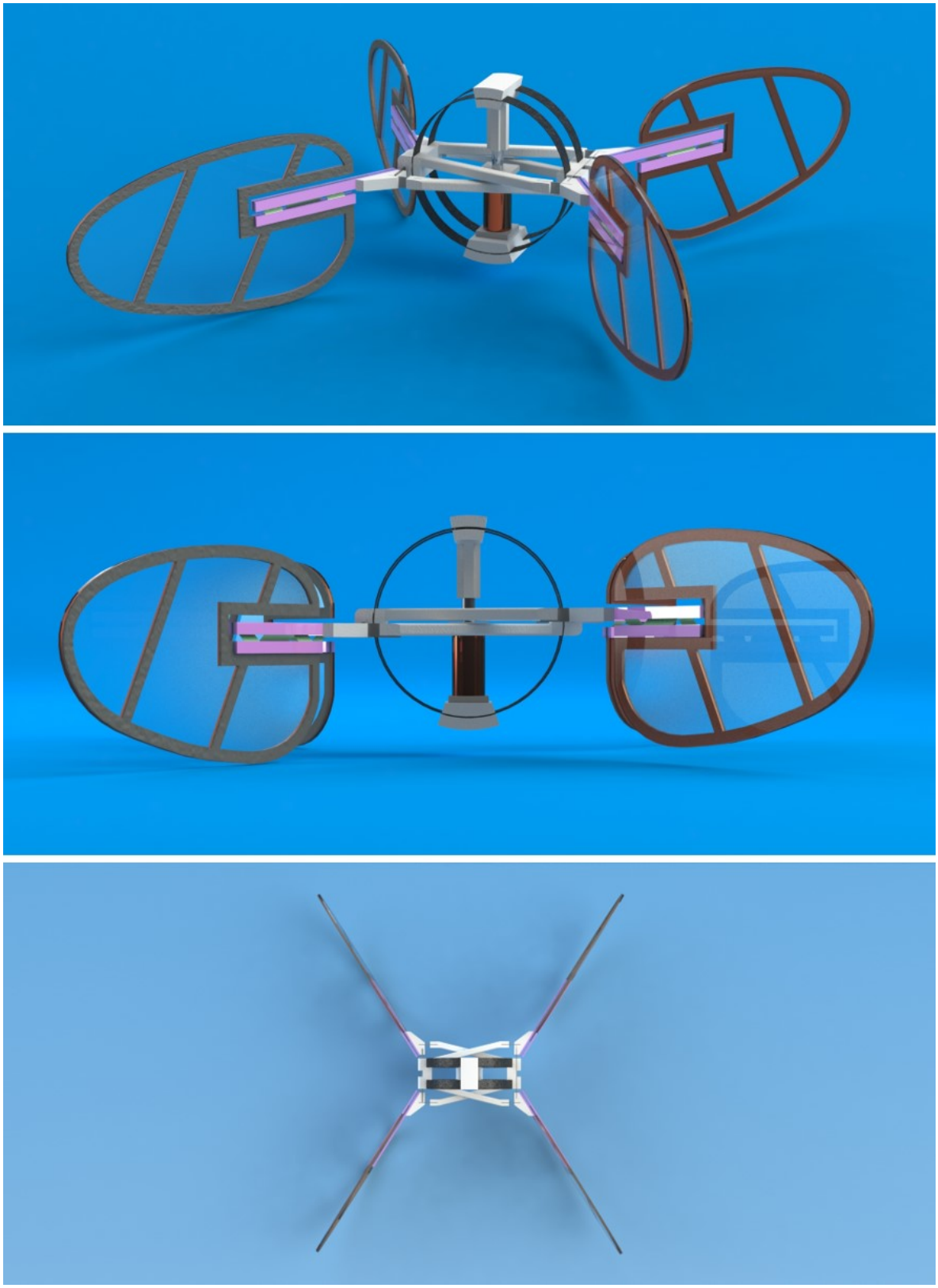

Figure A-2: Rendered images of the Atalanta with the new wing-system.

Bibliography

[1] C. T. Bolsman, *Flapping wing actuation using resonant compliant mechanisms*. PhD thesis, 2010.

[2] Q. Wang, *Modeling, Design and Optimization of Flapping Wings for Efficient Hovering Flight*. PhD thesis, 2017.

[3] H. J. Peters, *A Controllability Approach for Resonant Compliant Systems*. PhD thesis, 2016.

[4] NSF, "Open frame solenoid sdo-0415l." https://www.nsfcontrols.co.uk/NSF/media/NSF/0415L.pdf.

[5] L. Briët, E. Kistemaker, T. V. Krimpen, and E. Versluis, "Optimization of flexible flapping wings," tech. rep., 2019.

[6] X. Bao, A. Bontemps, S. Grondel, and E. Cattan, "Design and fabrication of insect-inspired composite wings for mav application using mems technology," *Journal of Micromechanics and Microengineering*, vol. 21, no. 12, p. 125020, 2011.

[7] A. Calderón, Y. Chen, X. Yang, L. Chang, X.-T. Nguyen, E. Singer, and N. Pérez-Arancibia, "Control of flying robotic insects: A perspective and unifying approach," *arXiv preprint arXiv:1910.11911*, 2019.

[8] K. Y. Ma, P. Chirarattananon, S. B. Fuller, and R. J. Wood, "Controlled flight of a biologically inspired, insect-scale robot," *Science*, vol. 340, no. 6132, pp. 603–607, 2013.

[9] C. Richter and H. Lipson, "Untethered hovering flapping flight of a 3d-printed mechanical insect," *Artificial life*, vol. 17, no. 2, pp. 73–86, 2011.

[10] D. Farhadi Machekposhti, N. Tolou, and J. Herder, "A review on compliant joints and rigid-body constant velocity universal joints toward the design of compliant homokinetic couplings," *Journal of Mechanical Design*, vol. 137, no. 3, 2015.

[11] V. Pini, J. Ruz, P. M. Kosaka, O. Malvar, M. Calleja, and J. Tamayo, "How two-dimensional bending can extraordinarily stiffen thin sheets," *Scientific reports*, vol. 6, no. 1, pp. 1–6, 2016.

[12] Ansys Granta, "Ces edupack material database." https://grantadesign.com/education/ces-edupack/, Accessed 24-June-2020.

[13] T. A. Ward, C. J. Fearday, E. Salami, and N. Binti Soin, "A bibliometric review of progress in micro air vehicle research," *International Journal of Micro Air Vehicles*, vol. 9, no. 2, pp. 146–165, 2017.

[14] D. Floreano and R. J. Wood, "Science, technology and the future of small autonomous drones," *Nature*, vol. 521, no. 7553, pp. 460–466, 2015.

[15] H. V. Phan and H. C. Park, "Insect-inspired, tailless, hover-capable flapping-wing robots: Recent progress, challenges, and future directions," *Progress in Aerospace Sciences*, no. September, 2019.

[16] H. Liu, S. Ravi, D. Kolomenskiy, and H. Tanaka, "Biomechanics and biomimetics in insect-inspired flight systems," *Philosophical Transactions of the Royal Society B: Biological Sciences*, vol. 371, no. 1704, 2016.

[17] J. W. Gerdes, S. K. Gupta, and S. A. Wilkerson, "A review of bird-inspired flapping wing miniature air vehicle designs," *Journal of Mechanisms and Robotics*, vol. 4, no. 2, 2012.

[18] C. H. Greenewalt, "The wings of insects and birds as mechanical oscillators," *Proceedings of the American Philosophical Society*, vol. 104, no. 6, pp. 605–611, 1960.

[19] M. Ras, "Design, fabrication and testing of a resonant flapping-wing micro air vehicle," Master's thesis, 2020.

[20] D. V. Amstel, G. D. Combe, H. Janmaat, and P. D. Zwart, "Het ontwerp van een vleugel-meetopstelling," tech. rep., 2011.

[21] R. Baksteen, R. de Gruiter, S. de Jong, and M. Rodermans, "FWMAV Test simulator," tech. rep., 2013.

[22] G. Bruining, D. Dijkshoorn, R. Noodelijk, and L. van der Spaa, "Ontwerp van een FWMAV actuator," tech. rep., 2013.

[23] F. Visscher, M. Krijnen, W. Feitsma, and I. van der Vossen, "Wing Manufacture for Micro Aerial Vehicles Using Additive Manufacturing Techniques," tech. rep., 2013.

[24] L. Sapin, O. Abolade, N. Willemstein, and L. V. Rijen, "Wing control of a Flapping Wing Micro Air Vehicle (FWMAV) using piezoelectrics," tech. rep., 2013.

[25] T. Lengkeek, W. Krijgsman, B. Fellinger, and J. Clarenburg, "Optic Flow karakteristiek van een optische muis sensor," tech. rep., 2014.

[26] B. L. V. Gaalen, H. K. Bijlsma, W. Veerhoek, and S. P. Aarts, "Out-of-plane motions of insects for flapping wing micro air vehicles," tech. rep., 2014.

[27] A. Hoogerbrugge, T. Drexhage, W. Nelissen, and D. Kappelle, "Controlling the bending stiffness of a cantilever hinge," tech. rep., 2015.

[28] P. van Esch, S. Nieuwenhuis, L. N. van Driessen, and E. L. Blansch, "A Compliant Mechanical Frequency Dividing Transmission Using Parametric Oscillation," tech. rep., 2019.

[29] A. Meskers, "High energy density micro-actuation based on gas generation by means of catalysis of liquid chemical energy," Master's thesis, 2010.

[30] H. J. Peters, "The Optimization of the Flapping Wings for a Micro Air Vehicle," Master's thesis, 2011.

[31] T. van Wageningen, "Design analysis for a small scale hydrogen peroxide powered engine for a Flapping Wing Mechanism Micro Air Vehicle," Master's thesis, 2012.

[32] Y. Lu, "Structural control method research motivated for MAV lift force modification," Master's thesis, 2013.

[33] M. Nugteren, "Dynamic Analysis of a Resonance Based Micro Air Vehicle Structure," Master's thesis, 2014.

[34] A. Selvan, "Simulation of optic flow based flight control for a flapping wing micro aerial vehicle," Master's thesis, 2014.

[35] H. van den Heuvel, "Conceptual Development of a Catalytic Expansion Actuator for a Resonating-body Flapping-wing Micro Air Vehicle," Master's thesis, 2015.

[36] N. K. Teunisse, "Maximization of the geometric non-linearities of a thin-walled structure in resonance," Master's thesis, 2015.

[37] R. Diekerhof, "Resonating structures with flapping wings," Master's thesis, 2016.

[38] D. van Vrede, "Flight Control and Collision Avoidance for Quadcopter and Flapping Wing MAV's using Only Optical Flow," Master's thesis, 2018.

[39] Q. Wang, J. Goosen, and F. Van Keulen, "Study of design parameters of flapping-wings," 2014.

[40] W. Shyy, C.-k. Kang, P. Chirarattananon, S. Ravi, and H. Liu, "Aerodynamics, sensing and control of insect-scale flapping-wing flight," *Proceedings of the Royal Society A: Mathematical, Physical and Engineering Sciences*, vol. 472, no. 2186, p. 20150712, 2016.

[41] J. P. Whitney, P. S. Sreetharan, K. Y. Ma, and R. J. Wood, "Pop-up book mems," *Journal of Micromechanics and Microengineering*, vol. 21, no. 11, p. 115021, 2011.

[42] R. J. Wood, S. Avadhanula, R. Sahai, E. Steltz, and R. S. Fearing, "Microrobot design using fiber reinforced composites," *Journal of Mechanical Design*, vol. 130, no. 5, 2008.

[43] Y. M. Chukewad, J. James, A. Singh, and S. Fuller, "Robofly: An insect-sized robot with simplified fabrication that is capable of flight, ground, and water surface locomotion," *arXiv preprint arXiv:2001.02320*, 2020.

[44] A. Bontemps, T. Vanneste, J. Paquet, T. Dietsch, S. Grondel, and E. Cattan, "Design and performance of an insect-inspired nano air vehicle," *Smart materials and Structures*, vol. 22, no. 1, p. 014008, 2012.

[45] P. S. Sreetharan, J. P. Whitney, M. D. Strauss, and R. J. Wood, "Monolithic fabrication of millimeter-scale machines," *Journal of Micromechanics and Microengineering*, vol. 22, no. 5, p. 055027, 2012.

[46] T. N. Pornsin-Sirirak, S. Lee, H. Nassef, J. Grasmeyer, Y. Tai, C. Ho, and M. Keennon, "Mems wing technology for a battery-powered ornithopter," in *Proceedings IEEE thirteenth annual international conference on micro electro mechanical systems (Cat. No. 00CH36308)*, pp. 799–804, IEEE, 2000.

[47] K. Meng, W. Zhang, W. Chen, H. Li, P. Chi, C. Zou, X. Wu, F. Cui, W. Liu, and J. Chen, "The design and micromachining of an electromagnetic mems flapping-wing micro air vehicle," *Microsystem technologies*, vol. 18, no. 1, pp. 127–136, 2012.

[48] G. C. De Croon, M. Groen, C. De Wagter, B. Remes, R. Ruijsink, and B. W. van Oudheusden, "Design, aerodynamics and autonomy of the delfly," *Bioinspiration & biomimetics*, vol. 7, no. 2, p. 025003, 2012.

[49] M. Karásek, F. T. Muijres, C. De Wagter, B. D. Remes, and G. C. de Croon, "A tailless aerial robotic flapper reveals that flies use torque coupling in rapid banked turns," *Science*, vol. 361, no. 6407, pp. 1089–1094, 2018.

[50] M. Keennon and J. Grasmeyer, "Development of two mavs and vision of the future of mav design," in *AIAA International Air and Space Symposium and Exposition: The Next 100 Years*, p. 2901, 2003.

[51] T. N. Pornsin-Sirirak, Y.-C. Tai, C.-M. Ho, and M. Keennon, "Microbat: A palm-sized electrically powered ornithopter," in *Proceedings of NASA/JPL Workshop on Biomorphic Robotics*, pp. 14–17, 2001.

[52] S. Ho, H. Nassef, N. Pornsinsirirak, Y.-C. Tai, and C.-M. Ho, "Unsteady aerodynamics and flow control for flapping wing flyers," *Progress in Aerospace Sciences*, vol. 39, no. 8, pp. 635–681, 2003.

[53] L. Hines, *Design and Control of a Flapping Flight Micro Aerial Vehicle*. PhD thesis, Carnegie Mellon University, 2014.

[54] M. Jaffar-Bandjee, J. Casas, and G. Krijnen, "Additive manufacturing: state of the art and potential for insect science," *Current opinion in insect science*, vol. 30, pp. 79–85, 2018.

[55] G. Goh, S. Agarwala, G. Goh, V. Dikshit, S. L. Sing, and W. Y. Yeong, "Additive manufacturing in unmanned aerial vehicles (uavs): Challenges and potential," *Aerospace Science and Technology*, vol. 63, pp. 140–151, 2017.

[56] Conrad , "Cured carbon plate." https://www.conrad.nl/p/carbonplaat-carbotec-l-x-b-340-mm-x-150-mm-030-mm-231663, Accessed 19-June-2020.

[57] Prof.dr.ir. Dannis Brouwer PDEng, "Lecture notes from the course me46015 precision mechanism design." University of Technology Delft, department of Precision and Microsystems Engineering, Accessed 19-June-2020.

[58] V. Tielen and Y. Bellouard, "Three-dimensional glass monolithic micro-flexure fabricated by femtosecond laser exposure and chemical etching," *Micromachines*, vol. 5, no. 3, pp. 697–710, 2014.

[59] Keyence, "Keyence vhx-6000 digitial microscope." https://www.keyence.eu/ss/products/microscope/vhx-7000/, Accessed 22-June-2020.

[60] Doug Brown, "Tracker video analysis and modeling tool." https://physlets.org/tracker/, Accessed 23-June-2020.

[61] Hoffmann Group, "Feeler gauge shim roll electronic catalogue." https://ecatalog.hoffmann-group.com/index.html?country=eng_WW_XXX/catalogs/&catalog=90000002#page_190, Accessed 24-June-2020.

[62] M. Taffetani, F. Box, A. Neveu, and D. Vella, "Limitations of curvature-induced rigidity: How a curved strip buckles under gravity," *EPL (Europhysics Letters)*, vol. 127, no. 1, p. 14001, 2019.

[63] C. Wang, Y. Xia, M. Friswell, and E. S. Flores, "Predicting global strain limits for corrugated panels," *Composite Structures*, vol. 231, p. 111472, 2020.

[64] Y. Xia, M. Friswell, and E. S. Flores, "Equivalent models of corrugated panels," *International Journal of Solids and Structures*, vol. 49, no. 13, pp. 1453–1462, 2012.

[65] Z. Ye, V. L. Berdichevsky, and W. Yu, "An equivalent classical plate model of corrugated structures," *International journal of solids and structures*, vol. 51, no. 11-12, pp. 2073–2083, 2014.

[66] B. Moulia, M. Fournier, and D. Guitard, "Mechanics and form of the maize leaf: in vivo qualification of flexural behaviour," *Journal of Materials Science*, vol. 29, no. 9, pp. 2359–2366, 1994.

[67] J. Tamayo, P. M. Kosaka, J. J. Ruz, Á. San Paulo, and M. Calleja, "Biosensors based on nanomechanical systems," *Chemical Society Reviews*, vol. 42, no. 3, pp. 1287–1311, 2013.